Volume 4 | Number 2 | December 2016 | ARO ISSN: 2410-9355 | DOI: 10.14500/2307-549X

ARO

The Scientific Journal of Koya University

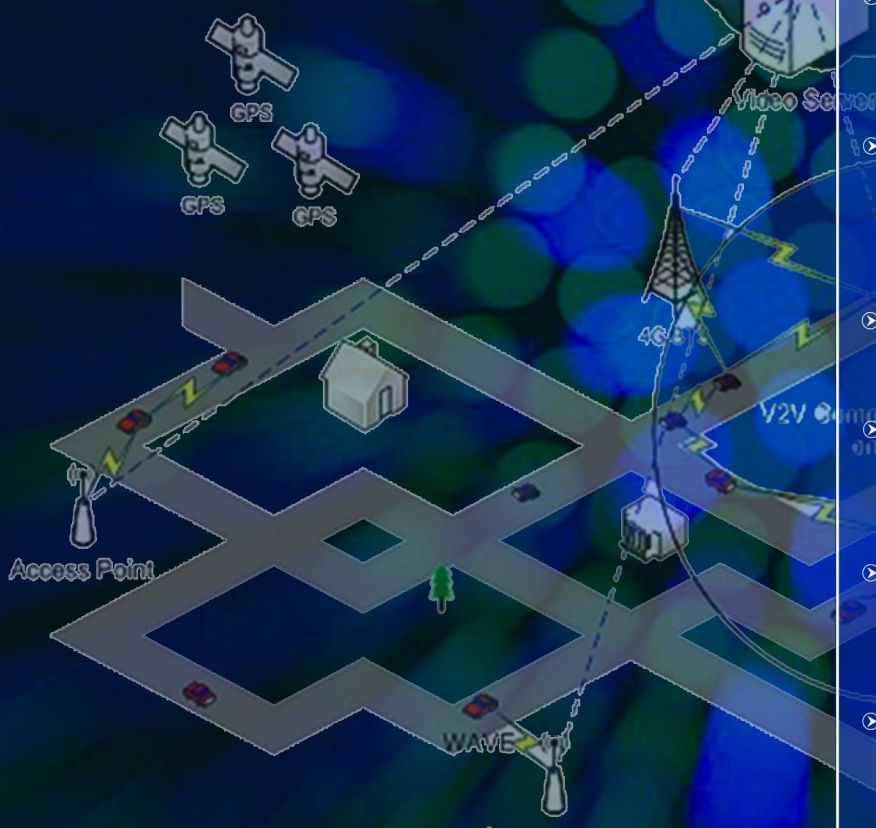

Issue Highlights

aro.koyauniversity.org

ARO-The Scientific Journal of Koya University

The Aro ("Today" in Hewramí Kurdish), is an international scientific journal published by the Koya University with p-ISSN: 2410-9355, e-ISSN: 2307-549X and DOI: 10.14500/2307-549X. Aro is a journal of original scientific research, global news, and commentary. The Aro Scientific Journal is a peer-reviewed, open access journal that publishes original research articles as well as review articles in all areas of Science.

ARO the Scientific Journal Office

Koya University
University Park
Danielle Mitterrand Boulevard, Koya KOY45
Kurdistan Region - F.R. Iraq

Tel.: +964 (0) 748 0127423
Mobile: +964 (0) 7502257080
E-mail: aro.journal@koyauniversity.org
url: aro.koyauniversity.org

December - 2016 | Befranbar- 2716

ARO

The Scientific Journal of Koya University

Vol IV, No 2(2016)

Contents

♦♦♦

DOI: 10.14500/2307-549X ARO p-ISSN: 2410-9355, e-ISSN: 2307-549X

ARO p-ISSN: 2410-9355, e-ISSN: 2307-549X DOI: 10.14500/2307-549X

Aro Editorial Words

Dear readers, you are holding the seventh issue (Vol IV, No 2) of Aro the Scientific Journal of Koya University in your hand. Aro is publishing its 2nd issue as an internationally listed Scientific Journal in Kurdistan Region/Iraq. Notably, Aro has been accepted for indexing in the Emerging Sources Citation Index (ESCI), a new edition of Web of Science™ as of Feb 2016. Content in this index is under consideration by Thomson Reuters to be accepted in the Science Citation Index Expanded™ (SCIE). All our individual articles are currently listed by Thomson Reuters using Aro's DOI numbers. This is a great achievement that we share with our academic communities. Aro is starting its fourth year journey in leading the quality of regional scientific publications with global impact. The editorial team is determined to keep the path of such a mission and sustain Aro's future publications with quality and reliability in mind.

Despite the continuous economic downturn and war on terror which have had a great impact on scientific research and funding of the universities of our region in particular, Aro is continuing to receive great numbers of well motivated quality papers which shows its steadily growing trust among researchers in the region, demanding the increased volume of publication. Nevertheless, Aro is finding more focus in applied sciences with research values in current regional issues having International impacts. Aro's Associate Editorial has grown larger and well dedicated and our meeting are more richer. Our colleagues with great passion are contributing to Aro's long-term visions.

Aro was created with a long-term visions of becoming accessible to all researchers in Kurdistan and beyond, and covering a wide range of scholarly disciplines in sciences. Aro aspires to become a channel for exchange of scholarly research by establishing academic connections between scholars globally.

Aro is a journal of original scientific research, global news, review paper, letters and commentary. The Aro Scientific Journal is a peer-reviewed, open access journal that publishes original research articles as well as review articles in areas of natural sciences and technology. In this issue you will have access to original research papers in variety of areas, such as Petroleum, Physics, Chemical Engineering, Biochemistry, Engineering and Materials Science.

The warm responses from researchers, academics and professionals in the last four years have made us to create a wider Editorial Board which serves the wider submitted scientific manuscripts. However, it is clear that having a dedicated and well organized editorial board for the journal is only one side of the coin. The other is the ability to attract submissions of quality research and scholarly work. We are thankful to all of those who put their trust in Aro and presented their original research work for publication in Vol IV, No 2 of the journal, as well as, our thanks are extended to the 16 peer-reviewers from the Universities worldwide for their efforts in reviewing and enabling this issue of Aro.

Your support and feedback are invited and appreciated.

Dilan M. Rostam
Editor-in-Chief

Wali M Hamad
Executive Publisher

Dilan M. Rostam, Salah I. Yahya, Shwan K. Rachid, Basim M. Fadhil, Fahmi F. Muhammad and Muhammed H. Zangana.
Executive Editorial Board

DOI: 10.14500/2307-549X ARO p-ISSN: 2410-9355, e-ISSN: 2307-549X

Correlation and Path Coefficient Analysis of Seed Yield and Yield Components in Some Faba Bean Genotypes in Sulaimani Region

Sherwan E. Tofiq[1], Omer K. Aziz[1] and Sazgar H. Salih[2]

[1]Faculty of Agricultural Science, University of Sulaimani, Kurdistan Region – F.R. Iraq

[2]Sulaimani Agricultural Research Center – Sulaimani, Kurdistan Region – F.R. Iraq

***Abstract*—The present study was conducted at Agricultural Research Center of Bakrajo, Sulaimani, Iraq during three successive seasons 2011-2014. This research was conducted using seven faba bean cultivars namely (Zaina, Seher, Yieldiz, Civilla, Luz di Otono, Tanyari and local). The following measurements and observations were made: 100 seed weight, first node height, number of seeds/plant, number of seeds/pod, pod length, number of pods/plant and seed yield. The results indicated that highly significant and negative correlations were presented between 100 seed weight and seed yield, whereas, significant and positive correlations were presented between the numbers of seed/plant and seed yield at the second season. In addition, the results of the third season indicate that the number of seeds/plant correlated significantly and positively with seed yield, and the number of seeds/pod correlated significantly and negatively with seed yield, whereas, number of pods/plant correlated high significantly and positively with the seed yield. The character first node height showed maximum direct effect value in seed yield at the first season and the third season, while number of pods/plant showed maximum direct effect value in seed yield at the second season.**

***Index Terms*—Broad bean, correlation, path analysis.**

I. Introduction

The Faba bean (*Vicia faba* L.) is a pulse crop and one of the most important legume crops in the Mediterranean Basin (Anonymous, 1997). It is one of the major winter sown legume crops, and has considerable importance as a low cost food rich in proteins and carbohydrates (Sepeto_lu and Grain, 2002). It is a diploid species ($2n = 12$). Botanically, it has been divided based on seed size into types as minor, equine and major, even though there is no discontinuity in seed size between them. This species originated in Southwest Asia but its immediate ancestor is not known. On the basis of morphological and geographical considerations, ancestors have been proposed within the species complex *Vicia narbonensis* L. ($2n = 14$) (Hawtin and Webb, 1982). Faba bean, is the only species known in cultivation of section Faba. It was divided two subspecies; *V. faba* subsp. paucijuga Murat and *V. faba* subsp. *faba* L.. The taxon *V. faba* subsp. *faba* L. was classified in three variety groups, var. minor, var. equine and var. *faba* (major). Variety groups were also referred to as tick bean, horse bean or field bean and broad bean (Duc, *et al.*, 2010). Faba bean is a self-pollinating plant with significant levels of outcross and inter-cross, ranging from 20 to 80% depending on genotype and environmental effects (Suso and Moreno, 1999). Faba bean is a grain legume and grown for its high protein content (25.4%) in the seed Karadavut, *et al.*, 2010). Yield improvement is a major breeding objective of most crop improvement programs (Ghobary and Abd-Allah, 2010). Yield in faba bean, similar to the other crops, is a complex trait and constitute by many of morphological and physiological traits. Seed yield is affected by genotype and environmental factors because it is a quantitative trait. Using as selection criteria of characters, direct relationship with seed yield increase the success of selection in plant breeding (Karasu and Oz, 2010). Therefore, progress of breeding in such traits are primarily conditioned by the magnitude and nature of variation and interrelationships among them (Raffi and Nath, 2004).

Mathematical applications have been widely used in different agricultural researches, Hamid and Abdullah (2008) used mathematical models in sustainable agriculture development as indispensable tool to increase the understand of rice growth, whereas different mathematical formulas represented as regression models were used as a non-destructive method for determine log volume for *Melia azedarach*

ARO-The Scientific Journal of Koya University
Volume IV, No 2(2016), Article ID: ARO.10081, 06 pages
DOI: 10.14500/aro.10081
Received 23 April 2015; Accepted 01 June 2015
Regular research paper: Published 20 June 2016
Corresponding author's e-mail: sherwan.tofiq@univsul.edu.iq

L. trees (Amin, 2014) and the leaf area of oleander (*Nerium oleander L.*) plants (Al-Barzinji and Amin, 2016). Another important mathematical application in agriculture is the correlation analysis, which describes the mutual relationship between different pairs of characters without providing the nature of cause and effect relationship of each character. Significant positive correlations were detected between faba bean seed yield and each of number of pods/plant, number of seeds/plant, seed weight/plant and biological yield (Alghamd, 2007). Tadesse, et al. (2011) indicated number of pods/plants, number of seeds/pod, thousand seed weight and plant height had significant association with seed yield/plot. The seed yield/plant exhibited positive and significant correlation with clusters/plant, pod length, plant height, branches/plant, pods/plant and hundred seed weight (Badolay, et al., 2009). Ulukan *et al.* (2003) also found positive and significant relationships between biological yield and plant height and grain number/pod. Keneni and Jarso (2002) indicated positive and significant correlation between Seed yield and number of pods/plant. Simple correlation analysis is not able to provide detailed and actual knowledge in the relation between dependent variable and predictor variables. Hence, the path analysis was also /formed to determine the direct and indirect contribution of each character to seed yield (Chitra and Rajamani, 2010). Path coefficient analysis has been widely used in crop breeding to determine the nature of relationships between grain yield and its contributing components and to identify those components with significant effects on yield for potential use as selection criteria (Mohammadi, et al., 2003). Correlation and path coefficient have been extensively conducted in various legume crops e.g., for instance, Bingliang and Mingliang (2003), Gonçalves, et al. (2003), Karasu and Oz (2010), Salehi, et al. (2010) and Sadeghi, et al. (2011) on bean, Arshad, et al. (2002), Sagir, et al. (2004) on chickpea, Karadavut (2009) on lentil, Ulukan et al. (2003) on faba bean, Hassan, et al. (2003) on mungbean, Nawab, et al. (2008) on pea, Dursun (2007) on bean, Malik, et al. (2007) on soybean etc. This study was aimed to determine the relationship among seed yield and yield components, and their direct and indirect effects of contributing characters to seed yield in faba bean.

II. Materials and Methods

The experiment was carried out at Bakrajo location during three successive seasons 2011-2014. Seven genotypes were used for this study namely Zaina, Seher, Yieldiz, Cirilla, Luz di Otono, Tanyari, and Local variety. The genotypes were arranged in randomized complete block design with three replications. Each ex/imental plot consisted of four rows four m long with inter-row spacing of 40 cm. Seeding rate was applied at the rate of 200 kg/ha and fertilizers were applied at the rate of 100 kg DAP/ha. Weeds were controlled by hand.

A. Correlation Coefficient (r)

Phenotypic correlation, the observable correlation between two variables, which includes both genotypic and environmental effects, and genotypic correlation, the inherent association between two variables were estimated using the standard procedure suggested by Miller, et al. (1958). Covariance analysis between all pairs of the variables followed the same form as the variance. Thus, estimates of genetic covariance component between two traits (σg_{xy}) and the phenotypic covariance component (σp_{xy}) were derived in the same fashion as for the corresponding variance components (Tadesse, et al., 2011).

$$r_{gxy} = \frac{\sigma g_{xy}}{\sqrt{\sigma^2 g_{yx} \times \sigma^2 g_y}} \quad (1)$$

$$r_{pxy} = \frac{\sigma p_{xy}}{\sqrt{\sigma^2 p_{yx} \times \sigma^2 p_y}} \quad (2)$$

where, σg_{xy} = genotypic covariance of two variables x and y, and σp_{xy} = phenotypic covariance of two variable x and y.

B. Path Coefficient Analysis

Path coefficient analysis is a statistical technique of partitioning the correlation coefficients into its direct and indirect effects, so that the contribution of each character to yield could be estimated. It is used in plant breeding programs to determine the nature of the relationships between yield and yield components that are useful as selection criteria to improve the crop yield. The goal of the path analysis is to accept descriptions of the correlation between the traits, based on a model of cause and effect relationship and to estimate the importance of the affecting traits on a specific trait (Cyprien and Kumar, 2011).

Path coefficient analysis was carried out using the phenotypic correlation coefficients as well as genotypic correlation coefficients to determine the direct and indirect effects of the yield components and other morphological characters on seed yield (Dewey and Lu, 1959).

The path coefficient is as follows;

$$r_{ij} = p_{ij} + \Sigma\, r_{ik}\, p_{kj} \quad (3)$$

Where, r_{ij} = mutual association between the independent character i and dependent character i as measured by the correlation coefficients. p_{ij} = components of direct effects of the independent character i on the dependent variable i as measured by the path coefficients, and $\Sigma r_{ik}\, p_{kj}$ = summation of components of indirect effects of a given independent

character i on a given dependent character i via all other independent characters k.

C. The Statistical Techniques

The data of seed yield and its components were analyzed by the following statistical procedures. Significance of correlation coefficients were tested in the probably levels of 0.05 and 0.01. These correlations were further analyzed using path coefficients as illustrated by LI (1968). The path analysis was done as given by Wright, (1921) and elaborated by Dewey and Lu (1959) to calculate the direct and indirect contribution of various traits to yield. Also, the relative importance of direct and indirect effects on seed yield was determined by path analysis. In path analysis, seed yield was the dependent variable and the other traits were considered as independent variables. All of the statistical analysis carried out using SAS 9.2 statistics program.

III. Results and Discussion

Data in Table I, explain the correlation coefficient among the characters for the first season (2011-2012), there were highly significant and positive correlation between the first node height with number of seeds/plant and pod length, while the first node height correlated significantly and positively with number of seeds/pod, and it correlated significantly and negatively with number of pods/plant. The character number of seed/plant associated high significantly and positively with pod length, while significantly and negatively correlated with number of pods/plant. Regarding to the character number of seeds/pod significant and positive correlation was observed with pod length, while highly significant and negative correlation was noticed with number of pods/plant. Pod length correlated significantly and negatively with number of pods/plant.

TABLE I
CORRELATION COEFFICIENT AMONG THE CHARACTERS FOR THE SEASON (2011 – 2012)

Traits	Seed yield (Kg/ha)	100 seed weight (gm)	First node height (cm)	No. of seeds/ plant	No. of seeds/ pod	Pod length (cm)
100 seed weight (gm)	0.264					
First node height (cm)	0.456	-0.160				
No. of seeds/plant	0.433	-0.046	0.917**			
No. of seeds/pod	-0.340	0.020	0.576*	0.523		
Pod length (cm)	0.331	-0.231	0.970**	0.842**	0.621*	
No. of pods/plant	0.228	0.254	-0.596*	-0.565*	-0.852**	-0.571*

The values do not bear star are not significant.
**Correlation is significant at the 0.05 level (2-tailed), $t_{0.05}(5)=2.571$.*
*** Correlation is significant at the 0.01 level (2-tailed, $t_{0.01}(5)=4.03$.*

Table II, explain the correlation coefficient among the characters for the second season (2012-2013), it was observed that the seed yield showed highly significant and negative correlation with 100 seed weight, while it correlated significantly and positively with number of seeds/plant. The character 100 seed weight gave highly significant and negative correlation with number seeds/plant. The character firs node height correlated height significantly and positively with pod length. The character number of seeds/plant showed significant and positive correlation with number of pods/plant.

TABLE II
CORRELATION COEFFICIENT AMONG THE CHARACTERS FOR THE SEASON (2012 – 2013)

Traits	Seed yield (Kg/ha)	100 seed weight (gm)	First node height (cm)	No. of seeds/ plant	No. of seeds/ pod	Pod length (cm)
100 seed weight (gm)	-0.721**					
First node height (cm)	-0.410	-0.069				
No. of seeds/plant	0.618*	-0.651**	-0.419			
No. of seeds/pod	-0.104	0.070	-0.099	0.288		
Pod length (cm)	-0.304	-0.337	0.904**	-0.202	-0.224	
No. of pods/plant	0.030	-0.392	0.095	0.614*	-0.182	0.357

The values do not bear star are not significant.
** Correlation is significant at the 0.05 level (2-tailed), $t_{0.05}(5)=2.571$.*
*** Correlation is significant at the 0.01 level (2-tailed), $t_{0.01}(5)=4.03$.*

Table III, explain the correlation coefficient among the characters for the third season (2013-2014), it was observed that the character seed yield produced significant and positive correlation with number of seeds/plant, while significantly and negatively correlated with number of seeds/pod and high significantly and positively correlated with number of pods/plant. The character 100 seed weight showed significant and positive correlation with first node height and pod length, while it correlated significantly and negatively with number of pod/plant. Regarding to the character first node height it was correlated high significantly and positively with number of seeds/pod and pod length. The character number of seeds/plant correlated significantly and positively with number of pods/plant. The character number of seeds/pod showed height significant and positive correlation with pod length, while it correlated height significantly and negatively with number of pods/plant. Regarding to the character pod length it showed significant and negative correlation with number of pods/plant. Cokkizgin (2007) also reported significant positive correlation between numbers of seed/plant with seed yield/plant. All other observed relationships among yield components were not significant. There was a significant correlation between biological yield and plant height as it was also reported by Ulukan, et al. (2003). Bianco, et al. (1979) found positive relationships between yield and plant height, number of branches and pods/plant, number of seeds/pod and 1000-seed weight, whereas, seed yield was negatively correlated with flowering date and the lowest node bearing pods. These findings indicate that selection for each or both of number of pods, nodes and biomass would be accompanied by high yielding ability under such conditions.

 http://dx.doi.org/10.14500/aro.10081

TABLE III
CORRELATION COEFFICIENT AMONG THE CHARACTERS FOR THE SEASON (2013 – 2014)

Traits	Seed yield (Kg/ha)	100 seed weight (gm)	First node height (cm)	No. of seeds/ plant	No. of seeds/ pod	Pod length (cm)
100 seed weight (gm)	-0.375					
First node height (cm)	0.132	0.080*				
No. of seeds/plant	0.572*	-0.225	0.381			
No. of seeds/pod	-0.559*	0.137	0.691**	0.015		
Pod length (cm)	-0.431	0.524*	0.710**	0.241	0.808**	
No. of Pods/Plant	0.896**	-0.577*	-0.051	0.617*	-0.621**	-0.509*

The values do not bear star are not significant.
** Correlation is significant at the 0.05 level (2-tailed),* $t_{0.05}(5)=2.571$.
*** Correlation is significant at the 0.01 level (2-tailed),* $t_{0.01}(5)=4.03$.

Data in Table IV, explain the path coefficient analysis between seed yield and its components in the first season. The character first node height showed maximum positive direct effect in seed yield with 1.001, while maximum negative direct effect exhibited by the character number of seeds/pod with -1.512. maximum positive indirect effect in seed yield produced by number of pods plant via number of seeds/pod which was 1.288 and followed by pod length via first node height with 0.971. Maximum negative indirect effect in seed yield was shown by pod length via number of seeds/pod with – 0.940.

TABLE IV
PATH COEFFICIENT ANALYSIS FOR THE CHARACTERS ON SEED YIELD AT SEASON (2011 – 2012)

Traits	*100 seed weight (gm)*	*First node height (cm)*	*No. of seeds/ plant*	*No. of seeds/ pod*	*Pod length (cm)*	*No. of pods/ plant*
100 seed weight (gm)	**0.683**	-0.109	-0.032	0.013	-0.158	0.174
First node height (cm)	-0.160	**1.001**	0.917	0.577	0.971	-0.597
No. of seeds/plant	0.015	-0.306	**-0.334**	-0.175	-0.281	0.189
No. of seeds/pod	-0.030	-0.871	-0.791	**-1.512**	-0.940	1.288
Pod length (cm)	-0.091	0.384	0.333	0.246	**0.395**	-0.226
No. of pods/plant	-0.153	0.358	0.339	0.511	0.343	**-0.600**
Seed yield **Correlation**	**0.264**	**0.456**	**0.433**	**-0.340**	**0.331**	**0.228**

Data in Table V, explain the path coefficient analysis between seed yield and its component in the second season. Maximum positive direct effect in seed yield observed by the character number of pods/plant with 19.310, while maximum negative direct effect exhibited by the character number of seeds/plant with – 28.589. Maximum positive indirect effect showed by the character 100 seed weight via number of seeds/plant with 18.622 and followed by the character number of seeds/plant via 100 seed weight with 13.146. Maximum negative indirect effect in seed yield observed by first node height via pod length with -22.410 and followed by number of pods/plant via number of seeds/plant with -17.566.

TABLE V
PATH COEFFICIENT ANALYSIS FOR THE CHARACTERS ON SEED YIELD AT SEASON (2012 – 2013)

Traits	*100 seed weight (gm)*	*First node height (cm)*	*No. of seeds/ plant*	*No. of seeds/ pod*	*Pod length (cm)*	*No. of pods/ plant*
100 seed weight (gm)	**-20.182**	1.388	13.146	-1.409	6.799	7.909
First node height (cm)	-0.525	**7.626**	-3.192	-0.754	6.890	0.725
No. of seeds/plant	18.622	11.968	**-28.589**	-8.238	5.772	-17.566
No. of seeds/pod	0.577	-0.818	2.381	**8.264**	-1.850	-1.506
Pod length (cm)	8.355	-22.410	5.008	5.551	**-24.801**	-8.843
No. of pods/plant	-7.568	1.836	11.865	-3.518	6.885	**19.310**
Seed yield **Correlation**	**-0.721**	**-0.410**	**0.618**	**-0.104**	**-0.304**	**0.030**

Data of path coefficient analysis between seed yield and their components in the third season are presented in Table VI.

TABLE VI
PATH COEFFICIENT ANALYSIS FOR THE CHARACTERS ON SEED YIELD AT SEASON (2013 – 2014)

Traits	*100 seed weight (gm)*	*First node height (cm)*	*No. of seeds/ plant*	*No. of seeds/ pod*	*Pod length (cm)*	*No. of pods/ plant*
100 seed weight (gm)	**-0.180**	-0.014	0.040	-0.025	-0.094	0.104
First node height (cm)	0.101	**1.264**	0.482	0.873	0.898	-0.065
No. of seeds/plant	-0.172	0.292	**0.764**	0.011	0.184	0.472
No. of seeds/pod	-0.176	-0.883	-0.019	**-1.278**	-1.033	0.794
Pod length (cm)	-0.419	-0.568	-0.193	-0.647	**-0.800**	0.407
No. of pods/plant	0.471	0.042	-0.503	0.507	0.415	**-0.816**
Seed yield **Correlation**	**-0.375**	**0.132**	**0.572**	**-0.559**	**-0.431**	**0.896**

Maximum positive direct effect in seed yield sowed by the character first node height with 1.264 , while maximum negative direct effect was -1.278 showed by number of seeds /pod. Maximum positive indirect effect in seed yield showed by pod length via first node height with 0.898 and followed by 0.873 for the character number of seeds/pod via first node height also. The highest negative indirect effect was -1.033 showed by the character pod length via number of seeds/pod. Previous results were obtained by Bakheit and Mahady (1998), Bora, et al. (1988) and Vandana and Dubey (1993). Abdelmula and Abdalla (1994) were reported that the number of pods/plant had the highest direct positive effect (7.02) on grain yield/plant, followed by 100-seed weight, number of branches/plant and number of seeds/pod. On the other hand, grain yield/plant was directly and negatively affected by number of nodes/stem (-2.85) and number of pods/node (-0.21). The highest negative indirect effects on grain yield/plant were caused by number of branches/plant (-6.93),100-seed weight (-5.38) and number of seeds/pod (-4.13), through number of pods/plant. Although number of nodes/stem and number of pods/node showed negative direct

effects on grain yield/plant, they had the highest positive indirect effects via number of pods/plant.

IV. Conclusion

Based on the results achieved in this study, it is concluded that yield components are interrelated with each other, and they affect grain yield/plant directly or indirectly, positively or negatively, through each other. It also concluded that the number of seeds/plant appeared to be the highest contributor to the grain yield. Therefore, direct and indirect selection for higher grain yield may be effective for improving this character, as had been shown by Peksen and Gulumser (2005), Sabokdast and Khyalparast (2008) and Atta, et al. (2008) in various studies on legume crops. Selection for increasing seed yield through these traits might be more successful.

References

Al-Barzinji, I.M. and Amin, B.M., 2016. Non-destructive method of leaf area estimation for oleander (*Nerium oleander* L.) cultivated in the Iraqi Kurdistan Region. *ARO-The Scientific Journal of Koya University*, 4(1), pp.22-26. Retrieved from http://dx.doi.org/10.14500/aro.10088

Abdelmula, A. A. and Abd alla, A.H., 1994. Path coefficient analysis in faba bean (*Vicia faba* L). *University of Khartoum Journal of Agricultural Science*, 2(1), pp.46-58.

Alghamd, S.S., 2007. Genetic behavior of some selected faba bean genotypes. *African Crop Science Conference Proceedings*, 8, pp.709-714.

Amin, T.M., 2014, Non-destructive method for estimating log volume for *Melia azedarach* L. trees in Erbil-Iraqi Kurdistan Region. *ARO-The Scientific Journal of Koya University*, 2(2), pp.32-36. Retrieved from http://dx.doi.org/10.14500/aro.10027

Anonymous, 1997. Food and Agriculture Organization of the United Nations (FAO). Production Year Book, FAO, Rome, Italy.

Arshad, M., Bakhsh, A. Bashir, M. and Haqqani, A.M., 2002. Determining the heritability and relationship between yield and yield components in chickpea (*Cicer arietinum* L.). *Pakistan Journal of Botany*, 34(3), pp.237-245.

Atta, B.M., Haq M.A. and Shah, T.M., 2008. Variation and inter-relationships of quantitative traits in chickpea (*Cicer arietinum* L.). *Pakistan Journal of Botany*, 40(2), pp.637-647.

Badolay, A., Hooda, J.S., Malik, B.P.S., 2009. Correlation and path analysis in faba bean (*Vicia faba* L.). *Journal of Haryana Agronomy*, 25, pp.94-95.

Bakheit, B.R. and Mahady, E.E., 1998.Variation, correlation and path coefficient analysis for some characters in collection of faba bean (*Vicia faba* L.). *Federal Board of Intermediate and Secondary Education (FBISE)*, 20, pp.9-14.

Bianco, V.V., Damato, G., Miccolis, V., Polignano, G., Poerceddu, E. and Scipa, G., 1979. *Variation in a collection of Vicia faba L. and Correlations Among Agronomically Important Characters. In: Some Current Research on Vicia faba in Western Europe.* Ed. D.A. Bond, G.T. Scarascia-Mugnozza and M.K. Poulsen. Pub. EEC, EUR 6244, pp.125-143.

Bingliang, W. and C. Mingliang, 2003. Path coefficient analysis of pod yield and its components in *Phaseolus vulgaris* L. var. humilis alef. *Journal of Biomathematics*, 18(3), pp.345-350.

Bora, G.C., S.N. Gupta, Y.S. Tomer, S. Singh and S. Singh, 1988. Genetic variability, correlation and path coefficient analysis in faba bean (*Vicia faba* L.). *Indian Journal of Agricultural Science*, 68(4), pp. 212-214.

Chitra, R., Rajamani, K., 2010. Character association and path analysis in glory lily (*Gloriosa su/ba* L.). *Communications in Biometry and Crop Science*, 5, pp. 78–82.

Cokkizgin, A., 2007. Research on *Determination of Botanical and Agronomic Pro/ties of Local Genotypes of Some Lentils* (*Lens culinaris Medik*.) *Selected From South And Southeastern Anatolian Regions In Turkey*. Ph.D. Thesis, Department of Field Crops Institute of Natural and Applied Sciences University of Cukurova, p.127.

Cyprien, M. and Kumar, V., 2011. Correlation and path coefficient analysis of rice cultivates data. *Journal of Reliability and Statistical Studies*, 4 (2), pp. 119-131.

Dewey, D.R. and Lu, K.H., 1959. A correlation and path coefficient analysis of components of crescent wheat grass seed production. *Agronomy Journal*, 51, pp.515-518.

Duc, G., Shiying, B., Baum, M., Redden, B., Sadiki, M., Jose Suso, M., Vishniakova, M. and Zong, X., 2010. Diversity maintenance and use of *Vicia faba* L. genetic resources. *Field Crops Research*, 115, pp.270–278.

Dursun, A., 2007. Variability, heritability and correlation studies in bean (*Phaseolus vulgaris* L.) Genotypes. *World Journal of Agricultural Sciences*, 3(1), pp. 12-16.

Ghobary, H.M.M. and Abd Allah, S.A.M., 2010. Correlation and path coefficient studies in common bean (*Phaseolus vulgaris* L.). *Journal of Plant Production*, 9, pp.1233–1239.

Gonçalves, M.C., Correa, A.M., Destro, D., Ferreira, L.C., and Sobrinho, T.A., 2003. Correlations and path analysis of common bean grain yield and its primary components. *Crop Breeding and Applied Biotechnology*, 3(3), pp.217-222.

Hamid, M.N. and Abdullah, M.Y., 2008, Contribution of mathematical model for the development of sustainable agriculture. 2008. *Malaysian Journal of Mathematical Science*, 2(2), pp.83-91.

Hassan, M., Zubair, M. and Ajmal, S., 2003. Correlation and path coefficient analysis in some promising lines of mashbean (*Vigna mungo*). *Pakistan Journal of Biological Sciences*, 6(4), pp.370-372.

Hawtin, G. and Webb, C., 1982. *Faba bean Improvement*. In: Proceeding of faba the bean Conference Cairo, Egypt, the International Center for Agricultural Research Center in the Dry Areas (ICARDA) Aleppo, Syria. Martinus Nijhoff Publisher for ICARDA/IFAD Nile Valley Project, The Netherlands, pp.19-23.

Karadavut, U., 2009. Path analysis for yield and yield components in lentil (*Lens culinaris Medik*.). *Turkish Journal of Field Crops*, 14(2), pp.97-104.

Karadavut, U., Ç. PALTA, Z. Kavurmaci, and Y. Bölek, 2010. Some grain yield parameters of multi-environmental trials in faba bean (*Vicia faba*) genotypes. *International Journal of Agriculture and Biology*, 12, pp.217–220.

Karasu, A. and Oz, M., 2010. A study on coefficient analysis and association between agronomical characters in dry bean (*Phaseolus vulgaris* L.). *Bulgarian Journal of Agricultural Science*, 16, pp.203-211.

Keneni, G. and Jarso, M., 2002. Comparison of three secondary traits as determination of grain yield in Faba bean on water logged vertisols. *Journal of Genetics and Breeding*, 56, pp.314-325.

LI, C.C., 1968. *Population Genetics*. The University of Chicago Press, Chicago. USA.

Malik, M.F.A., Ashraf, M., Qureshi A.S. and Ghafoor, A., 2007. Assessment of genetic variability, correlation and path analyses for yield and its components in soybean, *Pakistan Journal of Botany*, 39(2), pp.405-413.

Miller, P.A., Williams, J.C., Robinson, H.P. and Comstock, R.E., 1958. Estimation of genotypic and environmental variances and covariances in upland cotton and their implications in selection. *Agronomy Journal*, 50, pp.126-131.

Mohammadi, S.A., Prasanna B.M. and Singh, N.N., 2003. Sequential path model for determining interrelationships among grain yield and related characters in maize. *Crop Science*, 43, pp.1690-1697.

Nawab, N.N., Subhani, G.M., Mahmood, K., Shakil, Q. and Saeed, A., 2008. Genetic variability, correlation and path analysis studies in garden pea (*Pisum sativum* L.). *Journal of Agricultural Research*, 46(4), pp.333-340.

Peksen, E. and Gulumser, A., 2005. Relationships between seed yield and yield components and path analysis in some common bean (*Phaseolus vulgaris* L.) genotypes. *Journal of Faculty of Agricultural, Ondokuz Mayis University*, 20(3), pp.82-87.

Raffi, S.A., and Nath, U.K., 2004. Variability, heritability, genetic advance and relationships of yield and yield contributing characters in dry bean (*Phaseolus vulgaris* L.). *Journal of Biological Science*, 4(2), pp.157-159.

Sabokdast, M. and Khyalparast, F., 2008. A study of relationship between grain yield and yield component in common bean cultivars (*Phaseolus vulgaris* L.). *Journal of Water and Soil Science, Science & Technology of Agriculture & Natural Resources*, 11(42), pp.123-133.

Sadeghi, A., Cheghamirza, K. and Dorri, H.R., 2011. The study of morpho-agronomic traits relationship in common bean (*Phaseolus vulgaris* L.). *Biharean Biologist*, 5(2), pp.102-108.

Sagir, A., Bicer, B.T. and Sakar, D., 2004. Correlations among characters and ascochyta blight disease severities in chickpea breeding lines. *Plant Pathology Journal*, 3(1), pp.40-43.

Salehi, M., Faramarzi, A. and Mohebalipour, N., 2010. Evaluation of different effective traits on seed yield of common bean (*Phaseolus vulgaris* L.) with path analysis. *American-Eurasian Journal of Agricultural & Environmental Sciences*, 9(1), pp.52-54.

Sepeto_lu, H. and Grain, L., 2002. *Ege University, Faculty of Agriculture*, Publication: 24/4.262 p.

Suso, M.J., M.T. Moreno, 1999. Variation in outcrossing rate and genetic structure on six cultivars of *Vicia faba* L. as affected by geographic location and year. *Plant Breeding*, 118, pp.347-350.

Tadesse, T., Fikere, M., Legesse, T. and Parven, A., 2011. Correlation and path coefficient analysis of yield and its component in faba bean (*Vicia faba* L.) germplasm. *International Journal of Biodiversity Conservation*, 3, pp.376-382.

Ulukan, H., Culer, M. and Keskin, S., 2003. A path coefficient analysis of some yield and yield components in faba bean (*Vicia faba* L.) genotypes. *Pakistan Journal of Biological Science*, 6(23), pp.1951-1955.

Vandana, K., and Dubey, D.K.,1993. Path analysis in faba bean. *Federal Board of Intermediate and Secondary Education (FBISE)*, 32, pp.23-24.

Wright, S., 1921. Correlation and causation. *Journal of Agricultural Research*, 20, pp. 557–585.

In Vitro Effect of Sorghum (*Sorghum bicolor*) Seed Extracts as a Biological Acaricidal Against Some Hard Tick (Ixodidae) in Sulaimani Governorate - Kurdistan Region/Iraq

Bahzad H.S. Mustafa[1], Kadhm A. Mohammad[2] and Aram O. Mahammed[2]

[1]Department of Animal Production, Faculty of Agricultural Sciences, University of Sulaimani Sulaimani, Kurdistan Region – F.R. Iraq

[2]Department of Agribusiness and Rural Development, Faculty of Agricultural Sciences, University of Sulaimani Sulaimani, Kurdistan Region – F.R. Iraq

Abstract*—This study was conducted in Sulaimani governorate in order to identify the biological control of some Ixodidae genera among different flocks of cattle, sheep and goats. Four genera of Ixodidae; Boophilus spp, Hyalomma spp., Rhipicephalus spp. and Haemaphysalis spp., were identified in these infested animals. According to chi–square test, the highest distribution of Boophulis spp., was recorded in cattle (56.51%), and the highest distribution of Hyalomma spp., (49.82%) and Rhipicephalus spp., (28.16%) which were in sheep. The highest number of Haemophasylas spp., was obtained from goats (6.67%), whereas the lowest number of this genus (2.88% and 2.89%) was collected from cattle and sheep respectively. The toxicity of Sorghum bicolor seed extract was tested against the more distributed Ixodidae genera (Boophilus spp. and Hyalomma spp.) by immersion method on mature ticks, four concentrations (23.2, 17.4, 11.6 and 5.8 mg/dl), in addition to the control treatment (0 mg/dl) of the seed were used to evaluate the engorged females in vitro. The results showed that 100% of absolute cumulative mortality of Boophilus spp., was gain after 72 hr by 23.2 mg/dl extract concentration, followed by 17.4 mg/dl which gave 90% mortality, whereas 100% absolute cumulative mortality for Hyalomma spp., was obtained by 23.2 mg/dl extract concentration after 48 hr, followed by 17.4, 11.6 and 5.8 mg/dl concentration that gave 90%, 80% and 40% mortality after 72 hr.

***Index Terms*—Boophilus spp., Hyalomma spp., Sorghum bicolor seed extract**

ARO-The Scientific Journal of Koya University
Volume IV, No 2(2016), Article ID: ARO.10065, 04 pages
DOI: 10.14500/aro.10065
Received 14 December 2014; Accepted 23 April 2015
Regular research paper: Published 09 September 2016
Corresponding author's e-mail: bahzad.mustafa@univsul.edu.iq

I. Introduction

Ixodidae causes damage directly due to herd irritability, blood spoliation, hide and udder injuries and inoculation of toxins, and indirectly by transmission of *Babesia* spp., and *Anaplasma marginale* especially in cattle and other ruminants (FAO, 2004).

Pesticidal plants have great potential for impact in developing countries (Isman, 2008), but a scientific under-standing of their activity provides opportunities to optimize their use (Stevenson, et al., 2009). Acaricides are needed to control tick infestations and tick-borne diseases. However, the uses of acaricides are constrained by their high costs, tick resistance, concerns about residues in food and in the environment (Mekonnen, 1996). The use of acaricides has disadvantages, such as the selection of resistant tick populations and harmful effects on the animals, human beings and the environment (Garcia-Garcia, et al., 2000) and more toxic and harmful to arthropods than to warm-blooded vertebrates (Okello, et al., 2003). Natural products offer world's resource-poor farmers a cheaper alternative to synthetic acaricides. There is a great potential for the use of Africa's, Asia and South America tropical and subtropical region plants to develop sources of acaricides to reduce the cost of tick control. These plants, being locally available and potentially easy to be produced, locally processed and used by farmers themselves or by cottage industries are an asset for the use of these plants and their extracts by traditional farmers in poor regions of the world. Tick control in the habitat and vegetation requires modification of the plant cover by removal of vegetation that shelters ticks (Baars, 1999). Various stages of some ticks, e.g. *Boophilus* spp. attach themselves to the blades of grass and other vegetation and stealthily attach to the cattle passing nearby. Though clearance of vegetation will annihilate their places of shelter, this type of action, however, may encourage soil erosion and may be detrimental to the ecosystem (Muhammad, et al., 2008). Farmers also used alternative

methods as an herbicidal such as used engine oil (12%), Jeyes fluid (household disinfectant 24%) (Mbati, et al., 2002).

Abdel-Shafy and Zayed (2002) examined the acaricidal effect of plant extract of Neem seed oil (Azadirachta indica) on egg, immature and adult stages of *Hyalomma* spp. and concluded that Neem can be used for tick control at economic concentrations of 1.6% to 3.2%. So, although herbal medicine research in veterinary parasitology is a recent area in most country, it has shown the potential to become a future tool to reduce the problems faced by animal breeders, such as resistance and residues, also prolonging the useful life of commercial chemical products applied for parasite control through the association of bioactive plant substances with synthetic products (Chagas, 2008). Sheep, cattle and goats are very common in Iraq especially in rich areas with green pastures (Hasson, 2012).

II. Materials and Methods

A. Sample of Sorghum (Sorghum bicolor) and Preparation of Extract.

Sorghum Bicolor (seed)

Two hundred grams of *sorghum bicolor* seed (natural product available in Sulaimani market) were cut in to small pieces and crushed using mixer blinder, and then immediately extracted with 300 ml of distilled water for 24 hr and filtrated. The aqueous extracts were serially diluted to $^1/_2$, $^1/_3$ and $^1/_4$ of original solution with distilled water (Sheldrick, 1984), an experimental was carried out in the photochemistry laboratory, Faculty of Agricultural Sciences, University of Sulaimani.

Tick Collection and Identification

Engorged female of ixodidae were collected manually (using cotton and alcohol 70%) from different flocks of cattle, sheep and goat, They were placed individually into clean universal glass vials and kept in room temperature to counted and identified by morphological features according to (Hoogstraal, 1956; Walker, et al., 2003).

B. Laboratory Experiments

Study of the effects of *S. bicolor* extract seed on the activity of hard tick; using four concentration of the extract used for the study, whereas; 23.2 (100%), 17.4 (75%), 11.6 (50%) and 5.8 (25%) was exposed to hard tick (using 10 ml of each concentration of this extract in Petri dish and put the distilled water on one Petri dish as a control (0% concentration) with number of hard tick), The number of engorged female found dead in each plate was recorded and monitored at certain interval of time; 30 min, 1 hr, 2 hr, 4 hr, 6 hr, 12 hr, 24 hr, 48 hr and 72 hr, and the results were summarized.

C. The Statistical Analysis

After collecting the raw data, Statistical tests were performed according to chi-square test as a goodness of fit for the different species of Ixodidae between the studied animals namely; cattle, sheep and goats, and the mean of mortality and cumulative mortality and confidence interval 95% for mortality by the two species (*Boophilus* and *Hyalomma* spp.) were compared, using simple t-test between the two means (steel, et al., 1997).

III. Results

In this study, the overall hard tick 973 collected from 300 hundred isolated in infested animals (one hundred in each; cattle, sheep and goats), as the following, 591 hard tick in cattle, 277 in sheep and 105 in goats.

Table I identifies four genera of Ixodidae; *Boophilus* spp., *Hyalomma* spp., *Rhipicephalus* and *Heamophalus* spp., according to the X^2 (chi- square) test for equally distribution of these species among different studied animals, the results shows highly significant ($P < 0.01$) values of chi-square and they were not equally distribution. The highly distribution of *Boophulis* spp., observed in cattle 334 (56.51%) and in goat 47 (44.76), in sheep the highly distributed showed in *Hyalomma* spp., 138 (49.82%) and *Rhipicephilus* spp., 78 (28.16 %), whilst shows the lowest number of *Haemophasylas* spp. collected in cattle and sheep 17 (2.88), 8 (2.89) respectively.

TABLE I
DISTRIBUTION OF IXODIDAE SPECIES IN CATTLE, SHEEP AND GOAT IN DIFFERENT FLOCKS IN SULAIMANI GOVERNORATE

Animal	*Boophilus* spp. %	*Hyalomma* spp %	*Rhipicephalus* Spp %	*Haemophasylas* spp. %	Total
Cattle	334 (56.51)	174 (29,44)	66 (11.17)	17 (2.88)	591
Sheep	53 (19.13)	138 (49.82)	78 (28.16)	8 (2.89)	277
Goats	47 (44.76)	27 (25.71)	24 (22.86)	7 (6.67)	105

$\chi^2_{Cal.} = 36.61^{**}$

** χ^2_{Cal} *is highly significant at the 0.01 level (2-tailed),* $\chi^2_{0.01}(6) = 16.81$

Data in Table II shows the cumulative mortality % of the *Boophilus* spp., affected by different concentration of *Sorghum bicolor* seed extracts during 72 hr as shown the highest mortality caused by the crude extract which considered as 100% concentrated, while the lowest concentration 5.8 mg/dl or 25% concentration. The crude extract started after 2 hr but the lowest concentrate 25% stared after 48hr only the absolute cumulative mortality 100% shown by the crude extract after 72 hr followed by 90% mortality gained by the 2nd concentration while the 3rd and 4th concentration the mortality declined to 65% and 15% respectively. Increasing the concentration of the extract shows increasing in mortality as an average of the studied time the maximum value was 37.22% gained by the crude extract and the lowest mortality was 2.22% as an average of the fourth concentration. Overall the time the highest confidence intervals ($P = 0.95$) obtained by the crude extract lies between 11.64 - 62.80% followed by the 2nd concentration which was 5.77-56.45%, whilst the 3rd and 4th concentration shows lower levels of confidence intervals under 50%, which consider to be not effective.

Cumulative mortality % of the *Hyalomma* spp., affected by different concentration of *Sorghum bicolor* seed extracts during 48hrs as shown the highest mortality caused by the crude extract which considered as 100% concentrated, while the lowest concentration 5.8 mg/dl or 25% concentration. The crude extract started after 1hr but the lowest concentrate 25% and 50% stared after 2 hr. the absolute cumulative mortality 100% shown by the crude extract 23.2 mg/dl after 48 hr followed by 2nd concentration 90% and the 3rd 80% after 72 hr whilst the 4th concentration the mortality declined to 40% after the same time. Increasing the concentration of the extract shows increasing in mortality as an average of the studied time the maximum value was 48.33% gained by the crude extract and the lowest mortality was 11.66% as an average of the fourth concentration.

TABLE II
EFFECT OF DIFFERENT CONCENTRATION OF *SORGHUM BICOLOR* EXTRACT ON THE MORTALITY PERCENTAGE OF *BOOPHILUS* SPECIES THROUGH 72 HR.

Extract conc. (mg/dl)	Cumulative Mortality/Time (%)									$\overline{X}$	C.I (95%)
	1/2 hr	1 hr	2 hr	4 hr	6 hr	12 hr	24 hr	48 hr	72 hr		
Distilled water (Control)	0	0	0	0	0	0	0	0	0	0	0
23.2	0	5	10	20	30	45	55	70	100	37.22	11.64 – 62.80
17.4	0	0	5	10	20	30	55	70	90	31.11	5.77 – 56.45
11.6	0	0	5	5	20	25	45	55	65	24.44	5.33 – 43.56
5.8	0	0	0	0	0	0	0	5	15	2.22	0.00 – 6.11
$\overline{X} = 23.75$											

Overall the time the highest confidence intervals ($P = 0.95$) obtained by the crude extract lies between 18.83 – 77.84 % followed by the 2nd concentration which was 12.55 – 64.12%, whilst the 3rd and 4th concentration shows lower levels of confidence intervals under 50%, which consider to be not effective, this result shown in Table III.

TABLE III
EFFECT OF DIFFERENT CONCENTRATION OF SORGHUM BICOLOR EXTRACT ON THE MORTALITY PERCENTAGE OF *HYALOMMA* SPECIES THROUGH 72 HR.

Extract conc. (mg/dl)	Cumulative Mortality/Time (%)									$\overline{X}$	C.I (95%)
	1/2 hr	1 hr	2 hr	4 hr	6 hr	12 hr	24 hr	48 hr	72 hr		
Distilled water (Control)	0	0	0	0	0	0	0	0	0	0	0
23.2	0	5	15	30	50	60	75	100	---	48.33	18.83 – 77.84
17.4	0	5	10	20	35	45	60	70	100	38.33	12.55 – 64.12
11.6	0	0	5	10	20	30	40	55	80	26.66	5.58 – 47.75
5.8	0	0	5	5	5	10	15	25	40	11.66	1.52 – 21.81
$\overline{X} = 31.25$											

IV. DISCUSSION

Research involving using *sorghum bicolor* seed extract for control hard tick (Ixodidae) *Hyalomma* and *Boophilus* spp., on cattle, sheep and goats flocks in Sulaimani governorate. In vitro tests conducted with *S. bicolar* at 23.2 mg/dl (100%), 17.4 mg/dl (75%), 11.6 mg/dl (50%) and 5.8 mg/dl (25%); showed the highest cumulative mortality after 72 hr in 50% and 100% concentration on *Boophilus* spp., engorged female, In Iraq, this results agreement with Mustafa and Faraj (2013), which observed that the genera *Boophilus* spp., there were highly significant differences between other tick species when collected and calculated by Less Significant Differences test (LSD) in Kurdistan region/Iraq. Several in vitro studies have proven the potential use of medical herbs and their essential oils and isolated substance for control of the tick *Boophilus* spp. Essential oils are complex mixtures containing many tens or even hundreds of substance with varied chemical composition (ISO, 1997). Silva, et al. (2007) obtained extracted product (EP) of 42% on engorged R (*Boophilus*) microplus females of the Alcohol extract of cymbopogon citrates of 100% concentration. Olivo, et al. (2008) observed efficiency of 85% on engorged *Boophilus microplus* females of C. nordus essential oil at 10%. Farias, et al. (2007) obtained 100% efficacy in controlling *R* (*Boophilus*) *microplus* using seed oil of *C. guianesis* at concentration ranging from 10% to 100% and had 100% efficacy against engorged femals of *R. sanguine* and *Amblyomma nitens* (Farias, et al., 2009). Nahar, et al. (2005) revealed that Ata (*Annona retirulata*) and bishkatali (*polygonum hydropiper*) have great acaricidal value against *Boophilus microplus*. Described the *Hyalomma* spp., the widespread species presence between awassi sheep in Iraq and transmitted malignant ovine theileriosis, may be because Awassi sheep move between region to another; losses may be higher in important sheep (brown, et al., 1990). Razmi *et al*. (2003) demonstrated the *Rhipicephalus* spp. and *Hyalomma* spp., were the most common species in sheep and goats in Iran. While Nasiri, et al. (2010) identified two genera and five species of *Hyalomma* and *Haemaphysalis* in mountainous region in Iran. The cumulative mortality of *Hyalomma* spp., as a highest in 100% after 48 hr and 50% after 72 hr, and the sensitivity of *Hyalomma* spp., was more than *Boophilus* spp., may be due to *Hyalomma anatolicum* as a three host tick it may feed as larva or nymphs on gerbils, then on cattle or sheep as adults (Walker, et al., 2003), and attack mutable host for short time for feeding and have not time to expose to the acaricide and this leads to preserved to resistance and remaining for long time to survival, this behavior contrast with *Boophilus* spp., because remains continuously on the host from the moment of access as an unfed larva until its departure as an engorged female. This type of life-cycle is characteristic of *Boophilus* spp. (Minjauw and Mc Leod, 2003), and therefore more exposed to acaricide, according to the t-test, the high mortality % of *Hyalomma* spp., was 31.25% compared to the lower mortality % of *Boophilus* spp., was 23.75%, but their difference was not significant. Godara, et al. (2015) revealed that ethanolic extract obtained from the aerial parts of *Artemisia absinthium* has acaricidal properties and could be useful in controlling, adults, eggs and larvae of *Hyalomma anatolicum*.

V. Conclusions

Sorghum bicolor seed extract more significant (more toxic) effect (100% mortality) after 48 hr with *Hyalomma* spp., while shows the same concentration (23.2 mg/dl) a significant effect on *Boophilus* spp., after 72 hr to killed hard tick (ixodidae). Therefore, using of some plants extract which effected on the ixodidae, especially extract of *sorghum bicolor* seed have many advantages over synthetic chemical, loss toxicity of mammalian and environmental pollution, being less expensive and easily available for control hard tick (Ixodidae).

References

Abdel Shafy, S. and Zayed, A.A., 2002. In vitro acaricidal effect of plant extract of neem seed oil (Azadirachta indica) on egg, immature and adult stages of Hyalomma anatolicum excavatum (Ixodidea: Ixodidae). *Vet. Parasitol*, 106(1), pp.89-96.

Baars, R.M.T., 1999. The effect of rangeland fires on cattle tick infestation in western Zambia. Trop. *Anim. Health. Prod*., 31(5), pp.275-278.

Brown, C.G.D., Hunter, A.G. and Luckins, A.G., 1990. Diseases caused by protozoa, In: Sewell, M.M. H. and Brocklessly, D.W.(eds). Handbook of Animal Diseases in the Tropics. 4th Ed, (University Press Cambridge, U.K.).

Chagas, A.C.S., 2008. Metodologias in vitro para avaliaçao de fitoterapicos sobre parasitas e resultados de testes a campo. In: Congresso Brasileiro de Parasitologia Veterinaria, 2008, Curitiba. Anais do Congresso Brasileiro de Parasitologia Veterinaria. Curitiba: CBPV, 15, p.13.

FAO (Food and Agriculture Organization of the United Nations), 2004. Module 1. Ticks: acaricide resistance: diagnosis management and prevention. In: Guidelines Resistance Management and Integrated Parasite Control in Ruminants. FAO Animal Production and Health Division, Rome.

Farias, M.P.O., Sousa, D.P., Arruda, A.C., Arruda, M,S,P., Wanderley, A.G., Alves, L.C. and Faustino, M.A.G., 2007. In vitro effectiveness of the oil of the Carapa guianensis Aubl. (andiroba) in the control of Boophilus microplus (Acari: Ixodidae). *Rev. Bras. Plantas. Med. Botucat*., 9(4), pp.68–71.

Farias, M.P.O., Sousa, D.P., Arruda, A.C., Wanderley, A.G., Teixeira, W.C., Alves, L.C. and Faustino, M.A.G., 2009. Potencial acaricida do oleo de andiroba Carapa guianensis Aubl. sobre femeas adultas ingurgitadas de Anocentor nitens Neumann, 1987 e Rhipicephalus sanguineus Latreille, 1806. *Arq. Bras. Med. Vet. Zootec*., 61, pp.877–882.

Garcia-Garcia, J.C., Montero, C., Redondo, M., Vargas, M., Canals, M., Bone, O., Rodriquez, M., Joglar, M., Machado, H., Gonzalez, I.L., Valdes, M., Mendez, L. and de la Fuente, J.. 2000. Control of ticks resistant to immunization with Bm86 in cattle vaccinated with the recombinant antigen Bm95 isolated from the cattle tick. *Boophilus microplus. Vaccine*., 18(21), pp.2275-2287.

Godara, R., Parveen, S., Katoch, R., Yadav, A., Katoch, M., Khajuria, J.K., Kaur, D., Ganai, A., Verma, P.K., Khajuria, V. and Singh, N.K., 2015. Acaricidal activity of ethanolic extract of Artemisia absinthium against Hyalomma anatolicum ticks. *Exp. Appl. Acarol*., 65(1), pp.141-148.

Hasson, R.H., 2012. Tick distribution and infestation among sheep and cattle in Baghdad's south suburb. *Kufa J. Vet. Med. Scie*., 3(1), pp.77-90.

Hoogstraal, H., 1956. African Ixodidae. 1. Ticks of the Sudan. U.S. Naval Medical Research Unit No3. Cairo, Egypt.

Isman, M.B., 2008. Perspective Botanical Insecticides: for richer for poorer, *Pest Management Science*, 64, pp.8–11.

ISO - International organization for standardization 1997. Aromatic natural raw materials - Vocabulary: ISO 9235. Genebra, p.8.

Mbati, P.A., Hlatshwayo, M., Mtshali, M.S., Mogaswane, K.R., de Waal, T.D. and Dipeolu, O.O., 2002. Ticks and tick-borne diseases of livestock belonging to resource-poor farmers in the eastern Free State of South Africa. *Exp Appl Acarol*, 28(1-4), pp.217-224.

Mekonnen, S., 1996. Epidemiology of ticks and tick-borne diseases in Ethiopia: Future research needs and priorities. In: ILRI, *The International Livestock Research Institute*. Nairobi, Kenya, 12-13 March 1996, pp.17-29.

Minjauw, B. and Mc Leod, A., 2003. Tick-borne disease and poverty. The impact of ticks and tick-borne disease on livelihood of small –scale and marginal livestock owners in India and eastern and southern Africa. Research report, DFID Animal Health Programme. Edinburg: Center for Tropical Veterinary Medicine, University of Edinburgh, UK, pp.1-116.

Muhammed, G., Naureen, A., Firyal, S. and Saqib, M., 2008. Tick control strategies in dairy production medicine. *Pak. Vet. J.*, 28(1), pp.43-50.

Mustafa1, B.H.S. and Faraj, S.H., 2013. Resistance of Hard Tick (Ixodidae) with some Acaricide in Cattle (Naturally Infestation) in Sulaimani Governorate Fields-Kurdistan Regional/Iraq. *J. Agri. Sci. Techno*., A3, pp.927-934.

Nahar, L., Anisuzzaman., Alim, M.A., Karim, M.J., Islam, K.I. and Mondal, M.M.H., 2005. In vitro acaricidal effects of some indigenous plants against Boophilus microplus (Aracnida: Ixodidae). *Bangladesh.J.Vet.Med*., 3(2), pp.118-123.

Nasiri, A., Telmadarraiy, Z., Vatandoost, H., Chinikar, S., Moradi, M., Oshaghi, M.A., Salim abadi, Y. and Sheikh, Z., 2010. Tick Infestation Rate of Sheep and Their Distribut ion in Abdanan County, Ilam Province, Iran, 2007-2008. *Iranian. J. Arthropod-Borne. Dis*., 4(2), pp.56-60.

Okello. O.J., Tukahiriwa, E.M., Perry, D.B., Rowlands, G.J., Nagda, S.N., Musisi, G., Bode, E., Heinonen, R., Mwayi, W. and Opuda, A.J., 2003. The impact of tick control on the productivity of indigenous cattle under ranch condition in Uganda. *Trop. Anim. Health. Prod.*, 35(3), pp.237-247.

Olivo, C.J.l; Carvalho, N.M.; Da Silva, J.H.S.; Vogel, F.F.; Massariol, P.; Meinerz ,G.; Agnolin, C.; Morel, A.F. and Viau, L.V. (2008). Oleo de citronela no controle do carrapato de bovinos, *Cienc Rural*. 38, pp.406–410.

Razmi, G.R.; Naghibi, A.; Aslani, M.R.; Dast jerdi, K. and Hossieni, N. 2003. An epidemiological study On Babesia infection in small ruminants in Mashhad suburb, Khorasan province, Iran. *Small Ruminant Res*., 50(1), pp.39-44.

Silva, W.W., Athayde, A.C.R., Rodrigues, O.G., Araujo, G.M.B., Santos, V.D., Neto, A.B.S., Coelho, M.C.O.C. and Marinho, M.L., 2007. Effects of neem (Azadirachta indica A.Juss) and lemongrass [Cymbopogoncitratus(DC)Stapf]Boophilusmicroplus and Rhipicephalus sanguineus (Acari: Ixodidae) in the semiarid region of Paraiba State, Brazil. *Rev. Bras. Plant. Med. Botucatu*, 9(3), pp.1–5.

Sheldrick, B.H., 1984. Analytical methods manual. Land Resource research in states Ottawa, Ontario, LRRI contribution, pp.30-84.

Steel, R.G.D., Torrie, J.H., and Dickey, D.A., 1997. *Principles and procedures of statistics: A biometrical approach*. 3rd ed. Hill book Co. Inc. New York, pp.400-428.

Stevenson, P. C., Dyarathna, T. K., Belmain, S. R. and Veitch, N. C., 2009. Bisdemosidic saponins Securidace longepeduncu Lata Coleaptere (Polygalaceae) with deterrent and toxic properties to storge pests, *J. Agricul. F. Chemistry*., 57, pp.8860-886.

Walker, A.R., Bouattour, A., Camicas, J.L., Estrada-Pena, A., Horak, I.G., Latif, A., Pegram, R.G. and Preston, P.M., 2003. Ticks of domestic animals in Africa, A guide to identification of species. Bioscience. Reports. U.K, pp.86-214.

Absorption Parameters for Glucose Solution for Gamma Ray at 59.54 keV

Maan S. Al-Arif[1] and Diyaree O. Kakil[2]

[1]School of Medicine, Koya University
Daniel Mitterrand Boulevard, Koya KOY45, Kurdistan Region – F.R. Iraq

[2]Department of Physics, Faculty of Science and Health, Koya University
Daniel Mitterrand Boulevard, Koya KOY45, Kurdistan Region – F.R. Iraq

***Abstract*—Photon absorption parameters for glucose solution at different concentrations such as linear attenuation coefficient, mass attenuation coefficient, effective atomic number, electron density and density determined at 59.54 keV photon energy. The mass attenuation coefficient is calculated using the mixture rule and a correction factor to approximate the experimental model is added. Accordingly, the effective atomic number and electronic density appears to decrease with increasing glucose concentration. Moreover, the measured linear attenuation coefficient and the density for the solution are linearly increased with concentration. We can conclude that the electrical conductivity of the solution depends on the physical nature of the electrical charge carrier in the solution, concentration of the solute material, and the electronic density of the solution at the same time.**

***Index Words*—Atomic number, attenuation coefficient, density, photon absorption.**

I. Introduction

Solution density is often used as a point of identification in the determination of an unknown substance. When a substance is dissolved in pure water, the density of the solution will be different from that of the water itself. The determination of the density of certain physiological liquids is often an important screening tool in medical diagnosis. The method used in density determination depends on the type of sample and on the level of precision desired (Zamyatin, and Burkov, 2012; Terwilliger, 2002). The general method to determine the density involves measurement of the mass and the volume of the sample using different techniques. On the other hand, with the extensive use of gamma-active isotopes in medicine, industry and agriculture, the study of absorption of gamma rays in the composite materials has become an interesting and exciting field of research. The photon attenuation coefficient, effective atomic number, electron density are basic quantities required in determining the absorption of x-rays and gamma photons in matter. The knowledge of the absorption parameters such as mass attenuation coefficient (μ/ρ), linear attenuation coefficient (μ), total atomic cross-section (σ_a), electronic cross-section (σ_e), effective atomic number (Z_{eff}), and electron density (N_{eff}) play an important role in understanding the physical properties of composite materials. They are invaluable in many applied fields, such as nuclear diagnostics, radiation protection, and radiation dosimetry.

Some material when dissolve in solution has certain dosimetric properties after exposed to photon radiation (Soppe, 1993; Marzouguia, et al., 2008; Hamzaoui, et al., 2009). The effective atomic number of such solution becomes of high importance especially at low photon energies where the energy dependency increases.

Since the solution density is varied with solute concentration, the present work aims to determine the density of glucose in distilled water by measuring the photon attenuation coefficient. This technique tends to establish the relationship between glucose concentration and the density. Moreover, the effective atomic number, electronic density of the solution calculated using the measured density and linear attenuation coefficient. The linear attenuation coefficient for some chemical solutions have been studied which shows a linear relationships with concentration (Mitkar, and Dongarge, 2012a; Mitkar, and Dongarge, 2012b; Baldha, et al., 1997). Similar method will be used to establish the relationship between concentration of the solution and density, effective atomic number, and electronic density.

II. Theoretical Background

The intensity of gamma radiation after traversing the thickness, x, of chemical solution is given by:

$$I = I_0 e^{-\mu x} \quad (1)$$

μ represent the linear attenuation coefficient. The intensity of radiation can also be written in terms of the mass attenuation coefficient such as:

$$I = I_0 e^{-(\mu/\rho)x\rho} \quad (2)$$

ARO-The Scientific Journal of Koya University
Volume IV, No 2(2016), Article ID: ARO.10103, 04 pages
DOI: 10.14500/aro.10103
Received 09 June 2016; Accepted 08 August 2016
Regular research paper: Published 09 September 2016
Corresponding author's e-mail: maan.safa@koyauniversity.org

(μ/ρ) is the mass attenuation coefficient, and *ρ* is the density of the material. The total mass attenuation coefficient *(μ/ρ)* for chemical mixture at any reference photon energy is related to the *(μ/ρ)* of the constituent elements in the mixture (Baldha et al., 1997; Teli, and Chaudhari, 1995; Chaudhari, and Teli, 1996; Teli, and Chaudhari, 1996; Wang, et al., 1995; Singh et al., 2002) and is given by:

$$(\frac{\mu}{\rho})_{solution} = \sum_i w_i \, (\frac{\mu}{\rho})_i \quad (3)$$

Where, w_i, is the mass fraction of component *i*, $(\frac{\mu}{\rho})_i$ is the mass absorption coefficient of component *i*, and the summation is over all components of the mixture.

The density of the solution can then be determined as;

$$\rho_{solution} = \frac{\mu_{solution}}{\sum w_i(\mu/\rho)_i} \quad (4)$$

Where, $\mu_{solution}$, represent the experimental linear attenuation coefficient, and $\sum_i w_i(\frac{\mu}{\rho})_i$ is the calculated solution mass attenuation coefficient.

The mass attenuation coefficient values of the materials have been calculated using the WinXCom program (Gerward, et al., 2004). This well-known and widely used program provides the total mass attenuation coefficient and total attenuation cross-section data for approximately 100 elements, as well as the partial cross-sections for incoherent and coherent scattering, photoelectric absorption and pair production at energies from 1 keV to 100 GeV. For materials composed of multiple elements, the fraction by weight is given by:

$$w_i = \frac{n_i A_i}{\sum_i n_i A_i} \quad (5)$$

A_i represents the atomic weight of the *i-th* element and n_i is the number of formula units. The total atomic cross-sections σ_a for the sample can be obtained from the value of (μ/ρ) using the following relation (Baltej, et al., 2012):

$$\sigma_a = \frac{1}{N_A}\left[\frac{(\mu/\rho)_{compound}}{\sum_i \frac{w_i}{A_i}}\right] \quad (6)$$

N_A represents the Avogadro's number. The total electric cross section (σ_e) is given by the following formula [Nil et al., 2013]:

$$\sigma_e = \frac{1}{N_A}\left[\sum_i \left(\frac{f_i A_i}{Z_i}\right)(\mu/\rho)_i\right] \quad (7)$$

Where f_i is the number fraction of the atoms of element (*i*) relative to the total number of the atoms of all elements in the mixture, and Z_i is the atomic number of the *i-th* elements in the mixture. σ_a and σ_e are related to the Z_{eff} of the material through the following expression (Baltej, et al., 2012; Nil et, al., 2013):

$$Z_{eff} = \sigma_a/\sigma_e \quad (8)$$

The N_{eff} (number of electrons per unit mass) can be written as following:

$$N_{eff} = \left(\frac{N_A}{A_i}\right)(Z_{eff})\sum_i n_i = \frac{(\frac{\mu}{\rho})s}{\sigma_e} \quad (9)$$

III. Materials and Method

The extent of gamma ray penetration depends upon several factors including energy of radiation and nature of intervening material. Since $70\ ml$ of distilled water is used in the present work, the energy of the gamma source is selected so that significant intensity attenuation should occur throughout the sample. Therefore, ^{241}Am gamma source with energy of 59.54 keV and activity of $0.34\ MBq$ is selected to be use in the present work. The ^{241}Am source has low penetration power which reduces the amount of shield needed. The ^{241}Am source have a linear attenuation coefficient of about $0.206\ cm^{-1}$, and a half value thickness of about $3.25\ cm$ in distilled water. The alpha particle emitted with gamma ray from the ^{241}Am source is easily absorbed by $1.0\ mm$ thick piece of paper placed in the direction of the beam.

The experimental arrangement for measuring the attenuation coefficient of glucose solution is shown in Fig. 1. The Attenuation coefficient measurement is performed using NaI (TI) scintillation detector connected to a multi-channel analyzer (MCA) with an energy resolution of 7.5% at 662 keV.

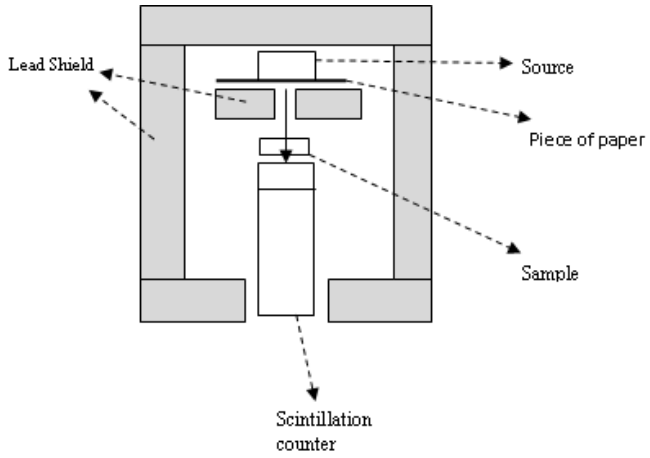

Fig. 1. Arrangement for measuring the attenuation coefficient.

The volume of liquid in the polyethylene container, with an inner diameter of $4.5\ cm$, increases from $10\ ml$ to $60\ ml$ in $10\ ml$ steps, and the fraction of the intensity transmitted are recorded. The temperature of the solution is kept at $20°C$ throughout the measurements. The actual height of the solution in the container is calculated by dividing the volume by the inner cross-sectional area. The transmission ratio for each solution height is recorded and used to calculate the linear attenuation coefficient according to (1).

The absorption coefficient for gamma rays is available for mixture of solid materials and solutions using various calculation techniques (Mitkar, and Dongarge, 2012a; Mitkar, and Dongarge, 2012b; Baldha, et al., 1997; Baltej, et al., 2012; Nil, et al., 2013; Singh, 2000). Most of them claim a good agreement with the well known mixture rule.

In the present work, the mixture rule is also used to calculate the mass attenuation coefficients for the solution at different glucose concentrations. In practice radiation suffers from

attenuation in passing through the solution, the base of the polyethylene container, and the aluminum layer covering the crystal of the scintillation detector. Since calculation based on mixture rule consider only the attenuation by the solution, therefore the attenuation of the $1\,mm$ thickness of the polyethylene base, and the attenuation of the 0.4 mm aluminum layer covering the crystal must be added to the calculation. The linear attenuation coefficient for aluminum layer is $0.7506\ cm^{-1}$ which attenuates the radiation beam intensity by 3%, and the attenuation coefficient for the polyethylene layer is $0.18518\ cm^{-1}$ which attenuates the radiation beam by 1.85%, at 60 keV (Hubbell, and Seltzer, 1995; NIST, 1996). Density of the solution at different glucose concentrations are then calculated according to (4).

Different concentrations of glucose solution expressed in terms of percent composition by mass (*% w/w*) are prepared and used in this work. The percent composition by mass is the mass of the solute divided by total mass of the solution (mass of solute plus mass of solvent), multiplied by 100. Table I shows the amount of glucose dissolved in distilled water corresponding to each arbitrary chosen concentration used in this investigation.

TABLE I
THE AMOUNT OF GLUCOSE DISSOLVED IN 70 ML OF DISTILLED WATER

glucose mass (g)	*% w/w*
4.66	6.66
6.99	9.09
13.99	16.66
17.50	20.00
27.99	28.57
34.94	33.30
48.98	41.17
70.0	50.00
105.0	60.00

IV. RESULTS AND DISCUSSION

The measured linear attenuation coefficient, the calculated mass attenuation coefficient (before and after correction) according to (3) is shown in Table II.

Solution density is gradually increases from $1.0\ g/cm^3$ at 0 % (*w/w*) concentration to a value of $1.393\ g/cm^3$ at 60 % (w/w) concentration.

The solution densities corresponding to each glucose concentration as a function of glucose concentration is shown in Fig. 2.

The variation of the effective atomic number and the effective electron density with glucose concentrations are shown in Fig. 3 and Fig. 4.

The effective atomic number and the effective electronic density of the solution decrease linearly and smoothly with increasing glucose.

TABLE II
EXPERIMENTAL AND CALCULATED ATTENUATION COEFFICIENTS AS A FUNCTION OF SOLUTION CONCENTRATION

Concentration (% w/w)	(μ) (cm^{-1})	(μ/ρ) Before Correction (cm^2/g)	(μ/ρ) After Correction (cm^2/g)
0	0.228	0.2057	0.2161
6.66	0.231	0.2048	0.2152
9.09	0.242	0.2045	0.2147
16.66	0.254	0.2036	0.2137
20	0.257	0.2032	0.2133
28.57	0.260	0.2021	0.2116
33.3	0.262	0.2015	0.2115
41.17	0.270	0.2006	0.2106
50	0.276	0.1995	0.2094
60	0.290	0.1982	0.2081

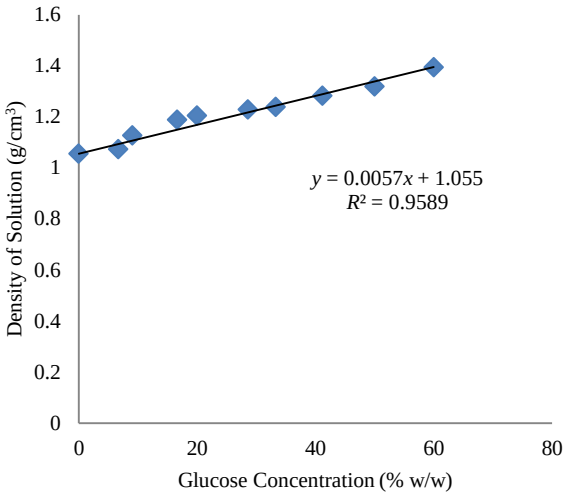

Fig. 2. Variation of the solution density with glucose concentration

V. CONCLUSION

A smooth linear relationship between concentration and density for the solution is obtained by means of measuring the linear photon attenuation coefficient. The density of the solution increases as the concentration increases.

The effective atomic number of the solution decreases with increasing the concentration. This indicates that as concentration increases, the solution physical property becomes approximately a tissue equivalent solution.

The electronic density for the solution decreases with increasing concentration. This trend of sugar solution agrees with some researchers (Marzouguia, et al., 2008). They found that higher electrical conductivity for sucrose solutions occur at concentration of $20\%\,(w/w)$ and tend to decrease with increasing concentration. Other researchers (Riyadh, and Abul-Hail, 2011) found that the electrical conductivity for sodium chloride solution increase with increasing concentration and was attributed to the ionic nature of the electrical charge carrier in the solution and not to the

electronic density. We suggested that the electrical conductivity of the solution depends on the physical nature, concentration of the solute material, and the electronic density of the solution. Moreover, higher value of the electronic density would indicate an increase in the probability of a photon-electron energy transfer and an energy deposition into the material. The present result indicates that the attenuation method is an excellent method to determine the unknown solution density, effective atomic number, and the electronic density. This method can be used with high accuracy in industry and research in cases where those photon absorption parameters are vital.

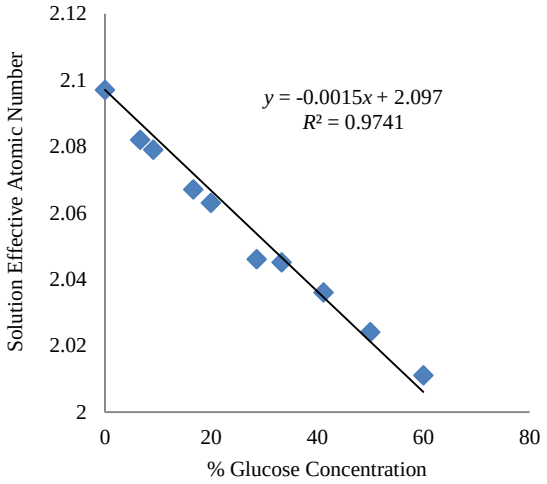

Fig. 3. Variation of the effective atomic number with glucose concentration.

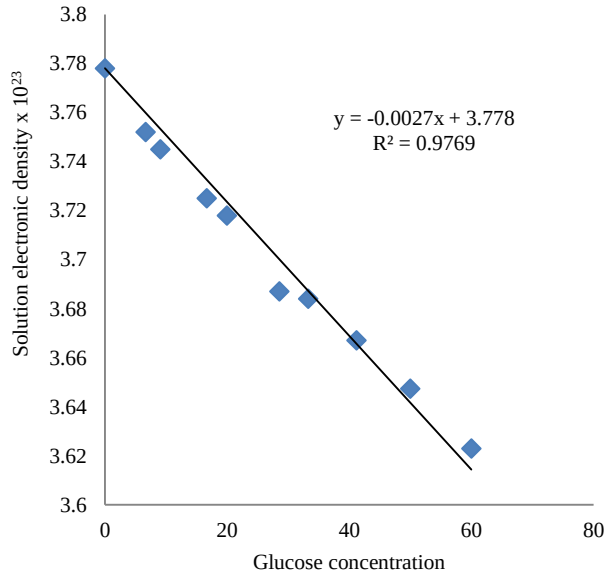

Fig. 4. Variation of the effective electronic density with glucose concentration.

REFERENCES

Zamyatin, I.V. Burkov, K.A., 2012. Determination of solutions density by the dilatometric titration method. *Russian Journal of General Chemistry*, 82(4), pp.639-642.

Terwilliger, T. C., 2002. Automated structure solution, density modification and model building. *Acta Cryst.* D58, 1937-1940, pp.3519-3540.

Soppe, W. J, 1993. Computer simulation of radiation damage in NaCl using a kinetic rate reaction model. *Journal of Physics: Condensed Matter*, 5 (22), pp.3519.

Marzouguia, K., Hamzaoui, A.H., Farah, K. and Ben Nessib, N., 2008. Electrical conductivity study of gamma-irradiated table sugar for high-dose dosimetry. *Radiation Measurements*, 43, pp. 1254–1257.

Hamzaoui, A.H., Farah, K., Marzougui, K., Horchani, S. , Ben Nessib, N. and M'Nif, A., 2009. PH-Metric study of gamma-irradiated table sugar for dosimetry purpose. *Radiation Measurements*, 44, pp.374–377.

Mitkar, S.R. and Dongarge, S.M., 2012a. Measurement of Linear and Mass Attenuation Coefficient of Alcohol Soluble Compound for Gamma Rays at Energy 0.511 MeV‖. *Archives of Applied Science Research*, 4(4), pp.1748-1752.

Mitkar, S.R. and Dongarge, S.M., 2012b. Study the Linear and Mass Attenuation Coefficient of Alcohol Soluble Compound for Gamma Rays at Energy 662 KeV. ***J***. *Chem. Pharm. Res.*, 4(8), pp.3944-3949.

Baldha, G.J., Raval, D.A., Subbarao, M.V., and Kulkarni, R. G., 1997. Attenuation Coefficient of Various Gamma Radiations by Solutions of Cobalt Sufate. *Applied Radiation and Isotopes*, 48(8), pp.1121–1124.

Teli, M.T.e and Chaudhari, L.M., 1995. "Attenuation Coefficient of 123 KeV Gamma-Radiation by Dilute- Solution of Ferrous Sulfate". *Indian Journal of Pure & Applied Physics*, 33(7), pp.395-397.

Chaudhari, L. M. and Teli, M.T., 1996. Linear Attenuation (or Absorption) Coefficient of Gamma Radiation For dilute-Solutions of Potassium-Chloride. *Applied radiation and isotopes, 47(3), pp. 365-367.*

Teli, M.T.e and Chaudhari, L.M., 1996. The Attenuation Coefficient of Ammonium-Chloride for 662 KeV Gamma-Radiation, Measured for Dilute – solutions‖. *Radiation physics and chemistry*, 47(4), pp. 531-534.

Wang, D.C., Ping, LA. and Yang, H., 1995. Measurement of the mass attenuation coefficients for SiH4 and Si. *Nucl Instrum Meth B*; 95, pp.161-165.

Singh, K., Singh, H. and Sharma, V et al., 2002. Gamma-ray attenuation coefficients in bismuth borate glasses. *Nucl Instrum Meth B;* 194, pp.1-6.

Gerward, L., Guilbert, N. and Jensen, KB et al., 2004. WinXCom–a program for calculating X-ray attenuation coefficients. *Radiat Phys Chem*, 71, pp.653-654.

Baltej, S.S. Dhaliwal, A.S. Mann, K.S. and Kahlon, K.S., 2012, Study of mass attenuation coefficients, effective atomic numbers and electron densities for some low *Z* compounds of dosimetry interest at 59.54 keV incident photon energy. *Annals of Nuclear Energy*, *(*42), pp.153–157.

Nil, K., Zeynal, T. and Merve, C., 2013. Determining photon energy absorption parameters for different soil Samples. *Journal of Radiation Research*, 54, pp.578–586.

Singh, G. K. Lark, B. S. and Sahota, H.S., 2000. Attenuation Measurements in Solutions of Some Carbohydrates‖. *Nuclear Science and Engineering*, 134 (2), pp.208-217.

Hubbell, J.H and Seltzer, S.M., 1995. Tables of X-Ray Mass Attenuation coefficients and Mass Energy Absorption Coefficients, 1 keV to 20 MeV for Elements Z=1 to 92 and 48 Additional Substances of Dosimetric Interest. *Radiation Physics Division, PML, NIST.*

The National Institute of Standards and Technology (NIST) is an agency of the U.S. Department of Commerce 1996. Available at: http://www.nist.gov/pml/data/xraycoef/index.cfm.

Riyadh, Ch. Abul-Hail, 2011. Electrical conductivity dosimetric characteristics of gamma-irradiated food salt. *Journal of Basrah Researches (Sciences)*, 37(4) A, pp.25-29.

Reconstruction the Missing Pixels for Landsat ETM+SLC-off Images Using Multiple Linear Regression Model

Asmaa S. Abdul Jabar[1,2], Ghazali B. Sulong[1], Loay E. George[3], Mohd Shafry[1] and Zinah S. Abduljabar[2]

[1]UTM-IRDA Digital Media Center (MaGIC – X), Faculty of Computing, Universiti Technologi Malaysia UTM Skudai, 81310 Johor, Malaysia

[2]Department of Computer, College of Science, University of Al-Mustansiriyah, Baghdad, F.R. - Iraq

[3]Department of Computer, College of Science, University of Baghdad, Baghdad, F.R. - Iraq

***Abstract*—On 31 May 2003, the scan line corrector (SLC) of the Landsat 7 Enhanced Thematic Mapper Plus (ETM+) sensor which compensates for the forward motion of the satellite in the imagery acquired failed permanently, resulting in loss of the ability to scan about 20% of the pixels in each Landsat 7 SLC-off image. This permanent failure has seriously hampered the scientific applications of ETM+ images. In this study, an innovative gap filling approach has been introduced to recover the missing pixels in the SLC-off images using multi-temporal ETM+ SLC-off auxiliary fill images. A correlation is established between the corresponding pixels in the target SLC-off image and two fill images in parallel using the multiple linear regressions (MLR) model. Simulated and actual SLC-off ETM+ images were used to assess the performance of the proposed method by comparing with multi-temporal data based methods, the LLHM method which is based on simple linear regression (SLR) model. The qualitative and quantitative evaluations indicate that the proposed method can recover the value of un-scanned pixels accurately, especially in heterogeneous landscape and even with more temporally distant fill images.**

***Index Terms*—ETM+SLC-off images, gap filling, multiple Linear Regression (MLR), simple linear regression (SLR).**

I. INTRODUCTION

Since the first launch of the Landsat satellite series in 1972, the Landsat program has provided the longest continuous multi-spectral data of the Earth's surface with excellent spatial resolution. The wealth of information that is provided from this observation has tremendously benefited and boosted scientists, researchers and common users in many fields such as soil mapping, agriculture, monitoring climate change, forestry, city planning, disaster response and relief, water management and other applications (Chen, Ye and Zhao, 2012; Zhu and Liu, 2014). In 1999, Landsat 7 with Enhanced Thematic Mapper Plus (ETM+), considered to be one of the most powerful satellites in Landsat program with the advancement of ETM+ over TM sensors, was launched. Consequently, it improved the spatial resolution of the thermal band 6 from 120 m to 60 m with the addition of a panchromatic band (band 8) of spatial resolution of 15m. Furthermore, the spatial resolution of the remaining multispectral bands (bands 1-5 and 7) is enhanced to 30 m. Notably, the ETM+ sensor visits every location on Earth every 16 days with a narrow field of view (15°) and swath of 185 km (Reza and Ali, 2008; Chen, et al., 2011).

The Scan Line Corrector (SLC) is an electromechanical instrument in the optical track of the ETM+ sensor on board of Landsat 7 which was exploited to compensate the forward motion of the satellite through the data gain (Markham, et al., 2004; Mohammdy, et al., 2014). Due to sudden and permanent collapse of this SLC instrument on May 31, 2003, nearly 20% of the pixels in an ETM+ image have not been scanned. These missing pixels caused the appearance of un-scanned locations (gaps) and severely hindered the use of these valuable data. Therefore, the individual image scans alternately overlapped instead of aligning in parallel scans thus creating such gaps ranging in width from a single pixel near the center of the scanned image to about 14 pixels toward the edges of the scene (Storey, et al., 2005; Wulder, et al., 2008).

Fortunately and despite the SLC failure, the radiometric and geometric qualities of the defective Landsat 7 images were not affected and about 80% of the pixels in the image were scanned in an appropriate manner without flaws (Chen, Tang

ARO-The Scientific Journal of Koya University
Volume IV, No 2(2016), Article ID: ARO.10147, 10 pages
DOI: 10.14500/aro.10147
Received 09 June 2016; Accepted 08 August 2016
Regular research paper: Published 09 September 2016
Corresponding author's e-mail: saasmaa2@live.utm.my

and Qiu, 2010). Since then, the ETM+ images acquired with the SLC failure are referred to as "Landsat 7 SLC-off images". In contrast, the images obtained prior to the SLC failure are referred as "Landsat SLC-on images". Several methods are proposed and developed for recovering the missing pixels in Landsat 7 SLC-off images. Generally, the gap filling algorithms which are found to be successful in such image recovery are classified into single source and multi-source approaches.

In a single source approach, typically the gapped areas are reconstructed using non-gapped areas in the defective image itself. Traditional interpolation approaches such as bilinear, bicubic and nearest-neighbor algorithms are used for filling the gap in Landsat 7 ETM+ SLC-off images. Despite their easy and simple implementation, the performance of these algorithms remains poor because of the occurrence of a clear boundary between the fill gaps locations and the target image. This is primarily produced due to the calculation of filled value from the pixels residing around the gap locations, and the information is not the reflection of land (Desai and Ganatra, 2012)

Zhang et al. proposed a geostatistical interpolation approach using ordinary kriging geostatistical technique to fill the data gaps in the Landsat 7 SLC-off images by considering the spatial structure of the anomalous ETM+ image itself in the interpolation process. The results indicate that this approach was appropriate for assessment of the mapping in large scale landscape areas but with inaccurate results in small scale applications (Zhang, Li and Travis, 2007).

Alternatively, in multi-source methods, auxiliary data derived from the images of the same place and over different time (multi-temporal images) are used to fill the gaps in Landsat 7 SLC-off images. The random occurrence of gaps through the multi-spectral bands in Landsat 7 images allows one to use both SLC-on and/or SLC-off image (multi-temporal) as auxiliary images to restore the gaps in target SLC-off image (Hu, et al., 2011).

Soon after the breakdown of the SLC, a study team from USGS/NASA (United States Geological Survey/National Aeronautics and Space Administration) developed and tested two phases of gap filling products. Both phases are based on utilizing a histogram based compositing technique by combining a SLC-off target image with one or more SLC-on and/or SLC-off fill images. In phase 1 product, a global histogram matching (GHM) and local linear histogram matching (LLHM) algorithms were used to locate a linear transformation between target SLC-off images and temporally SLC-on fill images. Although GHM method performs well over desert and rocky areas where the scenes consist of invariant terrain, in a LLHM algorithm a moving window is used for greater precision results than GHM method (Scaramuzza, Micijevic and Chander, 2004; He, et al., 2011). Also, in LLHM method all the valid neighboring pixels within a search window are taken into account, not the spectral similarity of these pixels and this reduces the accuracy of the estimated values which lead to difficulties with heterogeneous landscapes where the features are smaller than the local moving window size (Hossain, et al., 2015; Shen, et al., 2015).

Thereafter, in phase 2 product an adaptive window local histogram matching (AWLHM) algorithm was declared as an enhancement to LLHM method by using multiple auxiliary SLC-off images and with changeable size of moving window in recovering method (USGS & NASA., 2004; Rulloni, Bustos and Flesia, 2012). Generally, the result of AWLHM is more rational than LLHM especially in homogeneous landscape, but it has difficulty to obtaining suitable results when significant changes occur in areas smaller than the local moving window size within the scene (Jabar, Sulong and George, 2014). Generally, these products are limited in their performance and often provide an inaccurate reflection value if the scene is combined with long temporal variability, contains cloud or covered with snow in target or fill images (Prasomphan, 2012).

Maxwell introduced the spectral interpolation approach to fill the gap locations with the same scene spectral data guided by a segmentation model derived from earlier SLC-on image (Maxwell, 2004), then for further improvement a multi-scale segmentation model was utilized and performed on three different case studies. Although these approaches are demonstrated to be effective to fill the missing pixels in SLC-off images in some studies, such as forest and grass mapping, the accuracy of the reflectance prediction was low in a heterogeneous landscape, especially in narrow and tiny objects as in roads and rivers (Maxwell, Schmidt and Storey, 2007).

A multispectral projection transformation gap filling approach has been developed by Boloorani et al. using valuable pixels derived from earlier acquired auxiliary Landsat 7 SLC-on image. The results indicate the superiority of this approach in preserving the radiometric characteristics of multispectral data, but with visible gap lines still appearing in areas with sharp radiometric differences (Boloorani, Erasmi and Kappas, 2008).

A cokriging geostatistical technique was proposed by Pringle et al. to estimate the ETM+ missing values using multi-temporal auxiliary SLC-off images. This geostatistical approach was able to estimate missing values accurately, but with difficulties in well prediction of the reflectance at pixel level. In addition, the computational intensiveness of this approach limits its application for mass production (Pringle, Schmidt and Muir, 2009).

A weighted linear recovering model called Neighborhood Similar Pixel Interpolator (NSPI) was developed by Chen et al. by integrating the spectral and temporal information of the input data. Because it is a type of deterministic interpolation approach it can fill the gaps accurately even in a heterogeneous landscape. However, it cannot produce the statistical measure of the prediction (Che, et al., 2011). Subsequently, Geostatistical Neighborhood Similar Pixel Interpolator (GNSPI) approach was presented by Zhu et al. as an improvement to NSPI method using geostatistical theory. Generally, the GNSPI filled image has fewer striping effects than the previous geostatistical approach and it has more accurate estimating results than NSPI approach, especially

when there is a long time interval between the target SLC-off image and the multi-temporal auxiliary fill images (Zhu, Liu and Chen, 2012).

Later, a Weighted Linear Regression (WLR) was introduced by Zeng et al. as an integrated method to reconstruct the majority of data gaps in malfunction image by using multi temporal ETM+ SLC-off fill images as auxiliary information to build a weighted linear regression model between the corresponding pixels. When the auxiliary multi-temporal data cannot quite recover the missing pixels, a non-reference regularization algorithm is performed to accomplish the filling process. However, WLR algorithm fails to recover the images when the scene contains complicated textures together with abrupt changes (Zeng, Shen and Zhang, 2013).

Several studies using data from sensors other than Landsat7 have been established to contribute information derived from these sensors in recovering the gap locations in SLC-off target image. For instance, Boloorani et al. used the information observed by EO-1/ALI satellite in the recovery process (Boloorani, Erasmi, and Kappas, 2008), Reza and Ali used IRS products in estimating the value of the gap locations (Reza and Ali, 2008), while Roy et al. and Chen et al. adopted MODIS and CBERS data as auxiliary information, respectively (Roy et al., 2008; Jiang, Lan and Wu, 2009). Normally, the use of auxiliary images of other sensors is restricted to spatial resolution similarity, spectral compatibility, and economy (Zeng, Shen and Zhang, 2013).

In general, based on the advantages and at the same time the flaws of the above methods, it is determined that the multi-temporal data based approaches are more effective, multi-temporal Landsat7 data are also highly suitable as auxiliary fill images for gaps reconstruction in Landsat 7 SLC-off images. It is recognized that the gap locations may not be filled completely using one auxiliary image due to its lack of appropriateness. As a result, many auxiliary images are used in the progressive reconstruction process by considering the last filled image as a target in the next filled process. Therefore, by considering the limitation of such multi-temporal data based method in using only one auxiliary fill image in each step of reconstruction process, the main idea of this study is to develop an innovative multi- temporal reconstruction approach for filling the gaps in Landsat 7 SLC-off images by employing a system of linear equations derived from multiple linear regression (MLR) model using complementary information from two multi temporal Landsat 7 SLC-off fill images in parallel (parallel regression technique) with a high degree of accuracy. In addition, Cramer's rule has been used to calculate the MLR coefficients rather than using the mean and standard deviation.

The remainder of this paper is organized as follows: Section II describes the mathematical formulation of the proposed method and later on demonstrates the steps of the applied algorithm. Section III presents the results of applying the proposed algorithm on simulated and actual SLC-off images and comparing the results with multi-temporal data based method, LLHM, and finally in section IV the conclusions and discussion of the derived results have been presented.

II. Methodology

In this study and for the purpose of suitability, the SLC-off image to be recovered is defined as the target image (F_T) and the auxiliary images that are selected to fill the gaps in target images are defined as the fill images. Two fill images are simultaneously used and a system of multiple linear regression equations have been used to estimate the missing values in the target image (F_T) by exploiting the information extracted from two auxiliary images (F_1) and (F_2) in order to ensure that all gap locations have been filled.

A. Mathematical Formulation of the Multiple Linear Regression (MLR) Model

Overall, a regression model can be considered as a better method for estimating the values of the spatial data within a certain amount of correlated data sets (Jiang, Lan and Wu, 2009; Guo, et al., 2015). Earlier studies used a simple linear regression model (SLR) to recover every missing pixel in Landsat 7 SLC-off images by assuming a linear relationship between the target and one multi-temporal auxiliary fill scene. The calculation is performed on locally similar pixels that are derived from both target (F_T) and one fill image (F_F) using the following expression,

$$F_T(x,y) = B + GF_F(x,y) \quad (1)$$

where B and G are the linear regression coefficients for bias and gain, respectively, which are computed from the mean and standard deviation of the locally similar pixels (Lu and Wong, 2008). Generally, a progressive linear regression can be implemented by using another auxiliary fill image to recover the possible remaining gaps.

An extension to (SLR) model called multiple linear regression (MLR) is used to ensure the accurate recovery of all missing pixels. In this model the linear relationship between the target image and two fill images are established from the locally similar pixels extracted from them using the relation,

$$F_T(x,y) = b + G_1F_1(x,y) + G_2F_2(x,y) + \varepsilon_i \,. \quad (2)$$

where F_T is the pixel to be filled in the target SLC-off image at a location (x,y), F_1 and F_2 are the corresponding pixels in the first and second auxiliary fill images respectively and ε_i represent the random error term (Wooldridge, 2012). As in (SLR) model, the least square criteria are used for minimization the residuals using (Bonate, 2011).

$$S = \sum_{i=1}^{m} \varepsilon_i^2 = \sum_{i=1}^{m} (F_T(x,y) - G_1F_1(x,y) - G_2F_2(x,y) - b)^2 \quad (3)$$

where S is the sum of the square of the residuals. The minimization of S with respect to *G1*, *G2* and *b* yields;

 http://dx.doi.org/10.14500/aro.10147

$$\frac{\partial S}{\partial G_1} = \sum_{i=1}^{m} 2(F_T(x,y) - G_1F_1(x,y) - G_2F_2(x,y) - b) \quad (4)$$
$$(-F_1(x,y)) = 0$$

$$\frac{\partial S}{\partial G_2} = \sum_{i=1}^{m} 2(F_T(x,y) - G_1F_1(x,y) - G_2F_2(x,y) - b) \quad (5)$$
$$(-F_2(x,y)) = 0$$

$$\frac{\partial S}{\partial b} = \sum_{i=1}^{m} 2(F_T(x,y) - G_1F_1(x,y) - G_2F_2(x,y) \quad (6)$$
$$-b)(-1) = 0$$

Solving this system of linear equations, one gets,

$$\sum_{i=1}^{m} F_T(x,y)F_1(x,y) = G_1\sum_{i=1}^{m} F_1^2(x,y) + G_2\sum_{i=1}^{m} F_1(x,y)F_2(x,y) \quad (7)$$
$$+b\sum_{i=1}^{m} F_1(x,y)$$

$$\sum_{i=1}^{m} F_T(x,y)F_2(x,y) = G_1\sum_{i=1}^{m} F_1(x,y)F_2(x,y) + G_2\sum_{i=1}^{m} F_2^2(x,y) \quad (8)$$
$$+b\sum_{i=1}^{m} F_2(x,y)$$

$$\sum_{i=1}^{m} F_T(x,y) = G_1\sum_{i=1}^{m} F_1(x,y) + G_2\sum_{i=1}^{m} F_2(x,y) \quad (9)$$
$$+b\sum_{i=1}^{m} 1$$

These simultaneous linear equations are further solved sing Cramer's rule to obtain *G1,G2* and *b* in the form of determinants (Vavra and Fowler, 2010), given by:

$$G1 = \frac{\begin{vmatrix} \sum F_TF_1 & \sum F_1F_2 & \sum F_1 \\ \sum F_TF_2 & \sum F_2^2 & \sum F_2 \\ \sum F_T & \sum F_2 & \sum 1 \end{vmatrix}}{\begin{vmatrix} \sum F_1^2 & \sum F_1F_2 & \sum F_1 \\ \sum F_1F_2 & \sum F_2^2 & \sum F_2 \\ \sum F_1 & \sum F_2 & \sum 1 \end{vmatrix}} \quad (10)$$

$$G2 = \frac{\begin{vmatrix} \sum F_1^2 & \sum F_TF_1 & \sum F_1 \\ \sum F_1F_2 & \sum F_TF_2 & \sum F_2 \\ \sum F_1 & \sum F_T & \sum 1 \end{vmatrix}}{\begin{vmatrix} \sum F_1^2 & \sum F_1F_2 & \sum F_1 \\ \sum F_1F_2 & \sum F_2^2 & \sum F_2 \\ \sum F_1 & \sum F_2 & \sum 1 \end{vmatrix}} \quad (11)$$

$$b = \frac{\begin{vmatrix} \sum F_1^2 & \sum F_1F_2 & \sum F_TF_1 \\ \sum F_1F_2 & \sum F_2^2 & \sum F_TF_2 \\ \sum F_1 & \sum F_2 & \sum F_T \end{vmatrix}}{\begin{vmatrix} \sum F_1^2 & \sum F_1F_2 & \sum F_1 \\ \sum F_1F_2 & \sum F_2^2 & \sum F_2 \\ \sum F_1 & \sum F_2 & \sum 1 \end{vmatrix}} \quad (12)$$

B. Multi-Temporal Reconstruction Method based on MLR Model

As mentioned, the main idea behind the proposed approach is to fill the gap areas in Landsat 7 SLC-off images simultaneously by adopting a linear relationship between the missing pixel in the target image and the corresponding pixels in two fill images (parallel linear regression) using a multiple linear regression (MLR) model. Because the gaps in the defective Landsat 7 images do not overlap completely among scenes, it is reasonable to use multiple SLC-off ETM+ images as auxiliary images to fill the gaps in the target SLC-off image (Zhu, Liu and Chen, 2012). Therefore, in this study, a number of multiple SLC-off ETM+ images which cover the same area of the target image with different time acquisition are selected, then depending on degree of gap overlap between the target and these selected images, two auxiliary fill images will be chosen to ensure that for each missing pixel in the target image there is as much as possible a corresponding valid pixel in both fill images. Also, it is worth noting that the criteria for selecting the auxiliary SLC-off images are that the images be mostly free of clouds or snow cover, and their acquisition dates are close to that of the target image to minimize the seasonal differences and land cover change compared with the target image (Sulong, Sadiq and Edwar, 2015).

Fig. 1 illustrates the main steps of the parallel linear regression method based on the MLR model that is used for such recovery, for each band of the target image and the two fill auxiliary images. This new method is a three-step-process that allows the following:

Searching about the common valid pixels (K)

Extracting a moving window of size $(n \times n)$ around the missing pixel that was required to be filled in the target image F_T and the corresponding pixels in the two fill images F_1 and F_2. For each moving window on the target as well as the two fill images, find the number of the valid pixels in the target and the two fill images (common valid pixels). Fig. 2 presents a schematic diagram of determining the common valid pixels in all input images (F_T, F_1 and F_2), because this study is based on using two Landsat 7 SLC-off image as auxiliary images simultaneously. Then, each moving window contains valid pixels with a white color and missing pixels with a shadow color, whereas the intersection of the valid pixels that are located in the moving window and outside the gap locations in all input images, target and two fill images are selected as the common valid pixels that will be used in estimating the target

pixel value. It is also important to specify the minimum number of these common valid pixels as reference number (*RN*) that will be used in the prediction of the value of the target pixel. Beginning with the initial window size (3×3), the number of common valid pixels (K) is counted. If the minimum number of common valid pixels (*RN*) is not appropriately met, the moving window size is expanded by one pixel on each side (i.e., 5×5 to 7×7…), and the common valid pixels are counted again. The extension of the window size is continued until the minimum required number of common valid pixels (*RN*) is achieved. If the required number of common valid pixels is not met before reaching the maximum size of the moving window, then all commonly scanned pixels in the moving window are used to predict the target pixel value, regardless of the total number of common pixels. Also, the size of moving window is determined depending on the homogeneity of the scene. In case of heterogeneous landscape, a larger window size is required to guarantee that sufficient valid pixels will be selected. Considering that, the larger window size is found to yields essentially identical results, but also will consume more computing time. Therefore, in this study and because of using two fill images simultaneously and because of dealing with gaps with moderate size (6-8 pixels), then the maximum window size has to be set to 13×13 and the minimum number of common valid pixels (*K*) is set to 15. This means, a minimum number using 15 valid pixels at the same location from both auxiliary fill images in prediction of the target missing pixel value.

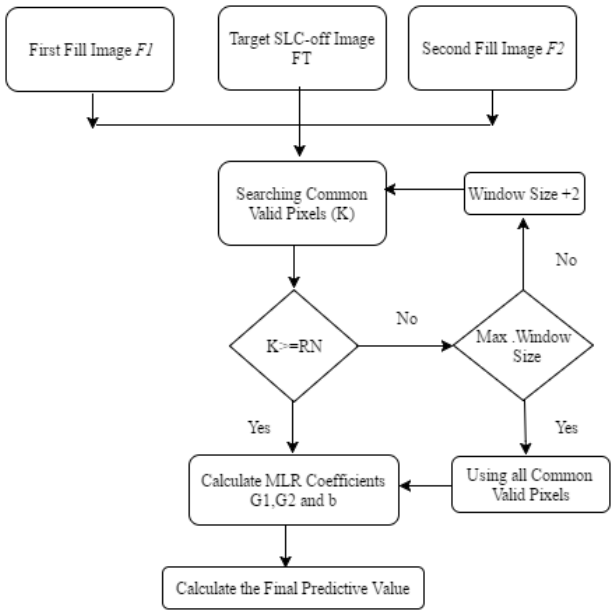

Fig. 1. The main steps of parallel linear regression method based on MLR model.

Calculating the Coefficients of MLR Model

The common valid pixels extracted from the target and two auxiliary fill images, first and second, in previous steps are used to calculate the three MLR model coefficients, *G1*, *G2* and *b* using 10,11 and 12 equations. It is noteworthy that each coefficient in the MLR model includes the summation of variables from F_T, F_1 and F_2 which is related to valid pixels in the target, first and second fill images, and these variables are extracted from the same locations in target and two fill images simultaneously.

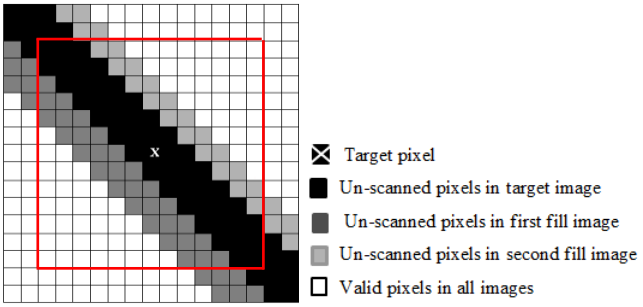

Fig. 2. Schematic diagram of the selection of common valid pixels from target and two SLC-off fill images within a moving window.

Calculating the Predictive Value:

After calculating the MLR coefficients, *G1*, *G2* and *b*, the estimated value of missing pixel in F_T is calculated using the following multiple linear equation;

$$F_T(x,y) = b + G_1 F_1(x,y) + G_2 F_2(x,y) \tag{13}$$

III. Experimental Results

To evaluate the performance of the proposed method, experiments were implemented on both simulated and real SLC-off ETM+ images with the gap width of approximately 6-8 pixels. The L1G product acquired from the USGS website (http://glovis.usgs.gov/) was used as a dataset and all data used in this study is stored as the original 8-Byte integer value. In the simulated experiments, the quantitative accuracy of the proposed MLR method is assessed by comparing the estimated or predicted pixel (X_E) with the actual or real pixel (X_A) through various statistical indices within the total number of gaps (N) in the scene. The precision of the recovered pixels is assessed by means of the Pearson correlation coefficient (r), Root Mean Square Error ($RMSE$) and Average Relative Error (ARE) given by:

$$r = \frac{\sum_{i=1}^{N}(X_E - \overline{X}_E)(X_A - \overline{X}_A)}{\sqrt{(X_E - \overline{X}_E)^2 (X_A - \overline{X}_A)^2}} \tag{14}$$

$$RMSE = \sqrt{\frac{\sum_{i=1}^{N}(X_E - X_A)^2}{N}} \tag{15}$$

 http://dx.doi.org/10.14500/aro.10147

$$ARE = \frac{(\sum_{i=1}^{N}(X_A - X_E / X_A))}{N} 100\% \quad (16)$$

where $\bar{X}_E$ and $\bar{X}_A$ are the mean of predicted and real values, respectively (Chen, et al., 2011; Zeng, Shen and Zhang, 2013).

Pearson indicator r measures the strength of the linear relationship between two input variables, which varies between -1 to +1. Perfect negative correlation gives r = -1, r = +1 signifies perfect positive correlation, and r = 0 implies the complete absence of any correlation. Mean Square Error (MSE), also known as residuals, determine the difference between X_E and X_A and RMSE is the square root of MSE. Also, ARE is used to assess how the predictive or forecasting value is close to the actual or real value which is calculated by dividing the relative error (RE) with the total number of gaps in the scene N, and the relative error is obtained by dividing the absolute error by real value. Both RMSE and ARE are used to measure the precision of the recovering method (Zeng, Shen and Zhang, 2013). The smaller the values of RMSE and ARE, the better of the prediction.

A. Experimental Results on Simulated SLC-off Images

The region that is covered by Path 169 and Row 37 in World Reference System 2 (WRS-2) is selected for experimentation. Three true color bands (Red = band 3, Green = band 2 and Blue = band 1) with 300 x 300 pixel sub images are used. An intensive study area located within the experimental region is chosen to simulate a SLC-off test image. It is consisting of the part of the Euphrates River with its surrounding arable land. The arable lands comprise green and non-green vegetation together with a bare ground that is displayed as a gray segment in the image.

In this work and in order to provide a comprehensive study to test the performance of the proposed method, four Landsat 7 SLC-on images that covered the same study area which were acquired on different dates in 2001 were selected to create one simulated target SLC-off image and a number of auxiliary fill SLC-off images. Fig. 3(a) – Fig. 3(d) shows the four Landsat 7 SLC-on images that are used to present the simulated images and which will then be used to test the proposed method. These images were acquired in 2001 on June 6, June 22, July 8 and September 10 respectively, while Fig. 3(e) - Fig. 3(h) shows the simulated SLC-off images generated from (a-d) respectively. The indicated simulated gaps in these tested images were generated by applying a gap mask from real or actual ETM+ SLC-off images acquired in 2007, where the zero values of the gap pixels replaced the pixel values in the same locations on the test images.

Subsequently, the simulated image in Fig. 3(g) acquired on July 8 is used as the target image to be filled while the remaining simulated images (e, f and h) are used as auxiliary fill images in two case studies and on each case study, both the proposed MLR and LLHM methods were implemented and compared.

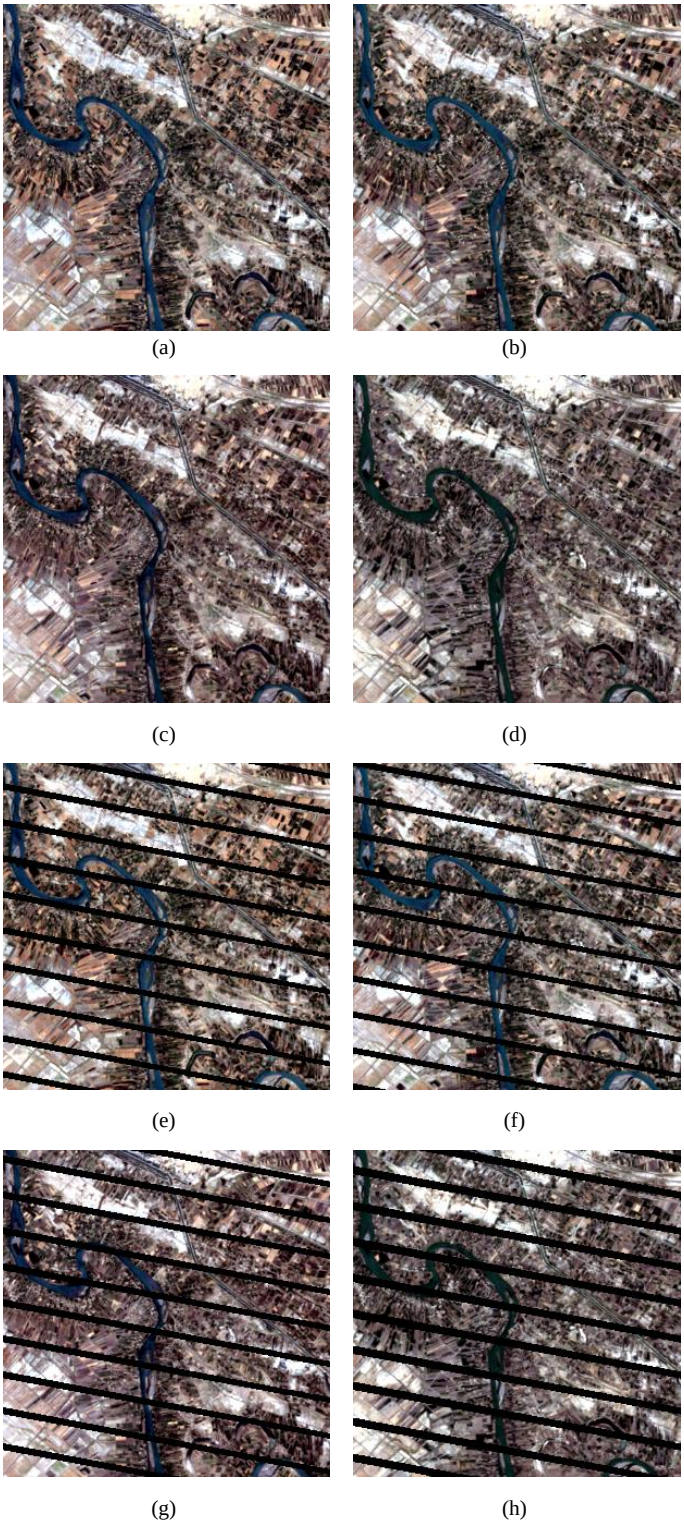

Fig. 3. Red-green-blue composites of Landsat7 SLC-on images acquired in 2001 for the simulation test: (a-d) acquired on June 6, June 22, July 8 and September 10 respectively. (e-h) the SLC-off image were simulated based on (a-d) respectively.

Fig. 4 shows the simulated images for the first case study, where the target SLC-off image (F_T) in (c) is filled using two previously SLC-off fill images (a and b), acquired on June 6 and 22 respectively, while with LLHM method a fill image that was most similar to the target images in seasonality,

which was acquired on June 22 and presented in Fig. 4(b), was used as a fill image.

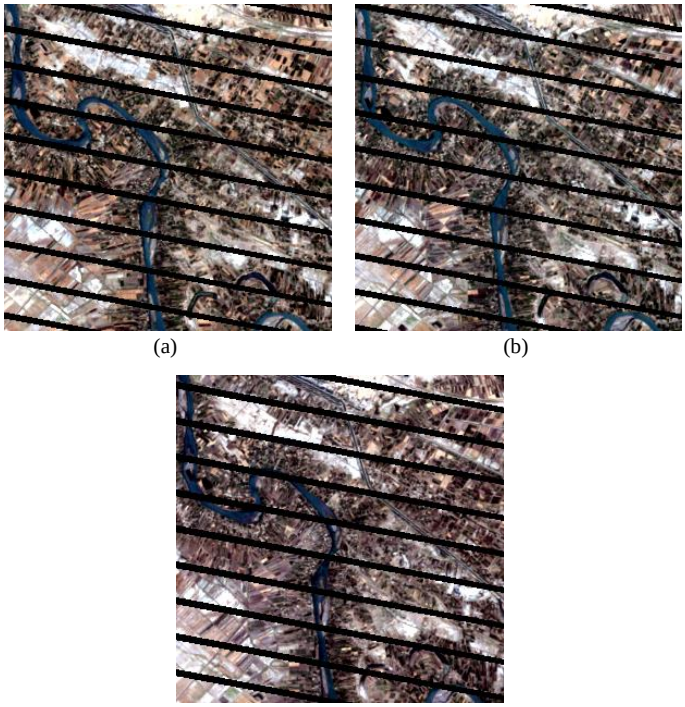

(a) (b)

(c)

Fig. 4. The simulated SLC-off images for the first case study: (c) is the target image to be filled which was acquired in 2001 on July 8 and (a and b) are the simulated auxiliary fill images that were acquired before the time acquisition of the target image (in 2001 on Jun 6 and 22) respectively.

For further performance evaluation of the proposed method, the fill image with time acquisition prior to the target image acquisition is used as first fill image (F_1) and the fill image with time acquisition after the target image acquisition is used as second fill image (F_2). Figure 5 shows the second case study where the same target SLC-off image (F_T) in Fig. 5 (b) is filled using two temporally distant fill images with time acquisition before and after the time acquisition of the target image simultaneously, on June 6 and September 10 respectively. It is obvious that the two images (a) and (b) are almost identical, but (b) and (c) are different, which is primarily attributed to the seasonal difference in the capture of these images, namely summer (image b) and autumn (image c). Also, with LLHM method, the simulated image in Fig. 5(a) that was acquired reasonably close to the date of the target image, June 6, was used as the fill image.

Finally, an actual SLC-on image (July 8, 2001) is used to validate the performance of the proposed MLR and the LLHM method by comparing the filled images with the real one.

Figure 6 demonstrates the filled results of the same target simulated SLC-off images in Fig. 4 and 5 by using fill images with different dates as presented in the two simulated case study, where Fig. 6 (a-b) displays the actual SLC-on image and the corresponding simulated target SLC-off image respectively, while Fig. 6(c) – Fig. (f) shows all the filled images of the same target image in Fig. 4 and 5 using the LLHM and the proposed MLR methods respectively. Remarkably, the images recovered by the MLR method are found to be very much closer to the real or actual image in Fig. 6(a) than the one recovered via LLHM despite using different auxiliary fill images with different time acquisitions.Furthermore, the zoomed areas of these filled images reveal superior visual details of the proposed method over the LLHM method even when using temporally distant fill images. The presence of visible errors in recovering images with L LHM, especially in the land surface with abrupt changes such as near the river, implies the inaccurate prediction by the LLHM method for heterogeneous landscapes. This notable alteration in the ground features may be due to the acquisition of one of the fill images (F_2 in the second case study) in a different season from the target image. Therefore, the implementation of the proposed MLR method is generally demonstrated to be better in terms of recovering the shape of ground features as compared to the LLHM method.

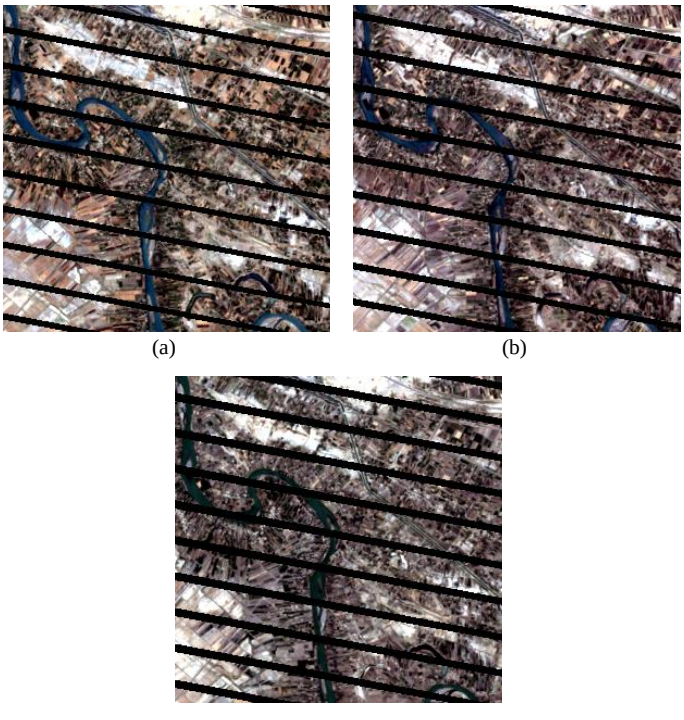

(a) (b)

(c)

Fig. 5. The simulated SLC-off images for the second case study: (b) is the target image to be filled which were acquired in 2001on July 8; (a and c) are the simulated auxiliary fill images acquired before (F_1) and after (F_2) the time acquisition of the target image (in 2001 on Jun 6 and September 10) respectively.

Table I summarizes the calculated values of r, RMSE and ARE of all three true color bands of the recovered pixels for both LLHM and MLR methods. These values are used for quantitative comparison of the predicted values of the gaps locations for the two methods. The proposed MLR method

 http://dx.doi.org/10.14500/aro.10147

and despite using more temporally distant fill images are found to achieve higher prediction accuracy in all indicators compared to LLHM method. In addition, the Pearson index (r) attained the highest values in all bands with a remarkable relative reduction in RMSE and ARE% values. This is essentially apparent when the time interval between acquisition dates of the fill and target images is larger as in the second case study. For example, for band 2, the proposed method slightly reduces RMSE values compared to the LLHM method (from 0.0555841 to 0.0531810) in the first case study when using temporally closer fill images, while for the same band there is a great reduction in RMSE (from 0.0707773 to 0.043823) using the proposed method when the more temporally distant fill images are used.

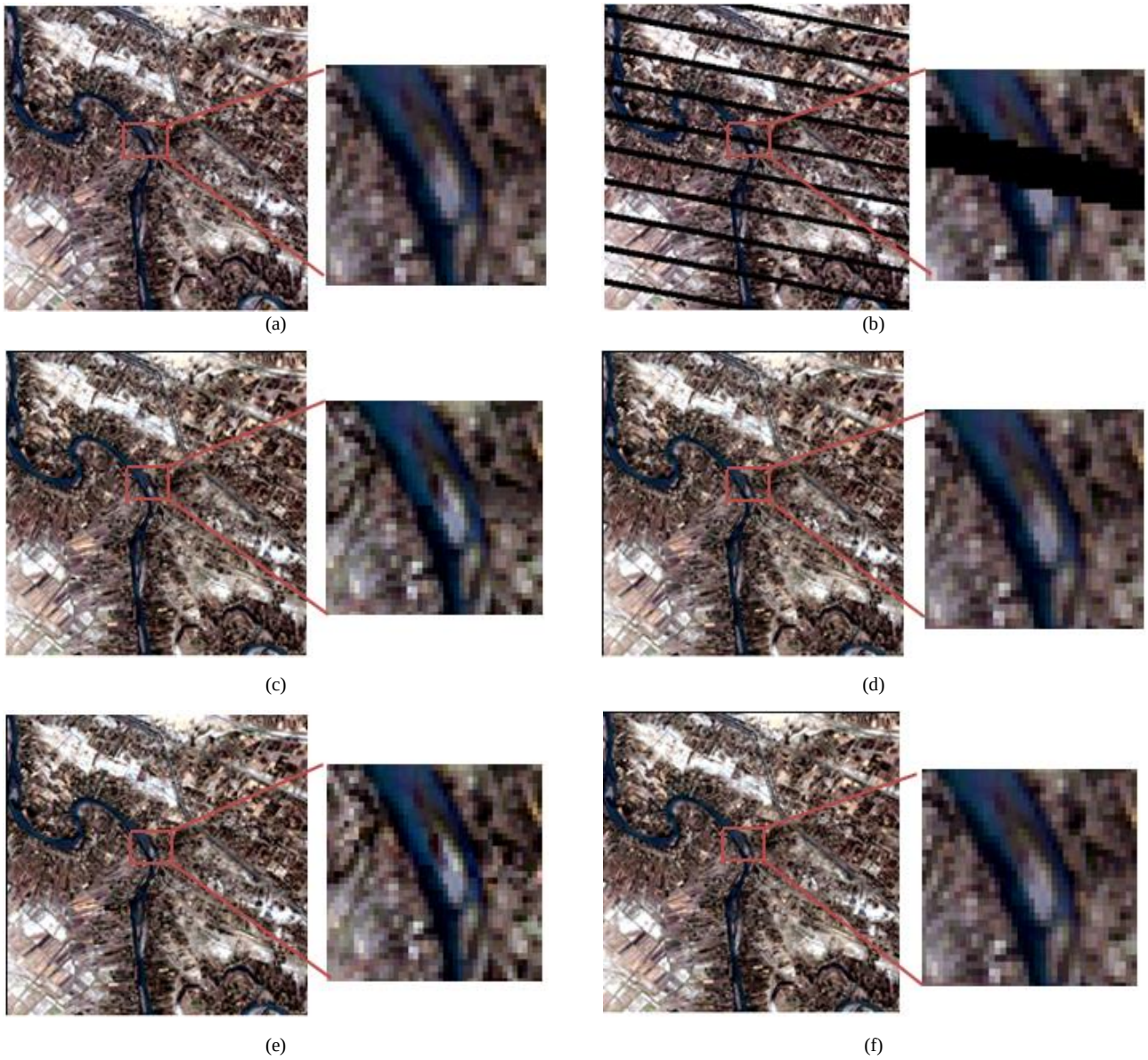

Fig. 6. .Results of gap-fill for the simulated SLC-off image: (a and b) the actual image and corresponding SLC-off simulated image respectively; (c and d) results of LLHM and MLR of fig. 4 (c) respectively using two previous fill images; (e and f) results of LLHM and MLR of fig. 5 (b) respectively using temporally far fill previous and fill next images.

B. Experimental Results on Actual SLC-off Images:

For further performance evaluation of the proposed method, both proposed MLR and LLHM methods have been carried out by applying them to the real or actual Landsat7 SLC-off images that were acquired in 2013. The actual SLC-off image acquired on July 25 as shown in Figure 7(b) is used as the target image to be filled (F_T). Meanwhile, the two SLC-off images taken on May 22 in Fig. 7(a) and September 27 in Fig. 7(c) is used as first (F_1) and second (F_2) fill images,

respectively, with the proposed MLR method while with LLHM method, the first fill image (F_1) was acquired reasonably close to the date of the target image, May 22, and presented in Fig. 7(a) was used as the fill image. Figs. 7(d) and 7(e) present the results of MLR and LLHM method respectively. The present MLR method is found to achieve excellent visual clarity, where most of the gaps are recovered with high superior quality of the filled image as compared to LLHM method which displays shadow in the recovered areas indicating inaccurate estimation of the missing values.

TABLE I
THE ACCURACY OF THE RECOVERED IMAGES OBTAINED FROM LLHM AND PROPOSED MLR METHOD IN TWO SIMULATED CASE STUDIES

		Filled results of Fig. 4 Case1		Filled results of Fig. 5 Case2	
Statistical Indicator	Band	LLHM	MLR	LLHM	MLR
r	B1	0.896294	0.929330	0.889631	0.927471
	B2	0.883729	0.927142	0.883677	0.925343
	B3	0.914987	0.943002	0.869451	0.917354
ARE%	B1	1.336410	1.323570	1.630620	1.360180
	B2	0.977490	0.956006	1.215000	0.970970
	B3	1.053240	1.091280	1.428940	1.137720
RMSE	B1	0.063971	0.061942	0.080026	0.062800
	B2	0.055584	0.053181	0.070777	0.043823
	B3	0.055884	0.054673	0.076265	0.056609

IV. DISCUSSION AND CONCLUSION

Despite the SLC failure, the radiometric and geometric quality of the ETM+ imagery is still excellent for many applications on regional and global scales over other satellite images. Therefore, a number of recovery techniques have been developed to fill the missing data locations in Landsat 7 SLC-off images.

In this study, a new multi-temporal recovering approach has been presented and evaluated for predicting the missing pixels in Landsat 7 SLC-off images by extending a standard multi temporal data method, LLHM, which is based on a simple linear regression model. This expansion was adopted through a multi-temporal reconstruction method based on multiple linear regression (MLR) models to precisely recover the mostly degraded pixels by exploiting information derived from two multi-temporal SLC-off auxiliary fill images simultaneously**.** The simulated and actual SLC-off images are analyzed using the proposed model and compared with the results of LLHM method. Also, with simulated case studies, the quantitative comparison was implemented by calculating the values of r, RMSE and IS metrics for both MLR and LLHM methods.

Generally, despite using different fill images situations, two previous fill images as in first simulated case study and more temporally distant fill previous and fill next images as in second simulated case study, the experimental results on both simulated and real case studies demonstrate that the proposed MLR approach provides a good tool in filling the missing pixels in SLC-off image where the filled locations are reasonable approximations of the actual SLC-on image more than LLHM approach. It is also obvious that the reconstructed images by the proposed method have good continuity and accuracy with no obvious shadows in filled images as in LLHM results. In addition, the statistical summary of the errors specifies that the new proposed method is found to achieve higher prediction accuracy. However, the present algorithm is tested only on specific gap width of 6 to 8 pixels. Further researches are required for estimating the missing values in the gaps with large width by assigning a suitable weight for each pixel contributing in the estimation process within the searching window.

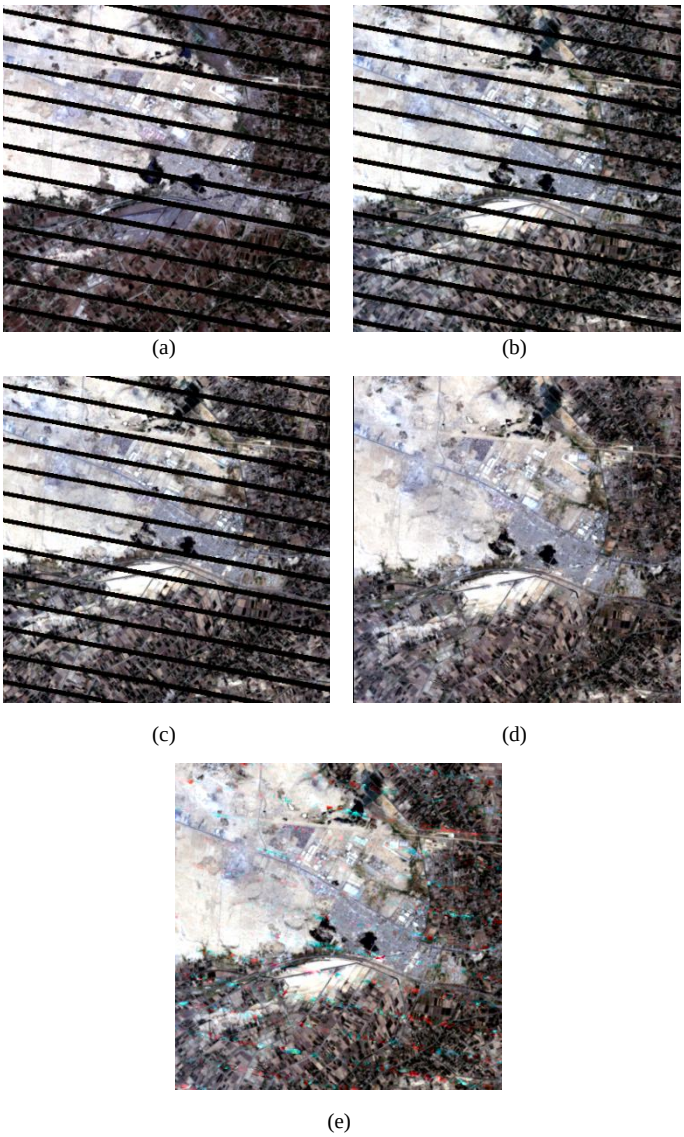

Fig. 7. The experiment results of actual Landsat7 SLC-off image (taken in 2013) (a) first fill image on May 22; (b) target image on July 25 and (c) second fill image on September 27; obtained result (d) from proposed MLR method and (e) from the LLHM method.

ACKNOWLEDGMENT

Asmaa S. Abdul Jabar is grateful to the Iraqi Ministry of Higher Education & Scientific Research and the University of Al-Mustansiriyah for their sponsoring her Ph.D. study.

REFERENCES

Boloorani, A.D., Erasmi, S. and Kappas, M., 2008, February. Multi-source image reconstruction: exploitation of EO-1/ALI in Landsat-7/ETM+ SLC-off gap filling. In *Electronic Imaging 2008* (pp. 681219-681219). International Society for Optics and Photonics.

Boloorani, A.D., Erasmi, S. and Kappas, M., 2008. Multi-source remotely sensed data combination: Projection transformation gap-fill procedure. *Sensors*, 8(7), pp.4429-4440.

Bonate, P. L., 2011. Linear Models and Regression:Ch.2, inUSA,(2nd Ed.): Pharmacokinetic- Pharmacodynamic Modeling and Simulation, Springer, Science+Business Media, LLC, pp.61-100.

Chen, F., Tang, L. and Qiu, Q., 2010, June. Exploitation of CBERS-02B as auxiliary data in recovering the Landsat7 ETM+ SLC-off image. In *Geoinformatics, 2010 18th International Conference on* (pp. 1-6). IEEE.

Chen, F., Tang, L., Wang, C. and Qiu, Q., 2011. Recovering of the thermal band of Landsat 7 SLC-off ETM+ image using CBERS as auxiliary data. *Advances in Space Research*, 48(6), pp.1086-1093.

Chen, F., Ye, H. and Zhao, X., 2012. *Making Use of the Landsat 7 SLC-off ETM+ Image Through Different Recovering Approaches*. Rijeka, Croatia: INTECH Open Access Publisher.

Chen, J., Zhu, X., Vogelmann, J.E., Gao, F. and Jin, S., 2011. A simple and effective method for filling gaps in Landsat ETM+ SLC-off images. *Remote Sensing of Environment*, 115(4), pp.1053-1064.

Desai, M. and Ganatra, A., 2012. Survey on gap filling in satellite images and inpainting algorithm. *International Journal of Computer Theory and Engineering*, 4(3), p.341.

Guo, G., You, W., Qian, G. and Shao, W., 2015. Parallel maximum likelihood estimator for multiple linear regression models. *Journal of Computational and Applied Mathematics*, 273, pp.251-263.

He, Q., Shan, B., Ma, H., Chen, Y. and Wang, X., 2011, July. Research on Algorithms for Recovering Landsat-7 Gap Data. In *Control, Automation and Systems Engineering (CASE), 2011 International Conference on* (pp. 1-4). IEEE.

Hossain, M. S., Bujang, J. S., Zakaria, M. H., and Hashim, M., 2015. Assessment of Landsat 7 Scan Line Corrector-off data gap-filling methods for seagrass distribution mapping. *International Journal of Remote Sensing*, *36*(4), pp 1188-1215.

Hu, W., Li, M., Liu, Y., Huang, Q. and Mao, K., 2011, June. A new method of restoring ETM+ SLC-off images based on multi-temporal images. In *Geoinformatics, 2011 19th International Conference on* (pp. 1-4). IEEE.

Jabar, A., S. , Sulong, G. and George, L.E., 2014. SURVEY ON GAP FILLING ALGORITHMS IN LANDSAT 7 ETM+ IMAGES. *Journal of Theoretical & Applied Information Technology*, 63(1).

Jiang, Y., Lan, T. and Wu, L., 2009, December. A Comparison Study of Missing Value Processing Methods in time series data mining. In *Computational Intelligence and Software Engineering, 2009. CiSE 2009. International Conference on* (pp.1-4). IEEE.

Lu, G.Y. and Wong, D.W., 2008. An adaptive inverse-distance weighting spatial interpolation technique. *Computers & Geosciences*, 34(9), pp.1044-1055.

Markham, B.L., Storey, J.C., Williams, D.L. and Irons, J.R., 2004. Landsat sensor performance: history and current status. *Geoscience and Remote Sensing, IEEE Transactions on*, 42(12), pp.2691-2694.

Maxwell, S., 2004. Filling Landsat ETM+ SLC-off gaps using a segmentation model approach. *Photogrammetric Engineering and Remote Sensing*, 70(10), pp.1109-1112.

Maxwell, S.K., Schmidt, G.L. and Storey, J.C., 2007. A multi-scale segmentation approach to filling gaps in Landsat ETM+ SLC-off images. *International Journal of Remote Sensing*, 28(23), pp.5339-5356.

Mohammdy, M., Moradi, H.R., Zeinivand, H., Temme, A.J.A.M., Pourghasemi, H.R. and Alizadeh, H., 2014. Validating gap-filling of Landsat ETM+ satellite images in the Golestan Province, Iran. *Arabian Journal of Geosciences*, 7(9), pp.3633-3638.

Prasomphan, S., 2012, December. Imputing Landsat7 ETM+ with SLC-off image using the similarity measurement between two clusters. In *Future Generation Communication Technology (FGCT), 2012 International Conference on* (pp.190-195). IEEE.

Pringle, M.J., Schmidt, M. and Muir, J.S., 2009. Geostatistical interpolation of SLC-off Landsat ETM+ images. *ISPRS Journal of Photogrammetry and Remote Sensing*, 64(6), pp.654-664.

Reza, M.M. and Ali, S.N., 2008. Using IRS products to recover 7ETM+ defective images. *American Journal of Applied Sciences*, *5*(6), pp.618-625.

Roy, D.P., Ju, J., Lewis, P., Schaaf, C., Gao, F., Hansen, M. and Lindquist, E., 2008. Multi-temporal MODIS–Landsat data fusion for relative radiometric normalization, gap filling, and prediction of Landsat data. *Remote Sensing of Environment*, 112(6), pp.3112-3130.

Rulloni, V., Bustos, O. and Flesia, A.G., 2012. Large gap imputation in remote sensed imagery of the environment. *Computational Statistics & Data Analysis*, 56(8), pp.2388-2403.

Scaramuzza, P., Micijevic, E. and Chander, G., 2004. SLC gap-filled products phase one methodology. *Landsat Technical Notes*. Available from http://landsat.usgs.gov/documents/SLC_Gap_Fill_Methodology.

Shen, H., Li, X., Cheng, Q., Zeng, C., Yang, G., Li, H., and Zhang, L., 2015. Missing information reconstruction of remote sensing data: A technical review. *IEEE Geoscience and Remote Sensing Magazine*, 3(3), pp.61-85.

Storey, J., Scaramuzza, P., Schmidt, G. and Barsi, J., 2005, October. Landsat 7 scan line corrector-off gap filled product development. In *Proceedings of Pecora*, 16, pp. 23-27.

Sulong, G.,Sadiq, A. and Edwar , L., 2015. Single and Multi-source Methods for Reconstruction the Gaps in Landsat 7 ETM+ SLC-off Images. *Research Journal of Applied Sciences, Engineering and Technology*, *11*(4), pp.423-428.

USGS & NASA., 2004, SLC-off Gap-Filled Products Gap-fill Algorithm Methodology: Phase2. Available from www.ga.gov.au/servlet/BigObjFileManager?bigobjid=GA4861.

Vavra, L. M., Fowler, D., 2010. Cramer's Rule.

Wooldridge, J.M., 2012. Chapter 3: Multiple regression analysis: Estimation, in USA (5th Ed.), Introductory Econometrics, A Modern Approach,South Western.

Wulder, M.A., Ortlepp, S.M., White, J.C. and Maxwell, S., 2008. Evaluation of Landsat-7 SLC-off image products for forest change detection. *Canadian Journal of Remote Sensing*, 34(2), pp.93-99.

Zeng, C., Shen, H. and Zhang, L., 2013. Recovering missing pixels for Landsat ETM+ SLC-off imagery using multi-temporal regression analysis and a regularization method. *Remote Sensing of Environment*, 131, pp.182-194.

Zhang, C., Li, W. and Travis, D., 2007. Gaps-fill of SLC-off Landsat ETM+ satellite image using a geostatistical approach. *International Journal of Remote Sensing*, 28(22), pp.5103-5122.

Zhu, X. and Liu, D., 2014. MAP-MRF approach to Landsat ETM+ SLC-Off image classification. *Geoscience and Remote Sensing, IEEE Transactions on*, 52(2), pp.1131-1141.

Zhu, X., Liu, D. and Chen, J., 2012. A new geostatistical approach for filling gaps in Landsat ETM+ SLC-off images. *Remote sensing of Environment*, 124, pp.49-60.

Video Streaming over Vehicular Ad Hoc Networks: A Comparative Study and Future Perspectives

Kayhan Z. Ghafoor

Department of Software Engineering, College of Engineering, Salahaddin University
Kirkuk Road Erbil, Kurdistan Region – F.R. Iraq

***Abstract*—Vehicular Ad Hoc Network (VANET) is emerged as an important research area that provide ubiquitous short-range connectivity among moving vehicles. This network enables efficient traffic safety and infotainment applications. One of the promising applications is video transmission in vehicle- to-vehicle or vehicle-to-infrastructure environments. But, video streaming over vehicular environment is a daunting task due to high movement of vehicles. This paper presents a survey on state-of-arts of video streaming over VANET. Furthermore, taxonomy of vehicular video transmission is highlighted in this paper with special focus on significant applications and their requirements with challenges, video content sharing, multi-source video streaming and video broadcast services. The comparative study of the paper compares the video streaming schemes based on type of error resilient technique, objective of study, summary of their study, the utilized simulator and the type of video sharing. Lastly, we discussed the open issues and research directions related to video communication over VANET.**

***Index Terms*—Applications of VANET video transmission, Cooperative collision avoidance, Vehicular networks, Video streaming.**

I. INTRODUCTION

Recent technology booming have a key role in developing various types of networks and then deploying them based on their specific applications. In the past decade, Vehicular Ad Hoc Network (VANET) has experienced more attention from the academia and automotive industries (Zeadally, et al., 2012; Bernsen and Manivannan, 2008).

Vehicular network is a type of wireless ad hoc network that enables ubiquitous connectivity among vehicles in the vicinity. At the present time, the importance of vehicular network is tremendously increased because of its unprecedented applications in transportation system - such as traffic management, safety, and efficiency as well as on-road infotainment (Hartenstein and Laberteaux, 2009). These traffic applications would appear through the existence of VANET because of its prompt convergence with Intelligent Transportation System (ITS). The promising future of vehicular network is a motive for automotive manufactures, researchers and governments to increase their efforts toward creating a standardized platform for vehicular communications. Particularly, the 5.9 GHz spectrum band has been allocated for licensed Short Range Communication (DSRC) between vehicles (Lochert, et al., 2007; Karadimas and Matolak, 2014). In the near future, more vehicles will be embedded with devices that facilitate communication between vehicles, such as Wire- less Access in Vehicular Environment (WAVE) (ITS-Standards, 1996). When vehicles are equipped with WAVE, they can communicate with nearby cars and access points within their coverage area. However, although many steps have been taken towards fulfilling the aforementioned applications efficiently, many challenging issue still remain to be solved due to its high topology changes, unreliable communication channel between vehicles and scarce of on-board resources (Whaiduzzaman, et al., 2014; Kakkasageri and Manvi, 2014; Dias, Rodriguesand and Zhou 2014).

Nowadays it is observed that car industries are manufacturing intelligent vehicles which are embedded with efficient storage, have good computation power and have the capability to communicate with other devices (Wired, 2014). Passengers also can use Internet inside their vehicle by using the emergence mobile internet technology like Long Term Evolution (LTE). Thus, in the near future road users can ubiquitously communicate with nearby wireless nodes and this will improve the driving safety, traffic efficiency and environment pollution (Chen, et al., 2010; Tripp-Barba, et al., 2014). However, these applications would provide clear vision to the drivers and passengers if high quality video is exchanged among nearby vehicles.

ARO-The Scientific Journal of Koya University
Volume IV, No 2(2016), Article ID: ARO.10128, 12 pages
DOI: 10.14500/aro.10128
Received 22 February 2016; Accepted 16 April 2016
Review paper: Published 22 October 2016
Corresponding author's e-mail: kayhan@ieee.org

We are motivated because video streaming over vehicular networks is significant to satisfy the passenger and driver requirements. Video camera has been embedded in many premium vehicles and trucks. This camera is not only provide a clear vision to the driver of the truck, but also increases the traffic awareness of nearby vehicle drivers if the video frames are shared with them. Moreover, video camera is installed in all intersections and all of them are embedded with wireless device. Thus, establishing a network of these cameras can be useful for tele-medicine. For example, a video camera captures traffic accident at the intersection and then it is forwarded to nearest hospital for required medicine (Wu and Ma, 2013; Asefi, 2011; Chaqfeh, Lakas and Jawhar, 2014; Chen, et al., 2014). Infotainment applications of video communication among vehicles are also helpful to make this emerging network quickly penetrate in the market. One of the interesting comfort-related applications is commercial advertisement on the road. For instance, a vehicle may visit a place for shopping purpose and it will receive video frames on current sales and special offers nearby supermarkets and shops (Wu and Ma, 2013; Asefi, 2011).

Although video streaming over vehicular networks is advanced and a become room for research, unfortunately there is no comprehensive survey to help the readers understand thoroughly the recent techniques of video streaming. In line with the growing interest of video streaming over VANET, this paper firstly presents a concise description of the background of vehicular networks and especially highlighting the video transmission over VANET. This is followed by presenting and elaboration of a comprehensive taxonomy for video streaming techniques in VANET. That is, multi-source video streaming, video broadcast and video content sharing. Then, each type of the aforementioned classification will be demonstrated and the motivation behind their design as well as trace the performance evaluation of the existing techniques. Finally, the paper discusses the possible future research directions. To the best of our knowledge, this review article is the first research study on advances of video streaming in vehicular networks.

The rest of the paper is structured as follow: Section II highlights vehicular networks. Section III thoroughly discusses the applications, requirements and challenges of video transmission among vehicles. An overview and motivation of video streaming over VANET are discussed in section IV, where we thoroughly highlighted the existing protocols under the categorization of multi-source video streaming, video broadcast and video content sharing, Section V discusses the prospective research opportunities and directions. Finally, Section VI concludes the paper and discusses important recommendations.

II. The Vehicular Network

Recently, auto car makers are made their efforts to design smart vehicles for the purpose of achieving safe and comfortable driving experience. These car innovations are observed in new cars as they are equipped with GPS, short range collision avoidance system, front and back camera, and embedded wireless sensors (Chen, et al., 2014). These facilities are necessary to warn the drivers for any possible abnormal road conditions and vehicle's mechanical defects. Moreover, vehicles have efficient on-board power, computation and communication capability (Xie, et al., 2007; Tonguz and Boban, 2010; Soldo, et al., 2008).

With these smart vehicles, cars are able to talk to each other and be aware about their neighbors. Thus, vehicular networks are a promising field of study and gained the attention of many researchers from both academia and industry. The deployment of such important system will open up a flourish path for safer driving experience (European-ITS, 2009). For instance, vehicles in the vicinity can exchange information for collision avoidance and traffic flow control. This will probably decrease death tolls on the roads. To support such important technology, an association of thirteen automobile companies assured that V2V has potential to reduce traffic accidents tremendously and hence save lives of people. For this reason, FCC allocated 5.9 GHz spectrum band for licensed Short Range Communication (DSRC) between vehicles.

III. Video Streaming Over Vehicular Networks: Applications and Requirements

This section presents prospective applications and implementation scenarios of video streaming over VANET (Belyaev, et al., 2014; Boukerche, et al., 2009; Belyaev, et al., 2014; Lin, et al., 2009). Table 1 presents video transmission applications and requirements which will be discussed in the following subsections.

A. Overtaken Maneuver

One main concern of traffic safety is wrong overtaking maneuver in highway or urban areas, which causes serious accidents. In real traffic scenarios, an accident due to wrong overtaking leads to a series of vehicle to vehicle crashes. This seriously obstructs the traffic fluidity and results the road congestion or another accident. These traffic accidents can be simply avoided if vehicular network technology is enabled between vehicles (Toledo-Moreo, et al., 2009; De Sousa Vieira, et al., 2013; Ruder, et al., 2002; Yasmeen, et al., 2015). More importantly, live video streaming from trucks to the following vehicles increases driver's aware- ness about oncoming vehicles and it is helpful to the driver for any overtaking decision. The crucial requirement of such system is strict end-to-end delay be- tween obstructing vehicle and overtaking cars. As it is mentioned by Vinel, et al., (2012), the required delay should not exceed 200 ms with acceptable perceived video quality. However, there are several challenges for real time video streaming over vehicular networks, such as unreliability of the wireless channel, shadowing and multi-path fading.

B. Pedestrian Crossing Assistance

Pedestrian is the ordinary people who use the roads and experience risk due to carelessness and erroneousness of

drivers or pedestrian themselves. One of the most glaring problems of transportation system is pedestrian-vehicle crashes since it is considered as a threat to human lives.

C. Public Transport Assistance

Recently the fuel cost is increasing as well as the researchers have alerted the high pollution of the environment due to carbon dioxide emission. These reasons made the people to use public transportation and their safety should be strictly considered. Uncommon vehicles (like ambulance, garbage truck or public bus) are embedded with video camera to provide cognizance capability to the drivers. The live video output of the camera would be useful to the vehicles which are close to the premium vehicle. In rare traffic scenarios, the vehicles that overtake the buses might hit the disembarking passengers. As it is illustrated in Fig. 1, vehicle number 2 might crash with the passenger who is just get off from the bus and intends to cross the road. This vehicular network application is considered as an important urban safety service that prevents passenger death or injury.

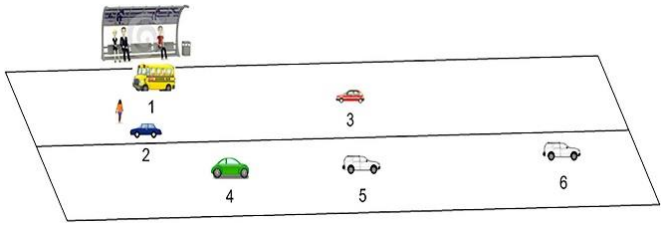

Fig. 1. Public Transport assistance.

The transmitted video should exhibit a strict low latency and good visual quality since this application treats the human lives. However, the main challenge with this scenario is the effect of Doppler phenomena that causes the frequency shifting between transmitter and receiver.

D. Video Surveillance

Nowadays anti-social behavior such as crimes, robbery, irritating people and terror acts are tremendously increased. Real time video surveillance in- side/outside vehicles are very crucial to prevent such behaviors. In this scenario, a vehicle transmits coded video to the infrastructure network and that video could be a call for traffic accident or heath condition of the passengers of crashed car. Furthermore, live video on moving public transport is streamed to the control center to abolish any crimes (Ahmad and Habibi, 2010). But, live video streaming for surveillance purpose is a daunting task due to harsh environment of vehicular network such as high mobility, large obstacles and bipolar traffic conditions.

E. Video Communication for Entertainment

Promising applications in vehicular network have been classified to traffic safety and management, and infotainment applications. The latter one provides comfort and entertainment- related information and useful advertisement to the passengers. This application contributes the success of vehicular network and speedup its market penetration (Campolo and Molinaro, 2011; Myllyniemi, Vehkapera and Peltola, 2007; Ghafoor and Bakar, 2010). Moreover, both academia and industry are approved the benefits of video communication for infotainment and advertisement services. Table I outlines the video transmission applications and requirements.

TABLE I
VIDEO TRANSMISSION: APPLICATIONS AND REQUIREMENTS

Video transmission applications	Benefits	Network Architecture	Requirements		Challenges
			End-to-end delay	Perceived video quality	
Overtaking maneuver	Highway traffic safety	Vehicle-to-Vehicle	Delay between video capturing and displaying should not exceed 200 ms.	The video quality should be acceptable	Obstruction of video transmission signal due to moving obstacles (vehicles) and high speed of vehicles.
Pedestrain crossing assistance	Urban traffic safety	Vehicle-to-Vehicle	Strict low latency	Acceptable video quality	Mobility is not a big concern since vehicle travel in low speed in pedestrian crossing areas. Moving or static obstacles are considered as great challenges.
Public transport assistance	Public transportation traffic safety	Vehicle-to-Vehicle	Strict low delay	Acceptable video quality	T bus stations, public transport vehicles broadcast live video to overtaken cars. In this case, Doppler frequency shifting would be the main issue.
Video surveillance	Public urban or highway security	Vehicle-to-Infrastructure	Delay should not exceed 6 sec as it is acceptable for video surveillance	Visual quality of not less than 25 dB is good	Mobility of in-road enabled video surveillance of wireless channel and obstacles
Video communication for entertainment	Infotainment	Vehicle-to-Vehicle and Vehicle-to-Infrastructure	Low latency	Average video quality of 29 dB is acceptable	High mobility of vehicles, radio obstacles, Doppler effect due to relative speed of vehicles.

As illustrated in Table I, infotainment relies on both V2V and V2I network architectures. Vehicles can exchange video information like games for entertainment while in V2I the infrastructure advertises contextual information about tourist places, updated news or locations that traffic jam occurs. Such video transmission requires low delay and acceptable video

 http://dx.doi.org/10.14500/aro.10128

quality as (29 dB). However, the delay and video quality for infotainment applications is not as strict as in the traffic safety services. The main challenge of video transmission in such harsh environment is the rapidly changing of network topology and radio obstacles.

IV. Video Streaming Over Vehicular Network

Video streaming over vehicular networks is a need for many applications. Video disseminating of news or commercial related information to the drivers/passengers can be considered as an important application for transportation systems. For safety applications video frames can be used to clearly show the traffic scene in the accident area. Also, video contents can save life of thousands during search and rescue operation in any unexpected event.

Video services are considered as one of the challenging issue in mobile wire- less networks (Bohrloch, et al., 2011). There are different factors that affect the vehicular network performance like high vehicle mobility, fast change of topology and fast and slow fading due to multi-path signal dissemination. The high speed of vehicles causes frequent connectivity interruption which leads to performance degradation.

As compared to data transfer application and even voice-over-IP or video conferencing, video content streaming requires bounded end-to-end delay and sufficient bandwidth. These requirements have long been addressed in cable networks while they still a room for research in mobile wireless networks like VANET. This is because vehicles use a shared medium and this will shrink the utilized bandwidth. With the challenges of VANET, providing a satisfactory perceived video quality to the client's needs more research. The overall structure of video streaming schemes is depicted in Fig. 2.

A. Video Content Sharing Mechanisms

As discussed in the aforementioned section, video streaming over vehicular network is a challenging task (Tal and Muntean, 2012; Park, et al., 2006; Ghafoor, et al., 2012; Venkataraman, et al., 2010; Dias, et al., 2011). The problem is more glaringly appear when a video data is transmitted via multi-hop towards a destination. The reason is that video data could not tolerate high end-to-end delay between source and destination. Thus, for smooth playback of video data at the destination tightly relies on the selection of most reliable and stable path toward the video receiver. On the other hand, vehicles are frequently changing their point of attachment from one network to the other and this leads to the intermittent of video streaming continuity. To tackle the aforementioned issues, the authors in (Asefi, 2011) proposed quality-aware geographical packet forwarding from a infrastructure network to the destination vehicle on the road. The startup delay and Peak Signal to Noise Ratio (PSNR) of delivered video frames are utilized as metrics for delivering video packets towards the destination. At the receiver, video playback depends on the collection and playback phases. The collection phase is defined as storing of incoming packets when the buffer is empty while the playback phase starts once the buffer is filled with threshold number of packets. Moreover, PSNR is used to select a high quality path with minimum end-to-end video frame distortion.

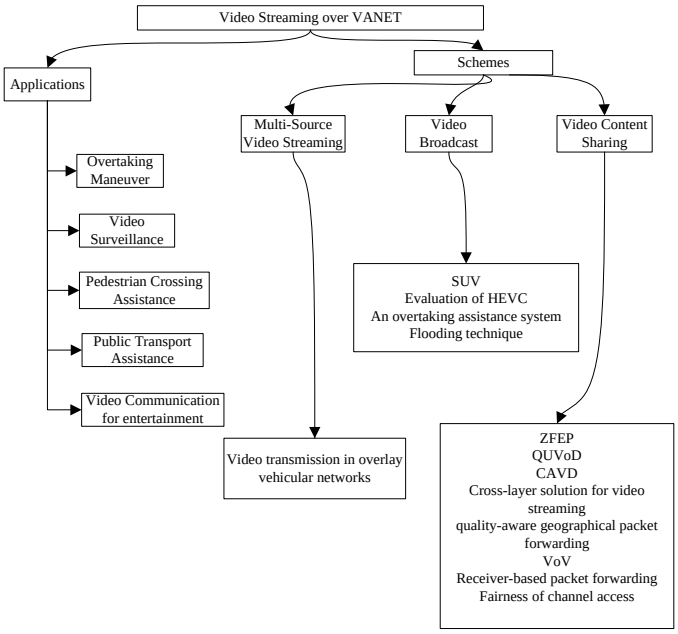

Fig. 2. Taxonomy of the literature on video streaming over VANET.

In vehicular environment, the destination vehicle usually moves from the coverage of one Access Point (AP) to the other one. Thus, the authors in (Asefi, 2011) also tackled IP mobility management for the purpose of improving visual quality of transmitted video, when the destination vehicle changes its point of attachment from one AP to the other one. Fig. 3 shows the vehicular network topology that is considered by the proposed solution. As can be seen, the radio communication range of every AP is 350 m and the APs are spaced with a distance of 1.2 Km. With this settings, two nearby APs could not cover 600 m distance and multi-hop V2V would be used for packet forwarding toward the infrastructure network. Simulation result shows that the proposed method improves the quality of transmitted video especially in dense traffic scenario than sparse distribution of vehicles.

To support video streaming from the Road Side Unit (RSU) to the destination vehicle, the authors in (Xing and Cai, 2012) proposed adaptive video streaming algorithm that composed of three main functions: neighbor discovery, next hop selection strategy, and video quality adaptation scheme. Firstly, the adaptive video streaming algorithm enables the vehicles to handshake and synchronizes by using beacon message. Through beacon message communication, vehicles can learn about their one-hop and two-hop neighbors. However, beacon message generates overhead on the wireless channel among vehicles. To tackle this problem, the authors bounded the number of neighbors to Z . In the other words, if the number of nearby vehicles exceeds Z , the overhead

mitigation mechanism randomly selects Z neighbors.

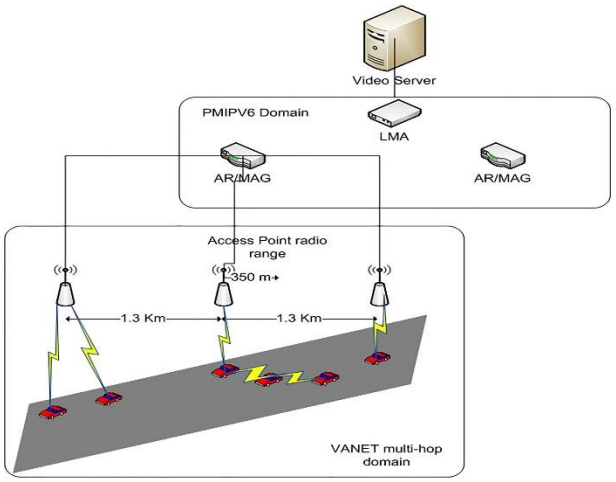

Fig. 3. VANET V2V and V2I scenario for the proposed mechanism in (Asefi, 2011).

In the second algorithm, the vehicle, which receives video data, searches for the next candidate relay vehicle within its radio coverage. A vehicle V C is considered as a best candidate if it has a highest link data rate (closest to the RSU) with the RSU. In addition, it is necessary to mention that the Scalable Video Coding (SVC) is used to encode the video frames into layers. In SVC, each video frame is coded into layers; a base layer and several enhancement layers. Base layer is very significant in the process of successful video file decoding at the receiver while enhancement layers have the role of improving the quality of video frames. In the other words, despite packet losses of the enhancement layer, the receiver can decode the video frames successfully.

The third part of proposed algorithm adapts the perceived video quality with the link data rate between a vehicle with the serving RSU and the receiver buffer level. More particularly, a vehicle adapts the requested number of enhancement layers from a RSU with respect of its buffer level and link data rate between itself and the RSU. To clarify, the link data rate is important for the receiver vehicle to support the acceptable video quality. Likewise, the receiver buffer level is crucial to be considered for video quality level tuning. The reason is that sometimes a vehicle may experience no connection with the RSU. In this case, the vehicle should buffer enough video frames for smooth playback in later time.

The authors conducted a performance evaluation of the proposed algorithm in MATLAB® and highway vehicular scenario with two lanes. The evaluation also considered real video traces of "Big Buck Bunny" which is consisted of 600 video segments. For benchmarking, the authors compared the proposed algorithm with the non-cooperative relaying mechanism by using startup latency, interruption ratio and average playback quality. The adaptive video streaming performs the best in terms of the aforementioned metrics as compared to the non-cooperative relaying approach.

Peer-to-peer (P2P) content distribution is witnessed to be a groundbreaking trend in vehicular networks. One of applications of P2P multimedia services is the vehicular Video-on-Demand (VoD) that provides edited video file to the vehicles on the road. Enhancement of Quality-of-Experience (QoE) of VoD applications is a pressing need. In this context, the authors in (Xu, et al., 2013) proposed inter- active quality-aware user-centric mobile VoD mechanism for VANET (QUVoD). As can be seen in Fig. 4, the QUVoD is based on multi-homed P2P/VANET architecture and mechanisms for storing video frames, video segment retrieval, and multi-path packet forwarding. Simulation results show the better performance of the proposed algorithms as compared with the state-of-the-arts solutions.

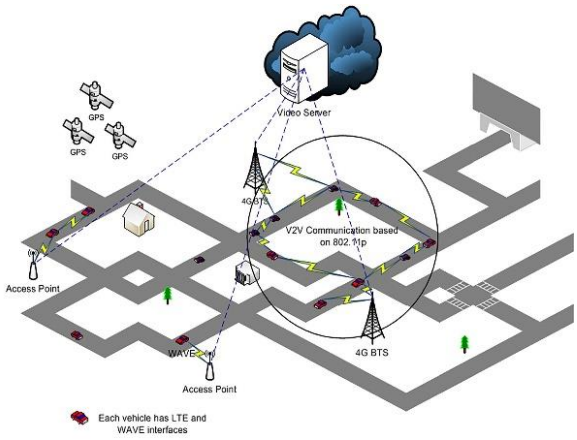

Fig. 4. QUVoD system for vehicular networks.

Traffic control system in world's countries use wireless enabled camera in order to let them be aware the traffic violation, car accidents or unusual transportation conditions. For instance, if a car crash occurs in urban or high- way vehicular environment, traffic control center informs nearest medical center to send ambulance to the accident area. With wireless enabled camera, paramedics could realize the required medical equipment to the accident scene. To achieve this scenario, the authors in (Wu and Ma, 2013) proposed existing traffic camera assisted (CAVD) live video streaming in VANETs. The purpose of CAVD is to stream the video frames from the accident spot to the mobile target vehicle (ambulance). For this purpose, they developed a scheme to optimally select intersection cameras using Optimal Buffering Point (OBP). Thus, the camera- based wireless network could forward the video frames with minimum start- up delay, reasonable perceived video quality and playback performance. In the performance analysis, the authors assured the superiority of their method as compared to the architecture of V3 that introduced by Guo, et al. (2005) - which streams video from a static node to the vehicles - and Trajectory-based statistical forwarding (TSF) (Jeong, et al., 2010).

As illustrated in Fig. 5, cameras are installed in all road junctions to monitor the traffic condition at the intersections. Each camera is equipped with wireless device to enable its communication with other devices. More

 http://dx.doi.org/10.14500/aro.10128

precisely, each camera could get the traffic information- vehicular arrival rate, speed and density- for each road segment and tag this information with time and then broadcast to all camera network. In this way, all cameras are aware about the traffic information of the whole city. Likewise, vehicles that they travel nearby the cameras will get such traffic information through wireless interface of the installed camera.

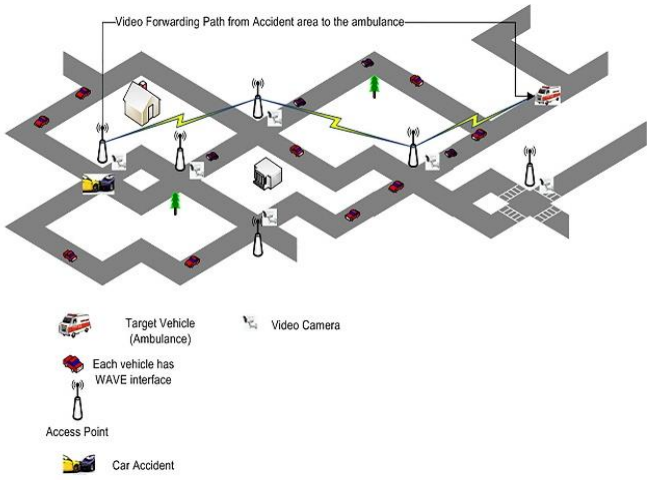

Fig. 5. Video streaming from accident area to the ambulance.

As it is witnessed by many researchers the network congestion will increase channel access delay at the MAC layer and hence some video frames will lately reach the destination. Thus, these delayed frames are not useful in recovering video file at the destination. To this end, the authors in (Puangpronpitag, Kasabai and Suwannasa, 2013) proposed the cross- layer solution for video streaming in a VANET application, which is overtaking assistance system. This V2V application uses windshield camera that mounted on vehicles. As illustrated in Fig. 6, the driver vision of vehicles 1 and 4 are blocked due to trucks 2 and 3. In this case, the video of the front scene is recorded by the trucks 2 and 3 and then streamed to the vehicles 1 and 4. With the help of this received video, the drivers of vehicles 1 and 4 can decide whether to overtake the trucks.

The proposed method adapts the video traffic with the current network capacity. More clarified, if the collision rate in the medium exceeds during a frame F transmission, discard this F frame and transcode frame F +1 and reduce the frame rate to half value. Usually if the time delay of a frame F exceeds the threshold value, this frame is useless in the decoding process of a video file. Thus, it is logical to skip this frame. Besides that, frame rate at the application layer is reduced if there is congestion in the network level. The frame rates of 30, 15, and 7.5 frames/second have been used in the performance evaluation. The simulation analysis was done in OMNeT++ packet level simulator with IEEE 802.11p MAC layer. The results show the acceptable network latency that is within the range of standard video frame delay - which is 100 ms - (Baldi and Ofek, 2000).

In some places on the highway or urban areas, vehicles want to download video files such as video news and entertainment games. In such environment, V2V is susceptible to intermittent connectivity likewise infrastructure is not promptly existing.

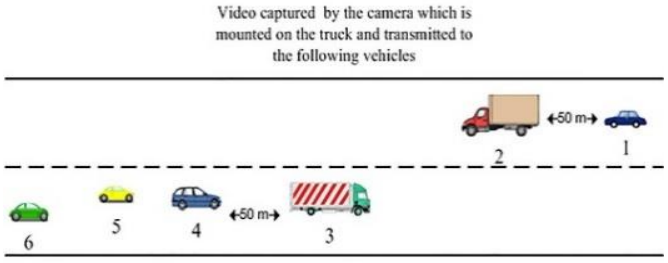

Fig. 6. Video streaming service to assist drivers during car overtaking.

For this case, exploiting both V2V and V2I is a significant need to support large file size downloading from neighbor vehicles or nearby infrastructure. To this end, the authors in (Sou, et al., 2011) proposed a Zone-based Frame Exchange Protocol (ZFEP) for video sharing among nearby peers. The idea of ZFEP is to exploit V2V and V2I for video communication among vehicles. For instance, drivers/passengers can exploit infrastructure to download video frames when neighbor vehicles are not exist in the area.

The users conducted numerical simulation and the results show their method is superior in terms of download speed and video quality. In another attempt, the same authors in (Shieh, et al., 2011) presented a mechanism for video frame sharing (VFSM) for sparse vehicular network. They improved the efficiency of video downloading from road side unit by enabling cooperation among vehicles that they have compatible interest. In such a way, vehicles can request video frames from the infrastructure using V2I whereas sharing the downloaded video with neighbor vehicles using V2V.

Toward the task of an efficient video dissemination in sparse and dense traffic conditions, the authors in (Maia, et al., 2013) proposed video transmission over VANET (VoV). In dense traffic condition, a mechanism has been developed for broad-cast overhead mitigation. The designed method partitioned the radio range to forwarding zones. A vehicle determines whether it's in the forwarding zone or not to compute the waiting time. The highest priority is given to vehicles that they are inside the forwarding zone and have farthest distance to the source. However, if the source faces the intermittent connectivity, that vehicle stores the message in its local cache for a limited period of time. Besides that, a vehicle that stores the messages inform nearby vehicles about the stored packets. This is done by piggybacking received message ID in the period of beacon exchanging and sending them to the vehicles in the vicinity.

Federal Communication Commission provided seven non-

overlapping channels in the frequency band of 5.85 GHz. One of these seven channels is allocated to transmit control information like beacon and event-driven messages. The rest of channels are used to transmit non-safety information. As all channels have one antenna, a transceiver hops from a SCH to the CCH or vice-versa. This channel switching generates a synchronization problem in IEEE 802.11p. As illustrated in Fig.7, MAC layer fetches a sequence of packets from the upper layer and at this moment the CCH channel is active for transmission. In this case, the received packets are saved in the local buffer of a vehicle until the SCH would be active. When the SCH become active, the MAC layer tries to forward all cached packets at the early first moments of SCH activation and this also happen in the nearby vehicles. Since all the vehicles want to transmit their buffered packets, the network performance will be drastically deteriorated. To address the aforementioned problem, the authors in (Maia, et al., 2013) proposed a rate control mechanism that finds out the rate at which the VoV should send packets down to the MAC layer.

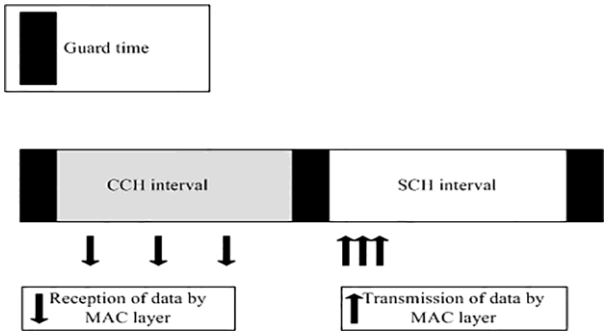

Fig. 7. Large number of packet transmission at the beginning of service channel.

Rezende, C. (2012) proposed receiver-based packet forwarding mechanism for video streaming in vehicular networks. Each relay vehicle uses the distance to the destination and contact time to calculate the waiting time that is utilized for vehicle's self-election. Particularly, the contact time represents a limited time window in which the winner relay vehicle will continue to forward packets without re-self-election of intermediate vehicle that occur in each single hop. This time window can be computed by the location tracking mechanism to predict the vehicle's future location and hence estimate the time window among neighbor vehicles. In such way, their method is trading-off between link stability and fast advancement of video packets transmission toward the destination.

The performance evaluation of the proposed solution and state-of-the-arts (normal receiver-based algorithm and Guided Gossiping (GG)) is simulated in NS2 and freeway mobility model. GG disseminates the packet toward the destination while receiver-based mechanism uses greedy metric for relay self- election. For the transmitted video, the MPEG video file with 300 frames and with resolution of 360×486 is used. The cost metric is measured by a ratio of total number of transmissions to packets sent. Simulation result shows that the proposed solution outperforms the benchmark schemes as it can forward more packets successfully with less frame loss and acceptable delay.

Following their work on improved receiver-based packet forwarding to minimize delay of routed video packets towards destination, Rezende et al. (2013) evaluated the performance, in terms of successful delivery rate and enhancement of video transmission quality, of two erasure techniques named random linear network coding (Li, et al., 2003) and XOR-based coding (Li, et al., 2004). The performance evaluation was done using freeway mobility model and NS2 simulation tool. Results have shown the XOR-based coding successfully forwards more packet than random linear network coding with similar rate of redundancy. Thus, in XOR-based mechanism, the majority video file content is recovered at the receiver vehicle.

The authors in (Xu, et al., 2012) implemented the performance analysis of different routing protocols (AODV, DSDV, GPSR) for video transmission over realistic VANET environment. The utilized simulation tool is incorporated myEvalvid (Ke, et al., 2006), NS2 (NS, 2011) and VANETMobiSim (VANETMobiSim, 2014). After conducting a comparative simulation in VANET-EvalVid realistic environment, the authors shows the superior performance of GPSR protocol with respect to the AODV and DSDV for good visual quality

of video frames. They also demonstrated that the quality of transmitted video is better in dense traffic condition than sparse distribution of vehicles.

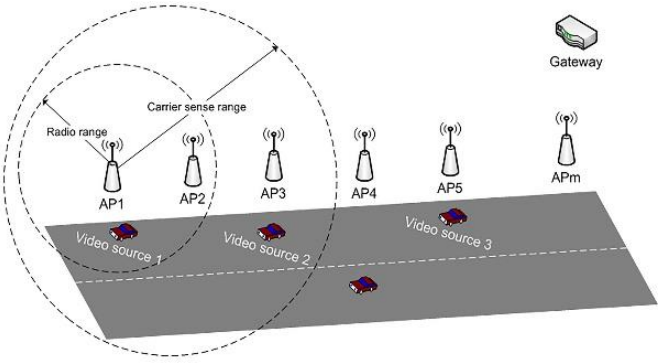

Fig. 8. Channel access starvation scenario in 802.11p.

As it is illustrated in a VANET scenario in Fig. 8, three vehicles under the radio coverage of three different APs are transmitting video frames towards the gateway. In this scenario, AP3 is starved of gaining the channel since the AP1 , AP2 , AP4 and AP5 are transmitting video packets toward the gateway. Thus, channel access starvation happens with the Carrier Sense Multiple Access (CSMA) of 802.11p. In an attempt, the authors in (Bellalta, et al., 2014) tried to improve the fairness of accessing the wireless channel between nearby vehicles. They also evaluated multi-hop video streaming from IEEE 802.11p enabled vehicular

surveillance network to the traffic management center. In their evaluation, Scalable Video Coding (H.264/SVC) and non-standard scalable video coding three dimensional discrete wavelet transmission (3-D DWT) (Belyaev, et al., 2013).

The transmitted video from the target vehicle/vehicles, which is multi-hops far away from the gateway, is assessed by end-to-end distortion. Moreover, they show that tuning of video data rate of a target vehicle is crucial and depends on the vehicular traffic density and location of participating vehicles.

B. Video Broadcast Mechanisms

Applications of video broadcast from a source to vehicles in the vicinity is very necessary. With this service, vehicles can be updated with latest news, traffic and tourist information, on-road advertisement, and video-application sharing. To efficiently broadcast video applications to urban vehicles, Soldo, et al. (2011) proposed Streaming Urban Video (SUV). The SUV enables video communication in V2V fashion. To achieve this, each relay vehicle utilizes the positional information and sensed power level to dynamically select the next candidate node. Moreover, the data channel is used to stream video and best- effort traffic based on the Time Division Multiple Access (TDMA) structure. More particularly, the data channel is organized as constant time frames with n number of similar time slots. In their work, the authors used graph-coloring algorithm to compute the value of time slots and a group of relay vehicles that they transmit over the specified time slot. They also proposed a collision resolution mechanism to handle the possible packet collisions in the link layer level.

In highways or urban scenarios, the drivers frequently need to overtake other vehicles that they comparatively drive slowly. In this case, sometimes the drivers of overtaking vehicles might underestimate the speed of the oncoming platoon of vehicles. Thus, an overtaking assistance system is very necessary as it helps the drivers to see on time and rightfully estimate the oncoming traffic. In recent studies, researchers highlighted two methods of cooperative overtaking assistance system: real time video transmission or beacon based system. In the former one, the video scene is captured by the windshield camera and then transmitted to the followed vehicles. In the second case, beacon messages with the carrying the positional information is exchanged among vehicles that will provide awareness to the drivers for the information of nearby vehicles. As illustrated in Fig. 9, truck 1 streams video about oncoming traffic to the following vehicles (such as vehicle 2) as well as the vehicles are aware about other vehicles in the vicinity by using beacon message communication. But, in such scenario when two platoons of vehicles reach each other, the overloading on the SCH would occur and thereby the transmitted video quality from truck 1 to the followed vehicles would degrade. To address this problem, Vinel, et al. (2012) combined the aforementioned two methods of overtaking assistance system. In essence, beacon message is useful to provide the information on oncoming platoon of vehicles through the CCH and this data can be used by a vehicle to estimate the channel throughput. Then, a vehicle can use channel through- put as a metric to adapt its video bit rate to the channel variation. With this joint beaconing and video streaming -assisted overtaking system, the end-to-end latency and visual quality of transmitted video are significantly improved.

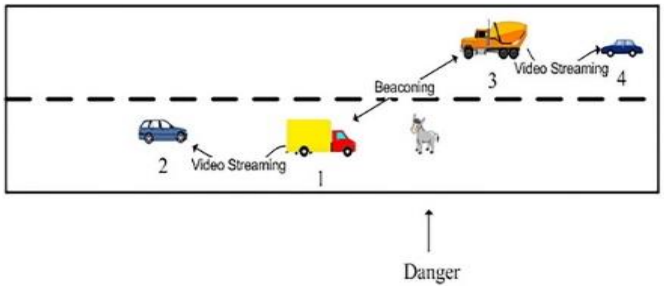

Fig. 9. Cooperative overtaking assistance system based on video streaming and beaconing.

Researchers are continuously devoting their efforts to improve the video compression standards. One of these new standards is High Efficiency Video Coding (HEVC) (Sullivan, et al., 2012) that doubles the coding efficiency of previous standard H.246/Advanced Video Coding (H.246/AVC). To show the efficiency and performance of HEVC VANET environment, Pinol, et al. (2011) evaluated the HEVC considering error-prone vehicular scenarios.

The simulation was done in OMNeT++ (OMNeT++, 2011) packet level simulator with SUMO mobility modeler. SUMO is considered as an efficient mobility model that simulates the movement behavior of vehicles, finding efficient trajectory of cars, interaction between vehicles and roads/ other vehicles and intersections. OMNeT++ supports the operation of service (SCH) and control channels (CCH) (multi-channel) in 802.11p. Another important characteristic of the used simulator is the ability to model obstacles that obstructs the communicated radio signal between vehicles. The authors developed a module to identify the video server and receivers. A server announces the video-related application through the CCH every 1 second. After receiving the existence of video services, the video receiver switches to a suitable SCH and hence downloads the video frames. Moreover, the “Race Horse” video sequence has been used with a frame transmission rate of 30 fps. The results of the experiments show the high sensitivity of HEVC to packet losses.

In the similar attempt, the authors in (Torres, et al., 2014) evaluated few flooding techniques for transmission of video frames over multi-hop and different vehicular densities. The evaluated flooding techniques were counter based algorithm, distance based scheme, backfire based algorithm (Osafune, Lin and Lenardi, 2006) and DECA algorithm (Nakorn and Rojviboonchai, 2013). For this evaluation purpose, the

authors use OMNeT++ packet level simulator and SUMO mobility model. Based on the simulation, they found that backfire algorithm, which is efficiently reduces the collision in the wireless medium as well as delivers more packets with low delay.

C. Multi-source Video Streaming Mechanisms

Following the trend of improving video streaming over VANET, the authors in (Qadri, et al., 2010) developed a method of video transmission in overlay vehicular environment. They used joint Multi-Description Coding (MDC) (Wang, Reibman and Lin, 2005) and spatial Flexible Macroblock Ordering (FMO) (Lambert, et al., 2006) to protect the video frames from the error-prone wireless channel. In FMO, which is considered as an error resilient mechanism for H.264/AVC, the video frames are divided into several slices in order to recover the lost macroblocks of neighbor slices.

The evaluation is based on the GloMoSim (Zeng, Bagrodia and Gerla, 1998) simulator and additive propagation model (Takai, Martin and Bagrodia, 2001) that uses a path loss model with multi-path fading in order to take into account consideration the signal obstruction and attenuation. The Rician fading model is used to incorporate the multi-path interference to the vehicles communication, which includes one line of sight and several non-line of sight components in the received signal. Moreover, the macro and micro mobility modeling are used to represent the realistic vehicular movement, behavior of drivers and urban street layout. Results show that different mobility models will affect the overhead and packet loss in the network. For instance, incorporating a precise driver behavior into vehicular mobility model will decrease packet loss in the network while including a lane changing model results a high movement of vehicles and leads to higher degradation of network performance. Furthermore, when the error of the wireless channel increases, the fading component (non-line of sight) of Rician distribution increases too. As consequence, the network performance is degraded, showing the effect of multi-path fading on the performance of the network.

V. Research Directions and Open Issues

The state of the arts video streaming over VANET solutions is reviewed, compared and criticized. These schemes can be counted as a foundation for video transmission in vehicular environments. However, they do not address many open issues yet. The following are some of the research directions.

Realistic Vehicular Network Scenarios: As it can be observed in the existing literature, the video streaming schemes were simulated in unrealistic scenarios, i.e., vehicular communications without considering wireless shadowing and fading channel deterioration. The difference between simulation experiments using realistic and unrealistic vehicular topologies may result in the expense of human lives which is not affordable. Therefore, the state of the arts solutions need to be reevaluated using realistic vehicular scenarios.

Considering Radio Obstacles in VANET: In highway or urban sites, obstacles like trucks (moving obstacles) and buildings (static obstacles) are exist. These radio obstacles obstruct the radio signal and hence will cause high video packet loss. Thus, considering radio obstacles in the proposed solutions is necessary.

Erasure coding: Transmitting video over such harsh environment is a daunting task. Error correction techniques need to be used to compensate the packet losses at the receiver. For instance, network coding, Multiple Description Coding (MDC) or forward error correction are suitable in vehicular network to boost the reliability of video packet transmission especially protecting most crucial information like I-frame.

Adaptive Video Streaming: Most video streaming solutions would not consider the characteristics of vehicular network. For instance, video streaming schemes is necessary to adapt with the traffic density or velocity of vehicles as both of them affect their scalability.

Video streaming over multi-radio enabled vehicular networks: Next Generation Network (NGN) aims to integrate different radio access technologies in order to provide seamless mobility and QoS at anywhere and anytime. Thus, it is crucial to design efficient video streaming scheme over different wireless access technologies (WiFi, WiMAX and LTE) and decision for optimal selection between them in heterogeneous vehicular networks.

VI. Conclusion

This paper presents a comprehensive review on new research direction, video streaming over VANET. More specifically, this survey discusses and highlights the taxonomy of video streaming protocols, significant applications and their requirements and challenges, and comparative study among existing solutions in the literature. Based on this review outcome, it can be observed that efforts have been made to develop efficient and VANET adaptive video streaming protocols. However, Table II shows the defects for most video streaming schemes since they utilized simulation or mathematical modeling. It is noteworthy that practical implementation verifies the assumptions made in the simulation as well as provides believability of the results which are obtained from simulation and mathematical analysis. Thus, considering more realistic vehicular environment, conducting test-bed experiments on video streaming, developing efficient video streaming protocols and embedding erasure coding in the developed schemes are worth the effort in the future research opportunities.

 http://dx.doi.org/10.14500/aro.10128

TABLE II
VIDEO STREAMING SCHEMES AND THEIR DEFECTS

Algorithm	Error Resilient Technique	Objective	Type of Video Sharing	Simulator and Video File	Evaluation Parameters	Simulation Results
Rezende et al. (2012)	None	Selecting more stable and shortest path	Video streaming unicast	NS2 and MPEG Akiyo CIF	Frame loss, delay and cost scenario	Their algorithm performs better in terms of frame loss, delay and cost of transmissions
Rezende, Almulla and Boukerche (2013)	Random linear network coding and XOR-based coding	Performance evaluation of two coding scheme	Video streaming unicast	NS2 and MPEG Akiyo CIF	Frame loss, delivery ratio and delay	XOR-based coding performs better as compared to the Random linear network coding
Soldo et al. (2011)	Multiple Description Coding	Efficient video Broadcast from one source to all vehicles	Broadcast	None	None	Comparisons with existing literature are not conducted in the paper
Puangpronpitag, Kasabai and Suwannasa, (2013)	Coded with H.264 standard	Suppressing MAC-level congestion by skipping frames, transcoding to next frames and halving the frame rate	Unicast	OMNeT++ and Fore- man CIF	Network latency	Comparisons with existing literature are not conducted in the paper
Xing, and Cai (2012)	Coded with Scalable Video Coding	To improve video quality of experience level by adaptively requesting number of enhancement video layers	Unicast	MATLAB® and video traces of Big Buck Bunny	Startup latency, interruption ratio and average playback quality	Performs better as compared to the non-corporative scheme
Vinel et al. (2012)	None	To improve video qual- ity and end-to-end de- lay by adapting video bit rate with the channel variation rate	Broadcast	Theoretical analysis	Throughput and PSNR	Improves the video quality and end-to-end latency
Maia et al. (2013)	None	To improve video dissemination by broadcast suppression, store and forward mechanism, and control of packet transmission rate	Broadcast	OMNeT++ and Akiyo CIF	Average frame loss, transmitted data message and average frame delay	Improves successful packet delivery rate
Wu and Ma (2013)	None	To improve start-up delay and required visual quality by using camera network to forward video packets through optimal path	Unicast	NS2 and foreman-qcif	Average start-up delay, average PSNR and average number of freezes	Improves startup delay and perceived video quality
Bellalta, et al. (2014)	Flexible macroblock ordering with two slice groups	To improve end-to-end distortion of target vehicle by dynamic adaptation of its video bit rate with vehicle density and position of participated vehicles	Unicast	Test-bed experiments and Tampere-04 (640×480, 300 frames)	Throughput and PSNR	Selecting best target vehicle's video bit rate provides good visual quality, this selection depends on the number of vehicles and their Position
Qadri, et al. (2010)	joint Multi-Description Coding (MDC) and spatial Flexible Macroblock Ordering (FMO)	To show the feasibility of multi-source video streaming under different conditions, mobility modeling, wireless channel condition and network size	Multi-source video streaming to a specific destination	GloMoSim and QCIF (176×144)	Control overhead, packet loss ratio, end-to-end delay and PSNR	Realistic mobility model, driver behavior and probabilistic fading model significantly affect network performance
Xu, et al. (2012)	None	To test the performance of several routing protocols in VANET environment	Unicast	NS 2.28 and Foreman (400 frames)	Frame loss rate and average PSNR	GPSR is more reliable for video streaming in dense traffic than AODV and DSDV routing protocols

REFERENCES

Ahmad, I. and Habibi, D., 2010. High utility video surveillance system on public transport using WiMAX technology In: *2010 IEEE Wireless Communication and Networking Conference*, Sydney, NSW, 2010, pp. 1-5.

Asefi, M., 2011. *Quality-driven cross-layer protocols for video streaming over vehicular ad-hoc networks.* Ph.D., University of Waterloo.

Baldi, M. and Ofek, Y., 2000. End-to-end delay analysis of videoconferencing over packet-switched networks. *IEEE/ACM Transactions on Networking*, 8(4), pp.479-492.

Bellalta, B., Belyaev, E., Jonsson, M. and Vinel, A., 2014. Performance Evaluation of IEEE 802.11 p-Enabled Vehicular Video Surveillance System. *IEEE Communications Letter*, 18(4), pp.1-4.

Belyaev, E., Egiazarian, K. and Gabbouj, M., 2013. A low-complexity bit-plane entropy coding and rate control for 3-D DWT based video coding. *IEEE Transaction on Multimedia*, 15(8), pp.1786-1799.

Belyaev, E., Vinel, A., Jonsson, M. and Sjoberg, K., 2014. Live video streaming in IEEE 802.11 p vehicular networks: demonstration of an automotive surveillance application. In*: 2014 IEEE Conference on Computer Communications Workshops (INFOCOM WKSHPS).* Toronto, ON, 2014, pp.131-132. doi: 10.1109/INFCOMW.2014.6849190

Belyaev, E. et al., 2014. Robust vehicle-to-infrastructure video transmission for road surveillance applications. *IEEE Transactions on Vehicular Technology*, (99), pp.1-15.

Bernsen, J. and Manivannan, D., 2008. Unicast Routing Protocols for Vehicular Ad hoc Networks: A Critical Comparison and Classification. *Pervasive and Mobile Computing*, Elsevier. 5(1), pp.1-18.

Bohrloch, T. et al., 2011. A methodology to evaluate video streaming performance in 802.11 e based MANETs. *In: The 10th International Conference Ad-hoc, Mobile, and Wireless Networks.* Paderborn, Germany, July 18-20, 2011, pp. 276-289.

Boukerche, A., Rezende, C. and Pazzi, R. W., 2009. Improving neighbor localization in vehicular ad hoc networks to avoid overhead from periodic messages. In: *Global Telecommunications Conference, 2009. GLOBECOM 2009.* IEEE, Honolulu, HI, 2009, pp.1-6.
doi: 10.1109/GLOCOM.2009.5425636

Campolo, C. and Molinaro, A., 2011. On vehicle-to-roadside communications in 802.11 p/WAVE VANETs. In: *2011 IEEE Wireless Communications and Networking Conference*. Cancun, Quintana Roo, 2011, pp.1010-1015. doi: 10.1109/WCNC.2011.5779273

Chaqfeh, M., Lakas, A. and Jawhar, I., 2014. A survey on data dissemination in vehicular ad hoc networks. *Vehicular Communications*, 1(4), pp.214-225.

Chen, M., Mau, D.O., Zhang, Y., Taleb, T. and Leung, V.C.M., 2014. VENDNET: VEhicular Named Data NETwork. *Vehicular Communications*, 1(4), pp. 208-213.

Chen, P.-Y., Liu, J.-W. and Chen, W.-T., 2010. A Fuel-Saving and Pollution-Reducing Dynamic Taxi-Sharing Protocol in VANETs. In: *Vehicular Technology Conference Fall (VTC 2010-Fall), 2010 IEEE 72nd*, Ottawa, ON, 2010, pp.1-5. doi: 10.1109/VETECF.2010.5594422

De Sousa Vieira, A. S., Celestino Jnior, J., Patel, A. and Taghavi, M., 2013. Driver assistance system towards overtaking in vehicular ad hoc networks. In: *AICT 2013: The Ninth Advanced International Conference on Telecommunications*, pp.100-107.

Dias, J. A. et al., 2011. Performance assessment of fragmentation mechanisms for vehicular delay-tolerant networks. *EURASIP Journal on Wireless Communications and Networking*, 2011(1), pp.1-14.

Dias, J. A., Rodrigues, J. J. and Zhou, L., 2014. Cooperation advances on vehicular communications: A survey. *Vehicular Communications*, 1(1), pp.22-32.

European-ITS, 2009. *EITS-Technical Report 102 638 v1.1.1*.

Ghafoor, K. and Bakar, K., 2010. Inter-Vehicle Communication Protocols for Multimedia Transmission. In: IMECS 2010: International MultiConference of Engineers and Computer Scientis 2010 Vol II. Hong Kong, pp.1234-1239, 17-19 March.

Ghafoor, K.Z., Abu Bakar, K., Zainuddin, Z.M., Chih-Heng K. and Gonzalez, A.J., 2012. Reliable Video Geocasting over Vehicular Ad Hoc Networks. *Ad Hoc and Sensor Wireless Networks*, 15, pp. 201-221.

Guo, M., Ammar, M. H. and Zegura, E. W., 2005. V3: A vehicle-to-vehicle live video streaming architecture. *Pervasive and Mobile Computin*, 1(4), pp.404-424.

Hartenstein, H. and Laberteaux, K. P., 2009. A tutorial survey on vehicular ad hoc networks. *IEEE Communications Magazine*, 46(6), pp. 164-171.

ITS-Standards, 1996. *Intelligent Transportation Systems.*

J. Jeong, J., Guo, S., Gu, Y., He, T. and Du, D.H.C., 2010. TSF: Trajectory-Based Statistical Forwarding for Infrastructure-to-Vehicle Data Delivery in Vehicular Networks. In: *2010 IEEE 30th International Conference on Distributed Computing Systems (ICDCS).* Genova, 2010, pp.557-566. doi: 10.1109/ICDCS.2010.24

Kakkasageri, M. and Manvi, S., 2014. Regression based critical information aggregation and dissemination in VANETs: A cognitive agent approach. *Vehicular Communications*, 1(4), pp.168-180.

Karadimas, P. and Matolak, D., 2014. Generic stochastic modeling of vehicle-to-vehicle wireless channels. *Vehicular Communications*, 1(4), pp. 153-167.

Ke, C.-H., Lin, C.-H., Shieh, C.-K. and Hwang, W.-S., 2006. A novel realistic simulation tool for video transmission over wireless network. In: IEEE International Conference on Sensor Networks, Ubiquitous, and Trustworthy Computing (SUTC'06), Taichung, pp. 7.doi: 10.1109/SUTC.2006.1636186

Lambert, P., De Neve, W., Dhondt, Y. and Van de Walle, R., 2006. Flexible macroblock ordering in H. 264/AVC. *Journal of Visual Communication and Image Representation*, Elsevier, 17(2), pp.358-375.

Li, F. and Wang, Y., 2007. Routing in Vehicular Ad hoc Networks: A Survey. *IEEE Vehicular Technology Magazine*, 2(2), pp.12-22.

Li, J. et al., 2004. On-the-fly verification of rateless erasure codes for efficient content distribution. In: *2004 IEEE Symposium on Security and Privacy*, 2004. pp.226-240. doi: 10.1109/SECPRI.2004.1301326

Lin, C.-H.et al., 2009. An adaptive cross-layer mapping algorithm for MPEG-4 video transmission over IEEE 802.11 e WLAN. *Telecommunication Systems*, 42(3-4. Springer), pp.223-234.

Li, S.-Y., Yeung, R. W. and Cai, N., 2003. Linear network coding. *IEEE Transactions on Information Theory*, 49(2), pp. 371-381. IEEE.

Lochert, C., Scheuermann, B., Caliskan, M. and Mauve, M., 2007. The feasibility of information dissemination in vehicular ad-hoc networks. In: *2007 Fourth Annual Conference on Wireless on Demand Network Systems and Services*, Oberguyrgl, 2007, pp.92-99. doi: 10.1109/WONS.2007.340478

Maia, G., Rezende, C, Villas A.L. and Loureiro, A., 2013. Traffic Aware Video Dissemination over Vehicular Ad Hoc Networks. In: The 16th ACM International Conference on Modeling, Analysis & Simulation of Wireless and Mobile Systems, At Barcelona, Spain pp.419-426. doi: 10.1145/2507924.2507962

Myllyniemi, M., Vehkapera, J. and Peltola, J., 2007. Fuzzy Logic-based Cross-layer Controller for Wireless Video Transmission. In: *Computers and Communications, 2007. ISCC 2007. 12th IEEE Symposium on*, Santiago, Portugal, 2007, pp.21-26. doi: 10.1109/ISCC.2007.4381641

Nakorn, K. N. and Rojviboonchai, K., 2013. DECA-bewa: Density-Aware Reliable Broadcasting Protocol in VANETs. *IEICE transactions on communications*, 96(5), pp.1112-1121.

OMNeT++, 2011. *OMNeT++ Simulator.*

Osafune, T., Lin, L. and Lenardi, M., 2006. Multi-hop vehicular broadcast (MHVB). In: *2006 6th International Conference on ITS Telecommunications.* Chengdu, 2006, pp.757-760. doi: 10.1109/ITST.2006.289011

Park, J.-S.et al., 2006. *Emergency related video streaming in VANET using network coding.* UCLA CSD Technical Report, pp.102-103.

Pedestrian and Center, B. I., 2014. *Pedestrian and Bicyclist Crash Statistics. Final Report; Michigan Department of Transportation.*

Piñol, P., Torres, A., López, O., Martínez, M. and M. P. Malumbres, M.P., 2011. Evaluating HEVC video delivery in VANET scenarios. In: *Wireless Days (WD), 2013 IFIP*, Valencia, 2013, pp.1-6. doi: 10.1109/WD.2013.6686539

Puangpronpitag, S., Kasabai, P. and Suwannasa, A., 2013. Cross-layer optimization of Vehicle-to-Vehicle video streaming for overtaking maneuver assistance systems. In: *2013 Fifth International Conference on Ubiquitous and Future Networks (ICUFN)*, Da Nang, 2013, pp.345-349. doi: 10.1109/ICUFN.2013.6614839

Qadri, N. N., Fleury, M., Altaf, M. and Ghanbari, M., 2010. Multi-source video streaming in a wireless vehicular ad hoc network. *IET on Communications*, 4(11), pp.1300-1311.

Rezende, C., Almulla, M. and Boukerche, A., 2013. The use of Erasure Coding for video streaming unicast over Vehicular Ad Hoc Networks. In: *Local Computer Networks (LCN), 2013 IEEE 38th Conference on*, Sydney, NSW, 2013, pp.715-718. doi: 10.1109/LCN.2013.6761318

Rezende, C., Ramos, H.S., Pazzi, R.W., Boukerche, A., Frery, A.C. and Loureiro, A.A.F., 2012. *Virtus: A resilient location-aware video unicast scheme for vehicular networks.* 2012 *IEEE International Conference on Communications (ICC)*, pp.698-702. doi: 10.1109/ICC.2012.6364470

Ruder, M., Enkelmann, W. and Garnitz, R., 2002. Highway lane change assistant. In: *Intelligent Vehicle Symposium, 2002. IEEE*, 2002, pp. 240-244 vol.1. doi: 10.1109/IVS.2002.1187958

Shieh, W.-C., Sou, S.-I. and Tsai, S.-Y., 2011. A study of video frame sharing in sparse vehicular networks. In*: Parallel and Distributed Systems (ICPADS), 2011 IEEE 17th International Conference on*, Tainan, 2011, pp.444-448. doi: 10.1109/ICPADS.2011.15

Soldo, F., Casetti, C., Chiasserini, C.-F. and Chaparro, P., 2008. Streaming media distribution in VANETs. In: *IEEE GLOBECOM 2008 - 2008 IEEE Global Telecommunications Conference*, New Orleans, LO, 2008, pp.1-6. doi: 10.1109/GLOCOM.2008.ECP.126

Soldo, F., Casetti, C., Chiasserini, C. and Chaparro, P. A., 2011. Video streaming distribution in VANETs. *IEEE Transactions on Parallel and Distributed Systems*, 22(7), pp.1085-1091.

Sou, S.-I., Shieh, W.-C. and Lee, Y., 2011. A video frame exchange protocol with selfishness detection mechanism under sparse infrastructure-based deployment in VANET. In: *2011 IEEE 7th International Conference on Wireless and Mobile Computing, Networking and Communications (WiMob*. Wuhan, pp.498-504. doi: 10.1109/WiMOB.2011.6085347

Sullivan, G. J., Ohm, J., Han, W.-J. and Wiegand, T., 2012. Overview of the high efficiency video coding (HEVC) standard. *IEEE Transactions on Circuits and Systems for Video Technology*, 22(6), pp.1649-1668.

Takai, M., Martin, J. and Bagrodia, R., 2001. Effects of wireless physical layer modeling in mobile ad hoc networks. In: *MobiHoc '01: Proceedings of the 2nd ACM international symposium on Mobile ad hoc networking & computing*

Tal, I. and Muntean, G., 2012. User-oriented cluster-based solution for multimedia content delivery over VANETs. In: *IEEE international Symposium on Broadband Multimedia Systems and Broadcasting*, Seoul, 2012, pp.1-5. doi: 10.1109/BMSB.2012.6264290

Toledo-Moreo, R., Santa, J. and Zamora-Izquierdo, M., 2009. *A Cooperative Overtaking Assistance System.* pp.50-56.

Tonguz, O. K. and Boban, M., 2010. Multiplayer games over vehicular ad hoc networks: A new application. *Ad Hoc Networks.* Elsevier, 8(5), pp.531-543.

Tripp-Barba, C., Urquiza-Aguiar, L., Igartua, M.A., Rebollo-Monedero, D., de la Cruz Llopis, L.J., Mezher, A.M. and Aguilar-Calderón , J.A., 2014. A Multimetric, Map-Aware Routing Protocol for VANETs in Urban Areas. *Sensors*, 14(2), pp.2199-2224.

VANETMobiSim, 2014. *Mobility Model.*

Venkataraman, H., D'Ussel, A., Corre, T., Muntean, C.H. and Muntean, G.-M.,, 2010. Performance analysis of real-time multimedia transmission in 802.11 p based multihop hybrid vehicular networks. In: *Proceedings of the 6th International Wireless Communications and Mobile Computing Conference.* ACM, New York, pp. 1151-1155. doi: 10.1145/1815396.1815660

Vinel, A., Belyaev, E., Egiazarian, K. and Koucheryavy, Y., 2012. An overtaking assistance system based on joint beaconing and real-time video transmission. *IEEE Transactions on Vehicular Technology*, 61(5), pp.2319-2329.

Wang, Y., Reibman, A. R. and Lin, S., 2005. Multiple description coding for video delivery. *Proc. of IEEE,* 93(1), pp.57-70.

Whaiduzzaman, M., Sookhak, M., Gani, A. and Buyya, R., 2014. A survey on vehicular cloud computing. *Journal of Network and Computer Applications*, Elsevier, 40(2), pp.325-344..

Wired, 2014. *Feds Will Require All New Vehicles to Talk to Each Other*. [Online] Available at <https://www.wired.com/2014/02/feds-v2v/>

Wu, H. and Ma, H., 2013. CAVD: A Traffic-Camera Assisted Live Video Streaming Delivery Strategy in Vehicular Ad Hoc Networks. In: *2013 IEEE 10th International Conference on Mobile Ad-Hoc and Sensor Systems*. Hangzhou, 2013, pp.379-383. doi: 10.1109/MASS.2013.55

Xie, F., Hua, K.A., Wang, W. and Ho, Y.H., 2007. Performance study of live video streaming over highway vehicular ad hoc networks. In: 2007 IEEE 66th Vehicular Technology Conference, Baltimore, MD, 2007, pp. 2121-2125. doi: 10.1109/VETECF.2007.445

Xing, M. and Cai, L., 2012. Adaptive video streaming with inter-vehicle relay for highway VANET scenario.In: *The 2012 IEEE International Conference on Communications (ICC).* Ottawa, ON, 10-15 June, pp. 5168-5172. doi: 10.1109/ICC.2012.6364143

Xu, C., Zhao, F. Guan, J, Zhang, H. and Muntean, G.M.., 2013. QoE-driven user-centric VoD services in urban multihomed P2P-based vehicular networks. *IEEE Transactions on Vehicular Technology*, 62(5), pp.2273-2289.

Xu, S., Zhou, H., Yu, Z. and Zhang, S., 2012. Simulated study on video communication over VANET. In: *Word Automation Congress (2012).* Puerto Vallarta, Mexico, 24-28 June, pp.221-225,

Yasmeen, F. et al., 2015. A Message Transfer Framework for Enhanced Reliability in Delay-Tolerant Networks. *Network Protocols and Algorithms*, 7(3), pp.52-88.

Zeadally, S., Hunt, R., Chen, Y.-S, Irwin, A. and Hassan, A., 2012. Vehicular ad hoc networks (VANETS): status, results, and challenges. *Telecommunication Systems.* Springer, 50, pp.217-241.

Zeng, X., Bagrodia, R. and Gerla, M., 1998. GloMoSim: a library for parallel simulation of large-scale wireless networks. In: *Twelfth Workshop on Parallel and Distributed Simulation, 1998. PADS 98. Proceedings.* Banff, Alta., 1998, pp.154-161.

Kinetics Study of the Formation of Pyrmidine Thione from the Reaction of 2,6-Dibenzylidinecyclohexanone and its Derivatives with Thiourea

Kosrat N. Kaka[1, 2], Abdulmajeed M. Dabbagh[1] and Wali M. Hamad[2]

[1] Department of Chemistry, Mosul University – F.R. Iraq

[2] Department of Chemistry, Koya University
Daniel Mitterrand Boulevard, Koya KOY45, Kurdistan Region – F. R. Iraq

***Abstract*—Kinetics of the addition of thiourea to 2,6-dibenzylidenecyclohexanone and its derivatives have been studied. The reaction is found as a pseudo-first order process which includes a nucleophilic attack by thiourea at the carbonyl group of the ketone system to produce the heterocyclic pyrimidine thione "thiopyrimidine" (Claisen route mechanism). The effect of the substituents at the para position of the 2,6-dibenzylidenecyclohexanone and its derivatives on the rate of reaction, at different temperatures, is studied. Arrhenius parameters, entropies, enthalpies and free energies of activations are estimated. A suitable mechanism, which is correspondent with the results and with Claisen routes mechanism, is suggested for this reaction.**

***Index Terms*—2,6-dibenzylidenecyclohexanone and its derivatives, mechanism route, kinetics study, thiourea, thiopyrimidine.**

I. Introduction

Thiopyrimidine derivatives are widely used as anticancer agents. They can be synthesized from the reaction of the phenyl thiourea and ethylcyanoacetate with aromatic aldehydes in ethanol to give a thiopyrimidine carbonitrile, as in the following reaction:

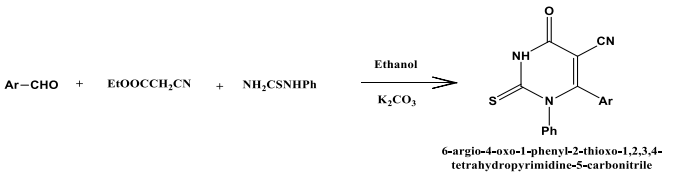

6-argio-4-oxo-1-phenyl-2-thioxo-1,2,3,4-tetrahydropyrimidine-5-carbonitrile

Thiopyrimidine carbonitrile, in turn, converts to a new derivative of thiopyrimidine which can also be used as anticancer precursor (El-Ansary, et al., 2015).

A considerable attention has been paid concerning the reactivity of carbonyl compound towards the addition of nucleophiles. Several factors influence the overall rate of reaction under various conditions. Among the crucial factors are structural features of the carbonyl compound, and the nature of the nucleophile, (Brown, Wheeler and Ichikawa, 1957; Clayden, et al., 2001). Another kinetic study was performed on condensation reaction of thiourea with substituted aldehyde to give Schiff-base compounds/ complexes. The rate constants of the reaction of Schiff-bases with Maleic acid, Succinic acid and Phthalic anhydride were studied and showed that the reaction was of first-order (Al-Hadithi, Al-Rawi and Al-Hity, 2007).

The present study is concerned with the kinetics of the formation of pyrimidine thione and its derivatives and to find out the electronic effect of substituents on the reaction rates and on the stability of the presumed activated complexes. The attained information was of great assistance in postulation of the mechanism which occurs under mild experimental conditions.

II. Experimental Part

The kinetic studies were monitored by uv-visible spectrophotometric method at fixed wavelengths. Agilent Cary-100 uv-visible was used to monitor the disappearance of the 2,6-dibenzylidenecyclohexanone and its derivatives under study at constant temperature with ± 0.01% ^{o}C, using a temperature controller in conjunction with uv-visible

ARO-The Scientific Journal of Koya University
Volume IV, No 2(2016), Article ID: ARO.10142, 06 pages
DOI: 10.14500/aro.10142
Received 05 December 2015; Accepted 28 September 2016
Regular research paper: Published 03 December 2016
Corresponding author's e-mail: kosrat.nazad@koyauniversity.org

http://dx.doi.org/10.14500/aro.10142

spectrophotometer. The kinetic runs were carried out using multicell holder at fixed $\lambda max = (339.00 - 364.00\, nm)$. Quickfit quartz cuvettes type (Q) were used. A working solution containing 0.1 M of thiourea and 2×10^{-4} M of 2,6-dibenzylidenecyclohexanone and its derivatives in dimethyl sulfoxide (DMSO) and absolute ethanol as solvent in strong basic medium ($pH \geq 12$) was used. A blank cell containing the same reaction medium except 2,6-dibenzylidenecyclohexanone and its derivatives was also used. All kinetic data were processed on computer programs using Microsoft Excel 2010 and Sigma Plot 11.0.

III. Results and Discussion

The kinetics of the reaction between thiourea and 2,6-dibenzylidenecyclohexanone and its derivatives in DMSO as a solvent and in basic medium of sodium ethoxide to form the thiopyrimidine have been studied. The reaction was found to be relatively slow, when monitored at a temperature range between (308.15-328.15)K; second order, presumably first order with respect to each of reactants (thiourea and 2,6-dibenzylidenecyclohexanone and its derivatives) when using 1:1 mixing mole ratio of reactants. The study also showed a pseudo first order decrease of the concentration of the 2,6-dibenzylidenecyclohexanone as shown in the Fig. 1., at 318.15 K, using a mole ratio of 1:500 (2,6-dibenzylidenecyclohexanone: thiourea). The decrease in concentration of 2,6-dibenzylidenecyclohexanone was monitored at different intervals and at fixed $\lambda max = (352.00\, nm)$.

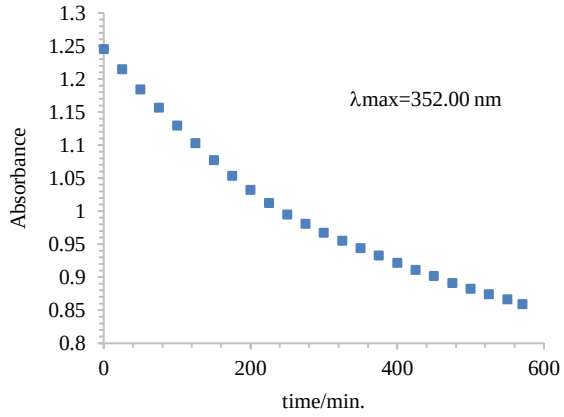

Fig. 1. Decrease of the concentration of 2,6-dibenzylidenecyclohexanone at different time at 318.15K.

At this wave length the monitored parent reactant neither interfered with thiourea $\lambda max = (264.00\, nm)$, nor with any of thiopyrimidine (product), $\lambda max = (263.00\, nm)$, and sodium ethoxide in ethanol, $\lambda max = (203.00\, nm)$ as shown in Fig. 2.

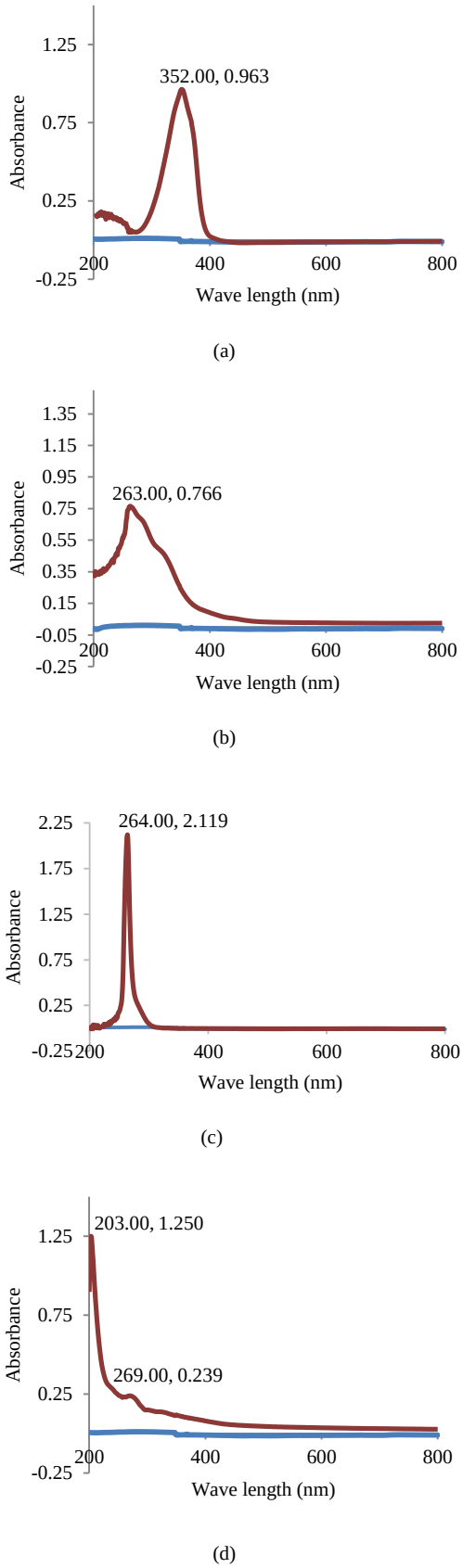

Fig. 2. Full spectra of individual reactants, product and used solvent; (a) λmax 2,6-dibenzylidenecyclohexanone in DMSO, (b) λmax thiopyrimidine-H product in DMSO, (c) λmax thiourea in DMSO and (d) λmax sodium ethoxide in ethanol.

The reaction was also monitored using a full scan uv-visible spectrum. No other products or side reactions were noticed and A∞ of the 2,6-dibenzylidenecyclohexanone and its derivatives was always approached to zero showing that no equilibrium process did ever exist. The products structure was confirmed by IR (Jihad, 2011) and (H^1, C^{13})-NMR (Appendix A). These observations suggest that the addition reaction proceeds clearly according to the simple stoichiometry of the reaction below:

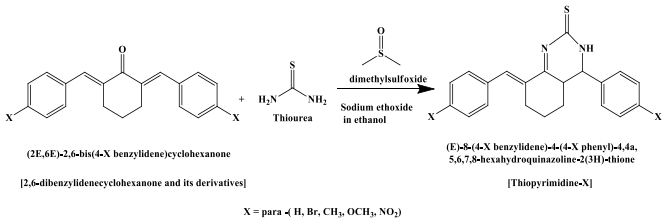

Typical runs found that the parent reactant or any of its derivatives follows the pseudo first order equation in terms of absorption functions at different temperatures [ln(A∞ − Ao)/(A∞ − At) vs. time]. The plots were found as linear for at least 90% of reactions.

$$ln(A\infty - Ao) \,/\, (A\infty - At) \;=\; kobs.t \qquad (1)$$

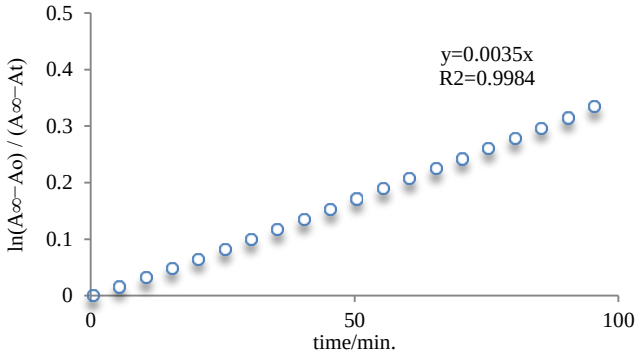

Fig. 3. Pseudo first order plot for the decrease in concentration 2,6-dibenzylidenecyclohexanone at 318.15K.

The results are shown in Table I.

TABLE I
OBSERVED RATE CONSTANTS FOR THE REACTION OF DIFFERENT 2,6-DIBENZYLIDENECYCLOHEXANONE AND ITS DERIVATIVES WITH THIOUREA AT DIFFERENT TEMPERATURES

Temp./ °K	10^5 kobs. / s^{-1}				
	p-H	p-Br	p-CH_3	p-OCH_3	p-NO_2
308.15	3.30±0.03	7.70±0.02	10.00±0.07	13.00±0.83	39.50±1.53
313.15	4.70±0.18	9.00±0.35	13.30±0.27	20.20±1.02	42.80±1.78
318.15	5.80±0.19	11.50±0.09	16.70±0.61	29.50±0.88	47.50±1.43
323.15	8.30±0.25	15.00±0.31	23.30±1.42	38.30±0.96	51.70±1.09
328.15	10.0±0.16	17.50±0.37	33.30±2.32	----------	55.00±1.04

Arrhenius plots (Dabbagh, 2010) were performed for all reactions; energies of activation, A-factors and entropies of activation at (318.15) K, were estimated as a listed in Table II:

TABLE II
ARRHENIUS PARAMETERS AND ENTROPIES OF THE ACTIVATION FOR THE REACTIONS OF DIFFERENT 2,6-DIBENZYLIDENECYCLOHEXANONE AND ITS DERIVATIVES WITH THIOUREA.

Compounds	E_a / kJ .mol^{-1}	A / s^{-1}	$\Delta S^{\#}$ / J.K^{-1}. mol^{-1}	$\Delta G^{\#}$ / kJ.mol^{-1}	R^2
diarylidene- H	46.6864	2.809×10^3	-187.7566	106.4212	0.9927
diarylidene-Br	36.2989	1.070×10^2	-214.9250	104.6773	0.9912
diarylidene-CH_3	49.7743	2.677×10^4	-169.0118	103.5454	0.9900
diarylidene-OCH_3	60.0404	2.051×10^6	-132.9374	102.3344	0.9908
diarylidene- NO_2	14.2826	1.045×10^{-1}	-272.5510	100.9947	0.9956

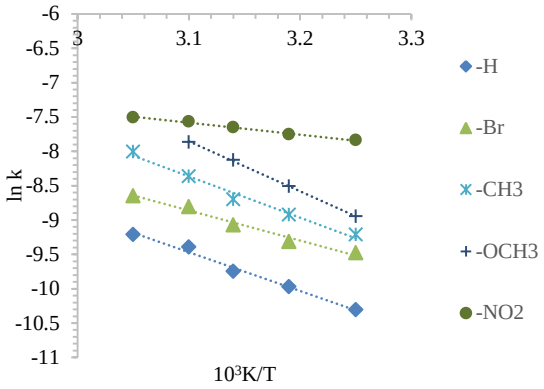

Fig. 4. Arrhenius plot for the reaction of different 2,6-dibenzylidenecyclohexanone and its derivatives with thiourea at different temperatures.

The electronic effects of all substituents at both sides of the 2,6-dibenzylidenecyclohexanone and its derivatives molecule play an important role on affecting the rate of reaction, since they either enrich or pauperize the reaction center at the α, β unsaturated system with electrons. The differences in rates were found to be in the following order at all reaction.

$$p\,p' - NO2 > \; p\,p' - OCH3 > \; p\,p' - CH3 > \; p\,p' - Br \; > \; p\,p' - H$$

This sequence of arrangements indicates that electronic effects play important role in enhancing or reducing the rate of reaction in comparison with the parent 2,6-dibenzylidenecyclohexanone. The p-OCH_3 and p-CH_3 groups which are electron donating groups (Dabbagh, et al., 2012), enrich the reaction center with electron density and increase the repulsive forces with thiourea nucleophile. As a result, the rate of reaction is reduced (Table I). On the other hand, electron withdrawing group such as p-NO_2 reduce the electron density at the reaction center resulting in partial positive reaction center, thus providing a better chance for thiourea nucleophile to attack, resulting a relative acceleration of reaction rate (Dabbagh and Al-Gwari, 2013).

It is concluded, from these observations, that the condensation process of the various 2,6-dibenzylidenecyclohexanone and its derivatives with thiourea proceeds via a nucleophilic addition reaction mechanism.

The values of the activation parameters are also important to discern the mechanism under all studied circumstances. The

 http://dx.doi.org/10.14500/aro.10142

activation energies for all reactants in the range between (14-60) kJ/mole. The variation in values may be attributed to the electron donating or withdrawing capabilities of the attacking group. These values come in the line with as discussed above, i.e. fast reaction requires low activation energy and vice versa, as in the following sequence:

$$p-NO2 > p-Br > p-H > p-CH3 > p-OCH3$$
Increase of the energy of activation

This observation is also explicable with the attack of the nucleophile to the partially positive reaction center. It is noticed that the values of E_a for the p-Br substituent and the parent 2,6-dibenzylidenecyclohexanone are very close to each other, this is unsurprising since the bromo group carriers dual donating and withdrawing character at the same time (Haji, 2013).

The entropies of activation $\Delta S^{\#}$, which are related to A-factor (Table II), are all largely negative values, indicating the formation of a restricted high polar transition state which suffers from lack of certain degrees of freedom as compared to the reactants (Dabbagh, Al-hamdany and Al-Sabawi, 2012). The decrease in the values of A-factor and correspondingly to ΔS# provides an important indication about the stability of the transition state and hence gives good support for explaining the reason of the differences in the values of rate constants. Again, it can be clearly discerned the effect of electronic properties of the different substituents on the transition state by noting the differences in $\Delta S^{\#}$ value for the p-NO_2 which is much lower than others due to the decrease of electron density at the reaction center leading to the formation of a highly oriented stable transition state. In contrast, the highest $\Delta S^{\#}$ value for the p-OCH_3 may be attributed to destabilized transition state since it enriches the reaction center with electron density. The –ve values of $\Delta S^{\#}$ thus suggested the formation of a restricted transition state which may occur via a cyclization process.

The values of the free energies of activation in Table II show a relative constancy for all reacting 2,6-dibenzylidenecyclohexanone and its derivatives. These results indicated that all the corresponding reactants were operative in similar mechanistic routes (Rajalakshmi and Ramachandramoorthy, 2013).

From these investigations it can be concluded that electronic effect plays an important role in the stabilization of the formed transition state. Also the reaction of the 2,6-dibenzylidenecyclohexanone and its derivatives with the thiourea nucleophile proceeds via the formation of a relatively slow step with adequate activation energies (Al-Hamdany, Dabbagh and Shareef, 2012).

The values of rate constants, Arrhenius parameters, $\Delta G^{\neq}$ and also the –ve values of $\Delta S^{\#}$ are all in quite agreement with the following mechanistic Claisen-routes steps:

First step: A fast nucleophilic attack by thiourea to the carbonyl group of the α, β unsaturated carbonyl system followed by proton transfer from nitrogen to form OH group as at the followings:

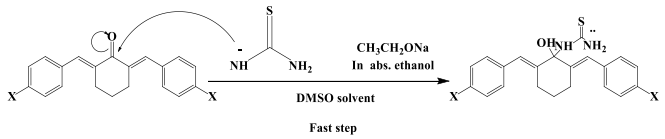

Second step: A fast step corresponding to a loss of water molecule to form a double bond:

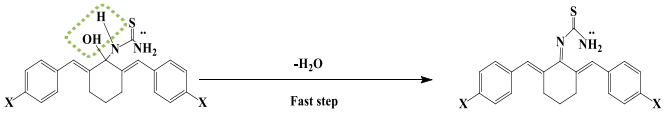

Final slow step: corresponds to a unimolecular cyclization process resulted by the intramolecular nucleophilic attack by the primary amine group of the thiourea side molecule to form the thiopyrimidine (keto-enol) product.

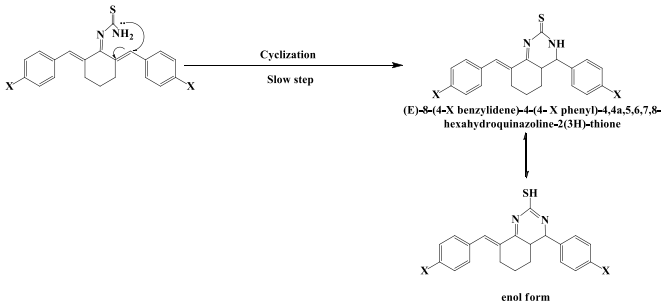

IV. Conclusion

In this paper we have studied the kinetics and the detailed mechanism of the reaction of para substituted 2,6-dibenzylidenecyclohexanone and its derivatives with thiourea in order to produce the corresponding thiopyrimidine. The reaction is a first order with both reactants. The low values of A-factor and correspondingly the negative values of $\Delta S^{\neq}$ provided a support to the restricted activated complex which lacked some degrees of freedom in the slow step. The order of reactivities with para substituents is;

$(p-NO2 > p-Br > p-H > p-CH3 > p-OCH3)$

and this supported the availability of electron density at the reaction center. The relative constancy of $\Delta G^{\neq}$ values indicated that the reaction of all the substituted 2,6-dibenzylidenecyclohexanone and its derivatives is operative in the same mechanism.

Acknowledgment

We offer our affection, appreciation and indebtedness to Koya University, Faculty of Science and Health, namely; Department of Chemistry, for their help in the practical part of the research in chemistry laboratories.

References

Al-Hadithi, M.A., Al-Rawi, K.F., AL-Hity, W.F., 2007. Synthesis, Characterization and Kinetic studies of Some Oxazepine and Oxazepane Derivatives. *J. of Al-Anbar University for Pure Science*, 1(3), p.19 pages.

Al-Hamdany, A.J., Dabbagh, A.M. and Shareef, O.A., 2012. Synthesis of Spiropyrrolidines via 1, 3 Anionic Cycloaddition. *Raf. J. Science*, 23(3), pp.94-105.

Brown, H.C., Wheeler, O.H. and Ichikawa, K., 1957. ketones, Chemical effects of steric strains—XIII: Kinetics of the reaction of sodium borohydride with carbonyl groups—a convenient tool for investigating the reactivities of aldehydes. *Tetrahedron*, 1(3), pp.214-220.

Clayden J., Greeves N., Warren S. and Wothers P., 2001. *Organic Chemistry*. Oxford edition, pp.234-237.

Dabbagh, A.M., 2010. *Chemical Kinetics*. Baghdad (2263): University of mosul (Ibn Ether Publisher).

Dabbagh, A.M. and Al-Gwari, S.S., 2013. Kinetics and Mechanistic Studies of the Bromination of some Derivatives of 1,3-diaryl-2-propen-1-one. *Raf. J. Science*, 24(1), pp.50-59.

Dabbagh, A.M., Al-Hamdany, A.J. and Al-Sabawi, A.H., 2012. Kinetics and Mechanistic Studies of the Bromination of some Substituted 2-Benzylidene-1, 3-indandione. *Raf. J. Sci*., 23(4), pp.83-92.

Dabbagh, A.M., Al-Hamdany, A.J., Shareef, O.A. and Al-Assaf, S., 2012. Kinetic studies of the formation of number of spiropyrrolidines. *Raf. J. Sci*., 23(3), pp.58-77.

El-Ansary, A.K., Mohamed, N.A., Mohamed, K.O., Abd-Elfattah, H.M. and El-Manawaty, M., 2015. A Simple and Convenient Synthesis of Novel Thiopyrimidine Derivatives as Anticancer Agents. *Research Journal of Pharmaceutical, Biological and Chemical Science*, 6(4), pp.1745-1752.

Haji K.A., 2013. Kinetics and mechanistic studies on the formation of some chalcones in different solvents and their reactions with bromine and hydrazine, PhD Thesis, Erbil: Salahaddin University, pp.169-170.

Jihad T.W., 2011. Synthesis and Antibacterial Evaluation of Some New Fused Cyclic Sulfoxides. *Raf. J. Sci*., 22(4), pp.62-74.

Rajalakshmi K. and Ramachandramoorthy T., 2013. Oxidation of Chalcones by Morpholinium Chlorochromate with Oxalic Acid as Catalyst: Kinetic and Mechanistic Study. *Journal of Chemistry, Hindawi Publishing Corporation*, Vol. 2013, p.5 pages.

APPENDIX A

IR, UV and (H^1, C^{13})-NMR of fused pyrimidine thiones:

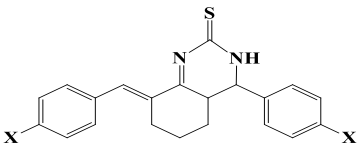

TABLE A-I
IR, AND UV-VISIBLE SPECTROPHOTOMETER FOR THE PRODUCTS OF FUSED PYRIMIDINE THIONE

Compounds Name	I.R. (KBr), υ (cm^{-1})										UV (DMSO solvent) λmax (nm)
	C≡C	C-H	C=N	C=C	N-H	C-O-C	C-Br	C-NO_2	C-C	C=S	
8-benzylidene-4-phenyl-4,4a,5,6,7,8-hexahydroquinazoline-2(3H)-thione	1539	1028	1623	1601	3199	------	------	------	------	1188	263
8-(4-bromobenzylidene)-4-(4-bromophenyl)-4,4a,5,6,7,8-hexahydroquinazoline-2(3H)-thione	1528	1071	1678	1589	3393	------	625	------	------	1011	264
8-(4-methylbenzylidene)-4-(p-tolyl)-4,4a,5,6,7,8-hexahydroquinazoline-2(3H)-thione	1539	1114	1647	1611	3188	------	------	------	951	1018	269
8-(4-methoxybenzylidene)-4-(4-methoxyphenyl)-4,4a,5,6,7,8-hexahydroquinazoline-2(3H)-thione	1539	1113	1636	1607	3208	2835	------	------	------	1028	284
8-(4-nitrobenzylidene)-4-(4-nitrophenyl)-4,4a,5,6,7,8-hexahydroquinazoline-2(3H)-thione	1516	1107	1644	1593	3321	------	------	1344	------	1017	272

 http://dx.doi.org/10.14500/aro.10142

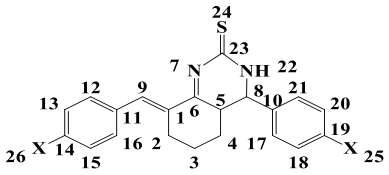

TABLE A-II
H^1-NMR FOR PRODUCTS OF PYRIMIDINE THIONE

Compounds Name	H^1-NMR (DMSO), ppm						
	H2, H22	H3, H4	H5	H8	H9	Ar-H	Others
8-benzylidene-4-phenyl-4,4a,5,6,7,8-hexahydroquinazoline-2(3H)-thione	2.800 3H, m	1.629 4H, m	2.267 1H, q	3.562 1H, d	6.476 1H, s	7.519 5H, m	------
8-(4-bromobenzylidene)-4-(4-bromophenyl)-4,4a,5,6,7,8-hexahydroquinazoline-2(3H)-thione	2.759 3H, m	1.448 4H, m	2.160 1H, q	3.294 1H, d	6.318 1H, s	7.606 5H, m	------
8-(4-methylbenzylidene)-4-(p-tolyl)-4,4a,5,6,7,8-hexahydroquinazoline-2(3H)-thione	2.800 3H, m	1.529 4H, m	2.267 1H, q	3.362 1H, d	6.476 1H, s	7.519 5H, m	Ar-CH_3 (2.350)6H,s
8-(4-methoxybenzylidene)-4-(4-methoxyphenyl)-4,4a,5,6,7,8-hexahydroquinazoline-2(3H)-thione	2.753 3H, m	1.201 4H, m	2.256 1H, q	3.334 1H, d	6.617 1H, s	7.885 5H, m	Ar-OCH_3 (3.778)6H,s
8-(4-nitrobenzylidene)-4-(4-nitrophenyl)-4,4a,5,6,7,8-hexahydroquinazoline-2(3H)-thione	3.003 3H, m	1.454 4H, m	2.264 1H, q	4.026 1H, d	6.585 1H, s	7.965 5H, m	--------

TABLE A-III
C^{13}-NMR FOR PRODUCTS OF PYRIMIDINE THIONE

Compounds Name	C^{13}-NMR (DMSO), ppm									
	C1	C2	C3, C4	C5	C6	C8	C9	C23	Ar-C	Ar-C-X
8-benzylidene-4-phenyl-4,4a,5,6,7,8-hexahydroquinazoline-2(3H)-thione	128.160	27.325	25.011	39.115	167.373	58.287	129.271	183.970	137.362	---
8-(4-bromobenzylidene)-4-(4-bromophenyl)-4,4a,5,6,7,8-hexahydroquinazoline-2(3H)-thione	124.362	26.854	24.012	39.154	165.013	54.227	127.490	181.033	132.590	---
8-(4-methylbenzylidene)-4-(p-tolyl)-4,4a,5,6,7,8-hexahydroquinazoline-2(3H)-thione	126.737	27.085	22.386	39.098	161.023	57.127	129.252	183.614	133.644	-CH_3 21.367
8-(4-methoxybenzylidene)-4-(4-methoxyphenyl)-4,4a,5,6,7,8-hexahydroquinazoline-2(3H)-thione	127.572	28.131	23.083	39.089	160.341	59.264	129.846	188.929	132.392	-OCH_3 54.905
8-(4-nitrobenzylidene)-4-(4-nitrophenyl)-4,4a,5,6,7,8-hexahydroquinazoline-2(3H)-thione	126.726	27.789	22.397	39.298	161.712	58.033	129.409	183.013	133.852	---

Application of Random Amplified Polymorphic DNA Markers for Genetic Diversity Assessment of Pomegranate (*Punica granatum* L.) Cultivars in Duhok Governorate – Kurdistan of Iraq

Dalal Y. Sinjare, Sabrya J. Zubair, Avesta M. Ali, and Jaladet M. S. Jubrael

Department of Scientific Research Center, College of Science, University of Duhok, Kurdistan Region, Iraq

***Abstract*–Random amplified polymorphic DNA (RAPD) markers were used to investigate the genetic diversity among 13 cultivars of pomegranate cultivated in Duhok governorate, Kurdistan region/Iraq. Unweighed pair-group method average clustering divided the 13 cultivars into three main groups. In RAPD analysis, 12 out of 30 employed random primers showed good amplification and polymorphism on pomegranate samples with a total of 107 bands. The percentage of polymorphic DNA bands ranged from 66.6% (OPX-17) to 100% (OPO-07, OPS-17, and OPE-18, OPP-02, OPK-08, OPL-17, and OPR-01) with an average of polymorphic rate of 94.39. According to matrix coefficient, the lowest genetic similarity was observed between Soormiz and Rash Dendikheer (0.1065). The Dereger and Kapepan populations were most similar ones with coefficient of 0.9374.**

***Index Terms*—Genetic diversity, Random amplified polymorphic DNA markers, Pomegranate.**

1. Introduction

The pomegranate (*Punica granatum* L.) is a woody perennial shrub or small tree (Shahbaz, 2010). It is an edible fruit tree and has been known as the richest dietary sources of antioxidant phenolics and anthocyanins. There is a wide variation among pomegranate genotypes in terms of these compounds (Ozgen, et al., 2008).

Pomegranate is a suitable crop for cultivation in arid and semi-arid regions it has also been considered as an important commercial fruit crop and is extensively cultivated in parts of Asia, North Africa, the Mediterranean, and the Middle East (Sarkhosh, et al., 2006). The origin of pomegranate is considered to be in central of Asia (Harlan, 1992), from where it has spread to the rest of the world (Levin, 1994; Verma, et al., 2010).

Using a sensitive and credible molecular, such as amplified fragment length polymorphism (AFLP), simple sequence repeat, and inter-SSR to detect the DNA variation and to identify the pomegranate germplasm, have become increasingly important way to help breeders and nurserymen with the selection and propagation of a cultivar (Nemati, et al., 2012).

The random amplified polymorphic DNA (RAPD) marker has been used to identify genetic diversity of many different plant species; the use of this reliable marker in pomegranate is limited (Dalal, 2013). The objective of this study is to characterize 13 pomegranate cultivars from the Duhok governorate in Kurdistan region/Iraq by RAPD markers, which will help breeders in parental selection in a pomegranate cultivar-breeding program.

II. Materials and Methods

A. Plant Material

Thirteen different cultivars of pomegranate were selected in Duhok governorate Kurdistan/Iraq. The cultivars names were Soormiz, Rash Dendikheer, Trshigalak, Trshinagala, Dereger, Shreennavekraq, Msafik, Mlese, Melsesharman, Nana (roman Zena), Kapepan, Zaxoly, and Henarok.

B. DNA Extraction and RAPD Analysis

DNA from fresh leaves was extracted following the protocol of Weigand, et al. (1993) using cetyltrimethyl ammonium bromide Protocol. The quantity and quality of isolated genomic DNA was determined using agarose gel (1% [w/v]) electrophoresis and a nanodrop spectrophotometer.

An initial screening with 30 primers (10-mers) from the kits OPA, from Operon Technologic was carried out.

ARO-The Scientific Journal of Koya University
Volume IV, No 2(2016), Article ID: ARO.10078, 4 pages
DOI: 10.14500/aro.10078
Received 17 April 2015; Accepted 26 October 2016
Regular research paper: Published 23 December 2016
Corresponding author's e-mail: avesta.ali@uod.ac

http://dx.doi.org/10.14500/aro.10078

12 informative primers were selected due to their ability to produce polymorphic, unambiguous and stable RAPD markers (Table I).

RAPD amplification was performed in a 25 µl reaction volume containing 50-100 ng genomic DNA, ×10 buffer (10 mM Tris-Hcl. pH 8.3, 50 mM KCl. 2 mM MgCl), 2.5 mM dNTPs, 10 pMOL of single 10-base primer and 1U *Taq* DNA polymerase (Sigma, USA). The thermocycler was programed as follows; initial cycle of 5 min at 94°C followed by 40 cycles of 1 min at 94°C, an annealing temperature of 36°C for 1 min, extension step of 2 min at 72°C, and a final extension step of 10 min at 72°C. Polymerase chain reaction products were separated by gel electrophoresis on 2% agarose gels with ×1 Trisma base, boric acid, ethylenediaminetetraacetic acid buffer, at 70 V/cm for 2 h. The gel was stained with 0.25 µg/ml ethidium bromide and stained gels were visualized by ultraviolet transilluminator and photographed. The molecular weights of bands were estimated using standard molecular markers.

C. Data Analysis

Data were recorded as discrete variables: 1 for the presence and 0 for the absence of a similar band. Only intense and reproducible bands appearing on the gel were scored. The data then entered into NTSYS-PC (Numerical Taxonomy and Multivariate Analysis System), Version 2.1 (Applied Biostatistics) program (Rohlf, 1993) using the program editor. The data were analyzed using Similarity for Qualitative Data routine to generate genetic similarity index (Nei and Li, 1979).

III. Result and Discussion

Thirteen selected cultivars were genotyped by RAPD markers. 12 informative primers were selected due to their ability to produce polymorphic RAPD markers (Fig. 1).

The range of the dissimilarity matrix obtained varied between 0.106 and 0.937 (Table II); the lowest genetic similarity was observed between Soormiz and rash Dendikheer cultivars (0.106) suggesting their close relatedness. The Dereger and Kapepan cultivars were most similar ones with coefficient of 0.937. The remaining cultivars shared intermediate genetic distance values. Low genetic distances between cultivars supported the inbreeding and low levels of genetic variation.

Genetic distances based on RAPD data and supported by the resulting dendrogram shown in Fig. 2. Three main groups could be identified. The first one is made up of the following cultivars, soormiz, rash Dendikheer, Dereger, Shreennafikreq, Zaxoly, Henarok, and Trshigalak. The second group consisted of Trshinegalak, Mlese, Melse Shaman and Msafik. The third group concluded of nano (romanzena) and Kapepan. The level of the genetic diversity highly correlated with the sample size; therefore, it would be worth mentioning that the used sample size was small in this study. Furthermore, another reason for the low genetic diversity could be due to the vegetative propagation (Behzadi Shahrbabaki, 1997). The results of this study are also in agreement with other studies in the Tunisian pomegranate using the same marker such as RAPD (Hasnaoui, et al., 2010), or different markers such as AFLP (Jbir, et al., 2008).

These primers generated a total of 107 RAPD bands (Table III); the percentage of polymorphic DNA bands ranged from 66.6% (OPX-17) to 100% (OPO-07, OPS-17, OPE-18, OPP-02, OPK-08, OPL-17, and OPR-01) with an average of polymorphic rate of 94.39, indicating a high degree of polymorphism among these pomegranate cultivars,

TABLE I
Represent the Operon Primers and their Sequences

Primer name	Sequence '5-3'
OPE-18	GGACTGCAGA
OPH-07	CTGCATCGTG
OPK-08	GAACACTGGG
OPL-17	AGCCTGAGCC
OPO-07	CAGCACTGAC
OPP-02	TCGGCACGCA
OPP-04	GTGTCTCAGG
OPQ-05	CCGCGTCTTG
OPR-01	TGCGGGTCCT
OPS-17	TGGGGACCAC
OPV-19	GGGTGTGCAG
OPX-17	GACACGGACC

TABLE II
Present Genetic Dissimilar it Coefficient Matrix of the Some Cultivars of *P. granatum*

Soormiz	0.000				
Rash dendikheer	0.106	0.00			
Trshigalak	0.392	0.337	0.000		
Trshinagala	0.687	0.792	0.483	0.000	
Dereger	0.308	0.322	0.278	0.492	0.000
Shreennavekrq	0.217	0.223	0.337	0.560	0.147
Msafik	0.821	0.814	0.722	0.508	0.684
Mlese	0.660	0.676	0.670	0.309	0.570
Melsesharman	0.579	0.616	0.573	0.246	0.489
Roman zena	0.676	0.743	0.839	0.576	0.799
Kapepan	0.699	0.689	0.928	0.840	0.937
Zaxoly	0.351	0.389	0.448	0.502	0.330
Henarok	0.339	0.307	0.469	0.644	0.296

P. granatum: Punica granatum

TABLE III
Represent the Total Number of Bands, Number of Polymorphism, and Polymorphism Rate of Pomegranate Cultivars

Primer name	Total number of bands	Number of polymorphic bands	Polymorphic percentage
OPE-18	7	7	100
OPH-07	10	9	90
OPK-08	8	8	100
OPL-17	14	14	100
OPO-07	10	10	100
OPP-02	8	7	87.5
OPP-04	7	6	85.7
OPQ-05	7	6	85.07
OPR-01	11	11	100
OPS-17	12	12	100
OPV-19	10	9	90
OPX-17	3	2	66.6
Total	107	101	94.39

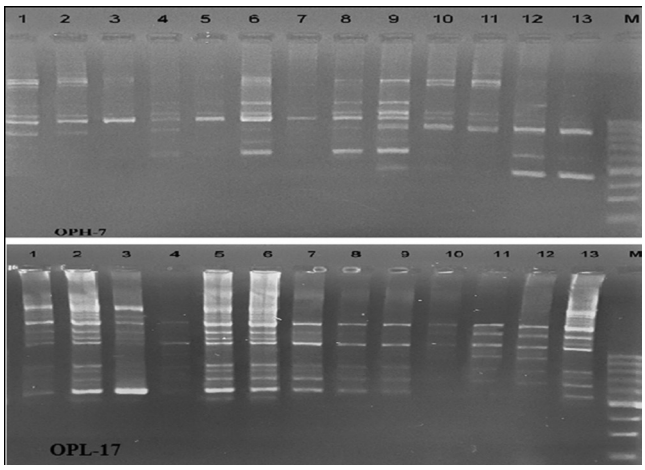

Fig. 1. Random amplified polymorphic DNA patterns representing examples of amplification produced using primers OPH-07 and OPL-17 performed on 2% agarose gel electrophoresis at 70 volt/cm for 2 h. Lane M represent λ DNA, Lanes 1 through 13 refer to pomegranate cultivars: Soormiz, Rash Dendikheer, Trshigalak, Trshinagala, Dereger, Shreennavekraq, Msafik, Mlese, Melsesharman, Nana (Roman Zena), Kapepan, Zaxoly, and Henarok

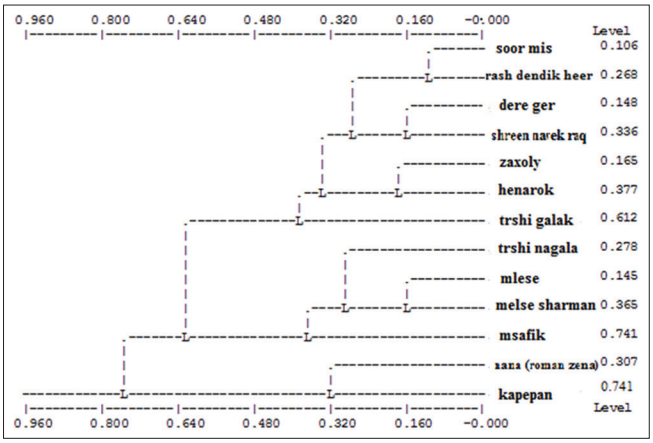

Fig. 2. A dendrogram neighbor joining tree representing the genetic relationships among pomegranate cultivars

which was greater than those reported for Iranian (Sarkhosh, et al., 2006; Zamani, et al., 2007) and Turkish (Durgac, et al., 2008) pomegranate cultivars, which were 57.3%, 57.0% and 22.0%, respectively, using RAPD markers.

The number of bands generated per primer was 8.92. In a study of Hasnaoui, et al. (2010), using four RAPD primers to estimate the genetic diversity among some pomegranate cultivars a total of 29 bands have been generated with a mean of 7.25 per primer.

Based on the pairwise analysis of the amplification products which been obtained with the 12 tested RAPD primers, all the tested pomegranate cultivars showed different relationships. Close genetic similarity was found in some of the cultivars analyzed as shown by high values of similarity index. This richness in genetic diversity could be the result of long-term evolution, and adapt to various environmental conditions (Ercisli, et al., 2011). However, RAPD marker revealed high genetic variability among pomegranate genotypes and it could be used for identification and characterization of pomegranate genotypes. In addition, complete comprehension of the genetic diversity within cultivars would contribute to a more efficient use of germplasm in plant breeding programs. Furthermore, it is essential to investigate other molecular markers linked closely to the morphological traits of pomegranate in the future. The *P. granatum* cultivars selected from Duhok governorate displayed very rich genetic variations.

IV. Conclusion

The results demonstrated that RAPD profiles are valuable tools with the great potential for classifications of pomegranate cultivars. In addition, complete comprehension of the genetic diversity within cultivars would contribute to a more efficient use of germplasm in plant breeding programs. Furthermore, it is essential to investigate other molecular markers linked closely to the morphological traits of pomegranate in the future.

V. Acknowledgment

The authors are thankful to the Scientific Research Center\ College of Science, University of Dohuk for providing all the necessary facilities for carrying out the study.

References

Behzadi Shahrbabaki, H., 1997. *Genetic Diversity of Pomegranate Genotypes in Iran*. Agriculture Education Publication, Karaj, Iran.

Dalal, Y.S., 2013. *Microsatellite Application and Genetic Characterization of Pomegranate (Punica granatum L.) in Duhok Province, Kurdistan region, Iraq*. MSc. Thesis. Duhok University.

Durgac, C., Ozgen, M., Simsek, O., Kacar, Y., Kiyga, Y., Celebi, S., Gunduz, K. and Serce, S., 2008. Molecular and pomological diversity among pomegranate (*Punica granatum* L.) cultivars in Eastern Mediterranean region of Turkey. *African Journal of Biotechnology,* 7, pp.1294-1301.

Ercisli, S., Agar, G., Yildirim, N., Duralija, B., Vokurka, A. and Karlidag, H., 2011. Genetic diversity in wild sweet cherries (*Prunus avium* L.) in Turkey revealed by SSR markers. *Genetics and Molecular Research,* 10, pp.1211-1219.

Harlan, J.R., 1992. *Crops and Man.* 2nd ed. American Society of Agronomy and Crop Science Society of America, Madison, WI. pp.289.

Hasnaoui, N., Mars, M., Chibani, J. and Trifi, M., 2010. Molecular polymorphisms in Tunisian pomegranate (*Punica granatum* L.) as revealed by RAPD fingerprints. *Diversity,* 2, pp.107-114.

Jbir, R., Hasanaoui, N., Mars, M., Marrakchi, M. and Trifi, M., 2008. Characterization of Tunisian pomegranate (*Punica granatum* L.) cultivars using amplified fragment length polymorphism analysis. *Scientia Horticulturae,* 115, pp.231-237.

Levin, G.M., 1994. Pomegranate (*Punica granatum*) plant genetic resources in Turkmenistan. *Plant Genetic Resource Newsletters,* 97, pp.31-36.

Nei, M. and Li., W.H., 1979. Mathematical model for studying genetic variation in terms of restriction endonucleases. *Proceedings of the National Academy of Sciences USA,* 76, pp.5269-5273.

Nemati, Z., Tehranifar, A., Farsi, M., Mirshamsi, K.A., Nemati, H. and Khayat, M., 2012. Evaluation of genetic diversity of Iranian pomegranate cultivars using fruit morphological characteristics and AFLP markers. *Notulae Botanicae Horti Agrobotanici Cluj,* 40(1), pp.261-268.

Ozgen, M., Durgac, C., Serce, S. and Kaya, C., 2008. Chemical and antioxidant properties of pomegranate cultivars grown in Mediterranean region of Turkey. *Food Chemistry,* 111, pp.703-706.

Rohlf, F.J. 1993. *NTSYS-PC Numerical Taxonomy and Multivariate Analysis System*. Vol. 11. Version 2. Exeter Software, Setauket, New York.

Sarkhosh, A., Zamani, Z., Fatahi, R. and Ebadi, A., 2006. *RAPD* markers reveal polymorphism among some Iranian pomegranate (*Punica granatum* L.) genotypes. *Scientia Horticulturae,* 111, pp.24-29.

Shahbaz, S.I., 2010. *Trees and Shrubs (A Guide of Trees and Shrubs of Kurdistan Region of Iraq)*. University Press, Duhok.

Verma, N., Mohanty, A. and Lal, A., 2010. Pomegranate genetic resources and germplasm conservation: A Review. *Fruit Vegetable Cereal Sci Biotechnol*, 4(2), pp.120-125.

Weigand, F., Baum, M. and Udupa, S., 1993. *DNA Molecular Marker Techniques, Technical Manual, No. 20 International Center for Agricultural Research in the Dry Areas (ICARDA*). Aleppo, Syria.

Zamani, Z., Sarkhosh, A., Fatahi, R. and Ebadi, A., 2007. Genetic relationships among pomegranate genotypes studied by fruit characteristics and RAPD markers. *The Journal of Horticultural Science and Biotechnology,* 82, pp.11-18.

The Zero Divisor Graph of the Ring (Z_{2^2p})

Nazar H. Shuker[1] and Payman A. Rashed[2]

[1]Department of Mathematic, College of Computer Sciences and Mathematic, University of Mosul, Mosul, Iraq

[2]Department of Mathematic, College of Basic Education, University of Salahaddin, Erbil, Kurdistan Region, Iraq

***Abstract*—In this paper, we consider the crossing number and the chromatic number of the zero divisor graph $\Gamma(Z_{2^2p})$ to show that this type of zero divisor graphs is bipartite graph, and the smallest cycle in $\Gamma(Z_{2^2p})$ is of length four this implies that the girth is equal four.**

***Index Terms*—Bipartite graph, crossing number, girth, planar graph, zero divisor graph of the ring (Z_{2^2p}).**

I. Introduction

The idea of zero divisor graph was first introduced by I. Beck in (1988), followed by Anderson and Livingston (1999), and some others Coykendall, et al., (2012) and Shuker, et al., (2012), showed that the zero divisor graph by $\Gamma(R)$ for commutative ring R, is always simple connected graph.

A planar graph is a graph that can be drawn on the plane in such a way that its edges are not intersecting each other (Harary, 1969). The crossing number $Cr(G)$ of a graph G is the minimum number of edge crossings of a plane drawing of the graph G according to Sankar and Sankeetha (2012). In graph theory, a planar graph is a graph that can be embedded in the plane, i.e. it can be drawn on the plane in such a way that its edges intersect only at their endpoints. In other words, it can be drawn in such a way that no edges cross each other's; such a drawing is called a plane graph or planar embedding of the graph. A plane graph can be defined as a planar graph with a mapping from every node to a point on a plane, and from every edge to a plane curve on that plane, such that the extreme points of each curve are the points mapped from its end nodes, and all curves are disjoint except on their extreme points (Harary, 1969).

In 2012, Sankar and Sankeetha posted two open conjectures, (*i)* For any graph $\Gamma(Z_{pq})$, where p and q are distinct prime numbers with $p < q$, then $Cr\Gamma(Z_{pq}) = (p-1)(p-3)(q-1)(q-3)/16$, (ii) for any graph $\Gamma(Z_{p^2})$, where p is any prime then $Cr\Gamma\left(Z_{p^2}\right) = (p-1)(p-3)^2(p-5)/64$. Furthermore in 2013, Malathi, et al., compare the rectilinear crossing number with the crossing number thereby forming an inequality by different conjectures.

In this environment, we study and address crossing number and chromatic number of the zero divisor graph Z_{2^2p} in which R is a commutative ring and $Z(R)$ is the set of zero-divisors of R. We associate a graph $\Gamma(R)$ to R with the set of vertices $Z^*(R) = Z(R)-\{0\}$, of non-zero zero divisor elements of R and for distinct v, $u \in Z^*(R)$, the vertices v and u are adjacent if and only if $vu = 0$. Throughout this work, we consider the ring Z_{2^2p}. This paper was organized as follows: Finding the crossing number of the zero divisor graph $\Gamma(Z_{2^2p})$ in the second section, in the third section we studied the girth, while in the four section we changed the style of zero divisor graph and proved it is bipartite graph and finally in the last section we find the chromatic number of the graph $\Gamma(Z_{2^2p})$. While in our conclusion, we find the precise number of the crossing number of the ring Z_{2^2p}. We also conclude that the chromatic number of Z_{2^2p} is equal two for all p.

II. The Crossing Number of a Zero Divisor Graph $\Gamma(Z_{2^2p})$

In this section, we consider the crossing number of the zero divisor graph of the ring Z_{2^2p}.

A. Definition (Malathi, et al., 2013)

The crossing number $Cr(G)$ of a graph G is the lowest number (minimum number) of edge crossings of a plane drawing of the graph G. For instance, a graph is planar if and only if its crossing number is zero. A good drawing of a graph G is "good" if and only if all edges intersect at most one.

We start this section with the following example.

Example 1: If $p = 7$, then the zero divisor graph $\Gamma\left(Z_{2^2p}\right) = \Gamma\left(Z_{2^27}\right) = \Gamma(Z_{28})$, and $Z^*(Z_{28}) = \{2, 4, 6, 8, 10, 12, 14, 16, 18, 20, 22, 24, 26, 7, 21\}$, with center $C = 2$ $P = 14$, has only two odd zero divisor elements, $p = 7$ and $3p = 21$.

The crossing number $Cr(Z_{28}) = 1 + 2 + 1 + 2 = 6$ as shown in Fig. 1.

ARO-The Scientific Journal of Koya University
Volume IV, No 2(2016), Article ID: ARO.10058, 04 pages
DOI: 10.14500/aro.10058
Received 23 October 2014; Accepted 20 September 2015
Regular research paper: Published 23 December 2016
Corresponding author's e-mail: payman.rashed@su.edu.krd

http://dx.doi.org/10.14500/aro.10058

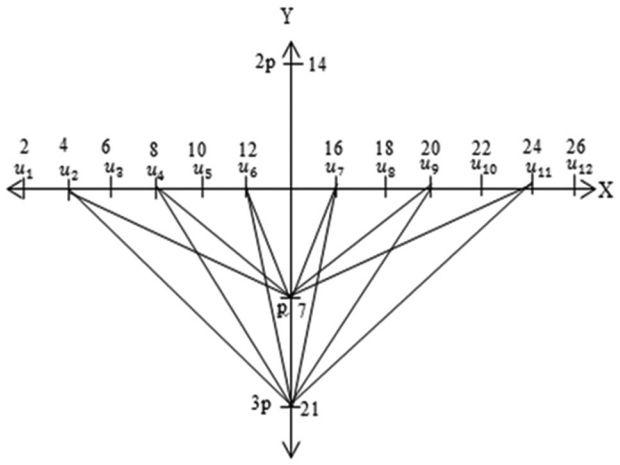

Fig. 1. Crossing number of the zero divisor graph $\Gamma(Z_{2^2 7})$

B. Definition (Bondy and Murty, 2013)

The degree of a vertex v in the graph G is the number of edges incident with v in the graph and denoted by $deg(v)$.

Recall that the center of the zero divisor graph $C = 2p$.

Next, we shall give the following result.

C. Theorem

The crossing number of $Z_{2^2 p}$, is $\left[\frac{p-1}{2}\frac{p-2}{2}\right]$.

Proof: The number of zero divisor elements (vertices) of the zero divisor graph $\Gamma\left(Z_{2^2 p}\right)$ is $(2p + 1)$, while the zero divisors are $\{2, 4, 6,\ldots,2p, 2p + 2,\ldots,4(p-1), p, 3p\}$, and the center of the zero divisor graph is $C = 2p$, for any prime p, and $deg(C) = 2p-2$.

Now, p and $3p$ are two vertices in the zero divisor graph of degree $(p-1)$ which are the greatest degree of the graph except the center.

Let $u = p$ and $v = 3p$, by degree of u and v there exist another vertices w_i distinct from u, v such that w_i is adjacent with both u and v, then $uw_i = 0$, $vw_i = 0$ for $I = 1, 2, 3,\ldots\ldots, p-1$.

But $uv = p.3p = 3p^2$ ($3p^2$ not divide 2^2p), this implies u and are non adjacent vertices but each u and v are adjacent with $p-1$ other vertices of $\Gamma\left(Z_{2^2 p}\right)$ which they are even vertices then we divide the zero divisor set Z^* of $\Gamma\left(Z_{2^2 p}\right)$ into two parts $V_1 = \{u, v, w\} = \{p, 2p, 3p\}$, and $V_2 = \{2, 4, 6,\ldots,(4p-2)\}$. Clearly any vertices u and v in V_1 are nonadjacent, same as in V_2, where $|V_1| = 2$ and $|V_1| = 2p-1$, since $|V| = 2p+1$, and $V(\Gamma\left(Z_{2^2 p}\right) = V_1 + V_2$, $V_1 \cap V_2 = \emptyset$.

Let $u = p$ and $v = 2$ in V_2, then 2^2 does not divide $uv = 2p$, if $u = p$ and $v = 8$ then 2^2p divides $uv = 2^3$, implies that the vertices u and v are adjacent with some vertices of V_1 and nonadjacent with the other vertices of V_2.

Let D be a good drawing of $\Gamma\left(Z_{2^2 p}\right)$, means it has a minimum number of crossing, the proof by method of induction on p.

If $p = 3$, then the crossing number is zero, if $p = 5$, then $|V| = 2p + 1 = 11$, $|V_1| = 3$ and $|V_1| = 3 = 11-3 = 8$.

Let the elements in V_1 be v_1, v_2, v_3 and elements in V_2 are $u_1, u_2, u_3, \ldots, u_{2p-2}$ denote by $Cr_D(v_i, u_j)$ the number of crossing of edges one terminate at v_i, the other at u_j and by $Cr_D(v_i)$ the number of crossing edges which are terminate at v_i.

Clearly the crossing number $\Gamma\left(Z_{2^2 p}\right)$.

$$Cr_D(\Gamma\left(Z_{2^2 p}\right)) = \sum_{i=1}^{i=3}\sum_{j=1}^{8} Cr_D\left(v_i, u_j\right)$$

We consider the vertices of V_1, the proof based on having all of the vertices on X and Y axis. The first thing is to place $|V_2|/2 = \frac{p-1}{2}$ vertices on one side of X axis and $|V_1| = 3$ vertices on the Y axis, then we connect all vertices on the X axis with the vertices on Y axis. The proof based on having all of the vertices of $\Gamma\left(Z_{2^2 p}\right)$ on X and Y axis. First, we place the vertices of V_2 on X axis such that 4 vertices on one side of X coordinate and other vertices of V_1 on the Y axis in a way that $2p = C$ in the positive and p, $3p$ on the negative side, respectively. Then, we connect the vertices of V_2 with $2p$ we get no crossing and connect the vertex p with the vertices of u_i of V_2 where $u_i = 0$ mod 4 on X axis also we get no crossing. Finally, when we connect the vertex $3pV$ with the vertices $u_i = 0$ mod 4, we get the crossing as follows:

$Cr(u_1) = Cr(u_3) = Cr(u_6) = Cr(u_8) = 0$

since they not adjacent with v_1, v_3

$Cr(u_2) = Cr(u_7) = 0$.

$Cr(u_4) = 1$ and $Cr(u_5) = 1$ in each side of X axis.

$Cr(\Gamma(Z_{2^2 p}) = \sum_{i=1}^{8} Cr(vi) = 2$ (1) since we have two side of X axis, then we must multiple by 2.

$$Cr(\Gamma(Z_{2^2 p}) = \left[\frac{4}{2}\right]\left[\frac{3}{2}\right] = \left[\frac{5-1}{2}\right]\left[\frac{5-2}{2}\right]$$

So $Cr(\Gamma(Z_{2^2 p}) = \left[\frac{p-1}{2}\right]\left[\frac{p-2}{2}\right]$

In general, we place $\left[\frac{2^2 p-2}{2}-1\right]$ (except the center $2p$) vertices on both side of X and Y axis such that p, $3p$ on one side of Y axis and $2p$ on the other side of it, see Fig. 2. The

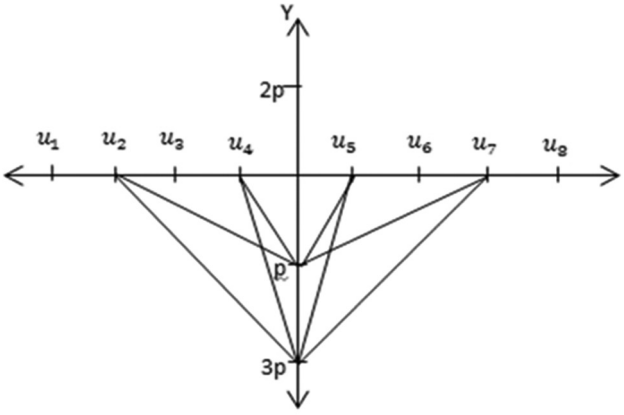

Fig. 2. Crossing number of the zero divisor graph $\Gamma(Z_{2^2 p})$

crossing happens when we connect v_3 with vertices u_i of V_2 if i is even, $i = 2, 4, 6, \ldots 2^2p-2$, i.e. $u_i = 0 \bmod 4$. And crossing is increase with increasing the vertices u_i in each side of X axis and its depend on p. then the number of vertices u_i adjacent with $v_3 = 3p$ are $\left[\frac{\frac{2^2p-2}{2}-1}{2}\right]$.

$= \left[\frac{2^2p-2}{4}-\frac{1}{2}\right] = \left[\frac{2^2p-2-2}{4}\right]$

$= \left[\frac{2^2p-4}{4}\right] = \left[\frac{4(p-1)}{4}\right] = p-1$ in each side of X axis as follow.

$Cr(u_2)=0$, $Cr(u_4)=1$, $Cr(u_6)=2$ and so on in this manner in one side of X axis till.

$Cr(u_{p-i}) = \left[\frac{p-2}{2}\right]$

Therefore $Cr_D(\Gamma(Z_{2^2p})) = \sum_{i=1}^{4p-4} Cr(v_3, u_i)) = 2[1 + 2 + 3 + \ldots + \ldots.]$

$= \left[\frac{p-1}{2}\right]\left[\frac{p-2}{2}\right]$

III. The Girth in the Zero Divisor Graph $\Gamma(Z_{2^2p})$

In this section, we consider the girth of the zero divisor graph of the ring $\Gamma(Z_{2^2p})$.

D. Definition (Beck, 1988)

The girth in the graph G is the smallest cycle contained in the graph. Next, we shall give the following result.

E. Theorem

The girth of the zero devisor graph $\Gamma(Z_{2^2p})$ is 4.

Proof: The vertices of the zero divisor graph is of the form $\{u_1, u_2, u_3, \ldots, u_n, v_1, v_2, v_3, \ldots, v_n, p, 2p, 3p\}$ where $2p$ is the center, p, $3p$ are odd zero divisors and u_i, v_j represented the even zero divisor of the form:

$u_{i+1} = ui + 4$, $i = 1, 2, \ldots, n-1$ and $j = 0 \bmod 4$, $j = 1, 2, \ldots, n$, $vn = 4p-4$ respectively.

Since each vertex u_i is of degree one, is adjacent to center only ($u_i.2p = 0$) and its not adjacent to any other vertex in $\Gamma(Z_{2^2p})$, $u_i.v_j \neq 0$, $u_i.p \neq 0$ and $u_i.3p \neq 0$, for all $i, j = 1,2, \ldots n$, then the $deg(u_i) = 1$.

But each v_i is adjacent to the odd vertices p, $3p$ and the center $2p$, $v_i.p = v_i.3p = v_i.2p = 0$, since $v_i = 0 \bmod 4$, then the smallest cycle in the zero divisor graph $\Gamma(Z_{2^2p})$ is as follow: Start from the vertex $2p$ to $v_m \to p \to v_k \to 2p$ for all m, $k \leq n$ then the girth of $\Gamma(Z_{2^2p}) = 4$, as shown in Fig. 3.

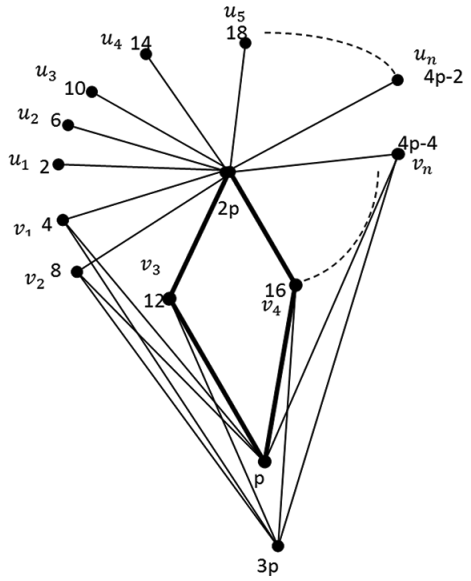

Fig. 3. The girth of $\Gamma(Z_{2^2p})$

IV. The Partition of the Zero Divisor Graph $\Gamma(Z_{2^2p})$

F. Definition

The graph G is said to be n-partite if V(G) divided in to subsets $V_1, V_2., V_n$ of vertices of the graph G, such that:

1. $V_i \neq \emptyset$, for $i = 1, 2., n$
2. $V_i \cap Vj = \emptyset$, for $i, j = 1, 2, \ldots, n$
3. $U_{i=1}^{n} V_i = V(G)$.

Provided that the vertices in each partition set V_i are nonadjacent, but they can be adjacent with each other. If $n = 2$, then the graph is called bi-partite graph.

G. Theorem

The zero divisor graph $\Gamma(Z_{2^2p})$ is bipartite graph.

Proof: Since the vertices of zero divisor graph $\Gamma(Z_{2^2p})$ with respect to the degree of vertices is of the form $\{u_1, u_2, u_3, \ldots, u_n, v_1, v_2, v_3, \ldots, v_n, p, 2p, 3p\}$ and up to zero divisor relation (two vertices a, b are adjacent if and only $ab = 0$) we divided the zero devisor set in to two subset of vertices $V_1 = \{u_1, u_2, u_3, \ldots, u_n, v_1, v_2, v_3, \ldots, v_n\}$ and $V_2 = \{p, 2p, 3p\}$ such that u_i is adjacent with center $2p$ only, while v_i is adjacent with p and $3p$ respectively. However, the vertices in the set V_1 are nonadjacent together so the vertices of the set V_2 are nonadjacent with each other as shown in the Fig. 4, implies that $\Gamma\left(Z_{2^2p}\right)$ is bipartite graph.

V. Chromatic Number of the Zero Divisor Graph $\Gamma\left(Z_{2^2p}\right)$

A coloring of a graph G is a mapping $Co: V(G) \to S$. The elements of S are called colors; the vertices of one color form a color class. If $|S| = k$, we say that Co is a k-coloring (often we use $S = \{1.,k\}$). A coloring is proper if adjacent vertices have different colors.

 http://dx.doi.org/10.14500/aro.10058

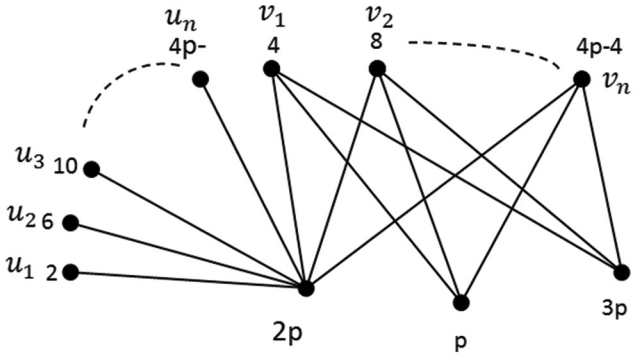

Fig. 4. The bipartite graph $\Gamma(Z_{2^2p})$

Consider a graph $G = (V, E)$ then edge coloring: No two edges that share an endpoint get the same color. Vertex coloring: No two vertices that are adjacent get the same color use the minimum amount of colors. This is the chromatic number denoted by $\chi(G)$.

A graph is k-colorable if it has a proper k-coloring. The chromatic number $\chi(G)$ is the least k such that G is k-colorable. Obviously, $\chi(G)$ exists as assigning distinct colors to vertices yields a proper $|V(G)|$-coloring. An optimal coloring of G is a $\chi(G)$-coloring, (Duana, 2006).

A graph G is k-chromatic if $\chi(G) = k$. In a proper coloring, each color class is a stable set. Hence, a k-coloring may also be seen as a partition of the vertex set of G into k disjoint stable sets $S_i = \{v|Co(v) = i\}$ for $1 \leq i \leq k$. Therefore, k-colorable are also called k-partite graphs. Moreover, 2-colorable graphs are very often called bipartite.

Clearly, if H is a subgraph of G then any proper coloring of G is a proper coloring of H. i.e., If H is a sub graph of G, then $\chi(H) \leq \chi(G)$.

Most upper bounds on the chromatic number come from algorithms that produce colorings. The most widespread one is the greedy algorithm. A greedy coloring relative to a vertex ordering $(v_1 < < v_n)$ of $V(G)$ is obtained by coloring the vertices in the order $v_1 \ldots v_n$, assigning to v_i the smallest-indexed color not already used on its lower-indexed neighborhood. In a vertex-ordering, each vertex has at most $\Delta(G)$ earlier neighbors, so the greedy coloring cannot be forced to use more than $\Delta(G) + 1$ colors.

H. Proposition (Beck, 1988)

$\chi(G) \leq \Delta(G) + 1$.

Next, we shall give the following result.

I. Theorem

The chromatic number of $\Gamma(Z_{2^2p})$ is 2.

i.e., $\chi\left(\Gamma\left(Z_{2^2p}\right)\right) = 2$

Proof: Since the graph $\Gamma\left(Z_{2^2p}\right)$ is bipartite graph (Theorem 4.2), then we use exactly two color, first color for vertices in each partite set V_1 and second to the other partite set V_2 where $V(G) = V_2 \cup V_2$, since no two vertices in V_1 neither in V_2 are adjacent together, then certainly they have the same color. Further, the total number of color used in the zero divisor graph is exactly two color, then $\chi\left(\Gamma\left(Z_{2^2p}\right)\right)$ is two and the graph $\chi\left(\Gamma\left(Z_{2^2p}\right)\right)$ is 2-colorable.

VI. Conclusion

In general, the crossing number of any zero divisor graph of the ring Z_n, is given by inequality (less than or greater than). In this work, we found the precise number of the crossing number of the ring Z_{2^2p}. We also conclude that the chromatic number of Z_{2^2p} is equal two for all p, and this graph can be drown as a bipartite graph up to the adjacency relation in the graph.

References

Anderson, D.D. and Livingston, P.S., 1999. The zero divisor graph of a commutative ring. *Journal of Algebra,* 217, pp.434-447.

Beck, I., 1988. Coloring of commutative ring. *Journal of Algebra,* 116, pp208-226.

Bondy, J.A. and. Murty, U.S.R., 2013. *Graph Theory and Application North.* Holland, New York. Amsterdam. Oxford.

Coykendall, J., Wagstaff, S.S., Sheppardon, L. and Spiroff, S., 2012. On zero divisor graph. *Journal of Commutative Algebra,* 2, pp.241-299.

Duane, A., 2006. Proper coloring and p-partite structures of the zero divisor graph. *Rose Holman Undergraduate Math Journal,* 7(2), pp.1-7.

Harary, F., 1969. *Graph Theory*. Addison-Wesley Publishing Company, California.

Harju, T., 2005. *Graph theory*, Department of Mathematics, University of Turku, Finland.

Malathi, M., Sankeetha, S. and Sankar, J.R., 2013. Rectilinear crossing number of a zero divisor graph. *International Mathematical Forum*, 8(12), pp583-589.

Sankar, J.R. and Sankeetha, S., 2012. Crossing number of a zero divisor graph. *International Journal of Algebra,* 6(32), pp.1499-1505.

Shuker, N.H., Mohammad, H.Q. and Ali, A.M., 2012. The zero divisor graph of Z_{p^nq}. *International Journal of Algebra,* 6, pp.1049-1055.

General Information

Aro's Mission: Aro seeks to publish those papers that are most influential in their fields or across fields and that will significantly advance scientific understanding. Selected papers should present novel and broadly important data, syntheses, or concepts. They should merit the recognition by the scientific community and general public provided by publication in Aro, beyond that provided by specialty journals.

We welcome submissions from all fields of natural science and technology, and from any source. We are committed to the prompt evaluation and publication of submitted papers. Aro is published biannually; selected papers are published online ahead of print.

Submission

Manuscripts should be submitted by the correspondent authors of the manuscript via the on-line submission page. Regardless of the source of the word-processing tool, only electronic Word (.doc, .docx, .rtf) files can be submitted on-line. There is no page limit. Only online submissions are accepted to facilitate rapid publication and minimize administrative costs. Submissions by any other one but the authors will not be accepted. The submitting author takes responsibility for the paper during submission and peer review. If for some technical reason submission through the email is not possible, the author can contact aro.journal@koyauniversity.org for support. Before submitting please check Aro's guide to authors thoroughly to avoid any delay in the review and publication process.

Authors are explicitly responsible for the language of their texts. Paper should be submitted in a well written in understandable English. Authors should not expect the editor or editorial board to rewrite their paper. Prior to submission, authors should have their paper proofread by a possible academic native speaker of English.

- Submit the Article with contact Information
- File name should be your article tittle
- Don't submit your article in multiple journal, we are taking only minimum time for review process. please don't waste our time
- Once the paper is accepted, it can't be withdrawn
- Please follow publication ethics and regulation
- Avoid plagiarism and copied material
- Strictly Follow Aro's Template

Terms of Submission

Papers must be submitted on the understanding that they have not been published elsewhere and are not currently under consideration by another journal or any other publisher. Aro accepts original articles with novel impacts only. Post conference papers are not accepted "as is", however, regular papers on the same topic but with a different title can be submitted. The new paper should contain significant improvements in terms of extended content, analysis, comparisons with popular methods, results, figures, comments, etc. Please do not forget that the publication of the same or similar material in Aro constitutes the grounds for filing of an (auto) plagiarism case.

The submitting author is responsible for ensuring that the article’s publication has been approved by all the other co-authors. It is also the authors’ responsibility to ensure that the articles emanating from a particular institution are submitted with the approval of the necessary institution. Only an acknowledgement from the editorial office officially establishes the date of receipt. Further correspondence and proofs will be sent to the author(s) before publication unless otherwise indicated. It is a condition of submission of a paper that the authors permit editing of the

paper for readability. All enquiries concerning the publication of accepted papers should be addressed to aro.journal@koyauniversity.org.

Peer Review

All manuscripts are subject to peer review and are expected to meet standards of academic excellence. Submissions will be considered by an editor and "if not rejected right away" by peer-reviewers, whose identities will remain anonymous to the authors.

Guide to Author

We welcome submissions from all fields of science and from any source. We are committed to the prompt evaluation and publication of submitted papers. Selected papers are published online ahead of print. Authors are encouraged to read the instructions below before submitting their manuscripts. This section arranged into an overview speedy guidelines below and more detailed at the bottom section of this page

Manuscript Preparation

Submitting your manuscript will be in two stages namely before final acceptance and after.

Stage one:

At the first stage manuscript needs to be prepared electronically and submitted online via the online submission page in a Word (.doc, .docx, .rtf) format of one column double-spaced page, Times New Roman font type, and 12 p font size. A pdf version of the submitted manuscript should be submitted too. All authors' names, affiliations, e-mail addresses, and mobile phone numbers should be typed on a cover page, indicating the correspondent author.

Stage two:

- File type: MS-Word version 2003 or later.
- Format: The preferred format of the manuscript two-column template with figures and captions included in the text. This template can be downloaded via the following link. Please follow instructions given in the template; http://aro.koyauniversity.org/about/submissions#onlineSubmissions
- Text: All text is in Times New Roman font. The main text is 10-point, abstract is 9-point font and tables, references and captions are 8-point font.
- Figures: Figures should be easily viewed on a computer screen.

Units of Measurement

Units of measurement should be presented simply and concisely using System International (SI) units.

Title and Authorship Information

The following information should be included;

- Paper title.
- Full author names.
- Affiliation.
- Email addresses.

Abstract

The manuscript should contain an abstract. The abstract should be self-contained and citation-free and should not exceed 200 words.

Introduction

This section should be succinct, with no subheadings.

Materials and Methods

This part should contain sufficient detail so that all procedures can be repeated. It can be divided into subsections if several methods are described.

Results and Discussion

This section may each be divided by subheadings or may be combined.

Conclusions

This should clearly explain the main conclusions of the work highlighting its importance and relevance.

Acknowledgements

All acknowledgements (if any) should be included at the very end of the paper before the references and may include supporting grants, presentations, and so forth.

References

References must be included in the manuscript and authors are responsible for the accuracy of references. Manuscripts without them will be returned. Aro is following Harvard System of Referencing. (Learn how to import and use Harvard Styling in your Microsoft Office by following this link: http://bibword.codeplex.com/releases/view/15852)

Preparation of Figures

Upon submission of an article, authors are supposed to include all figures and tables in the PDF file of the manuscript. Figures and tables should embedded in the manuscript. Figures should be supplied in either vector art formats (Illustrator, EPS, WMF, FreeHand, CorelDraw, PowerPoint, Excel, etc.) or bitmap formats (Photoshop, TIFF, GIF, JPEG, etc.). Bitmap images should be of 300 dpi resolution at least unless the resolution is intentionally set to a lower level for scientific reasons. If a bitmap image has labels, the image and labels should be embedded in separate layers.

Preparation of Tables

Tables should be cited consecutively in the text. Every table must have a descriptive title and if numerical measurements are given, the units should be included in the column heading. Vertical rules should not be used.

Copyright

ARO Reviewer/Associate Editor Application Form

Aro is a scientific journal of Koya University (p-ISSN: 2410-9355, e-ISSN: 2307-549X) which aims to offer a novel contribution to the study of Science. The purpose of Aro is twofold: first, it will aim to become an ongoing forum for debate and discussion across the sciences and Engineering. We hope to advance our problem solving capacity and deepen our knowledge regarding a comprehensive range of collective actions. Second, Aro accepts the challenges brought about by multidisciplinary scientific areas and aspires to expand the community of academics who are able to learn from and help to produce advances in a variety of different disciplines.

The Journal is seeking reviewers who can provide constructive analysis of papers thus enhancing overall reputation of the Journal. If any expert is interested in participating of the review process, we highly encourage you to sign up as a reviewer for our Journal and help us improve our presence in domain of your expertise. Appropriate selection of reviewers who have expertise and interest in the domain relevant to each manuscript are essential elements that ensure a timely, productive peer review process. We require proficiency in English.

How to apply

To apply for becoming a reviewer of Aro, please submit the application form by following the link:
http://aro.koyauniversity.org/user/register
To apply for becoming a member of the Editorial Board of Aro, please submit the application form by following the link: http://aro.koyauniversity.org/pages/view/AEB

Both Associate Editor and Reviewers should specify their areas of research and expertise. Applicants must have a doctorate (or an equivalent degree), and if Master degree they need to have significant publishing experience. Please note that;

- You will need to write your full official name.
- Please provide an email which reflects your official name, such as nameOne.NameTwo@... , or your institute's official email.
- All data need to be written in English.

Note: For more information, kindly visit the following websites:

1. Aro.koyauniversity.org.
2. http://libweb.anglia.ac.uk/referencing/harvard.htm.
3. http://bibword.codeplex.com/releases/view/15852.

Koya University is a young university established in 2003 and it is located in the city of Koya (Koysinjaq), short distance to the East of regional capital city of Erbil (Arbil, Hewler) in Kurdistan Region of Iraq. It is on the foothills of beautiful high mountain. Its campus has been carefully laid out to em-brace the beautiful mountainous nature. The Koya University has a faculty system which enhances the interactions be-tween similar academic fields. Today the University has 4 Faculties; Engineering, Sciences and Health, Humanities and Social Sciences, Education and a School of Medicine, which consist of 25 departments in different fields, such as Petroleum Engineering, Geotechnical Engineering, Physics, Clinical Psychology, Social Science and Medical Microbiology as well as Sport Education.

KOYA UNIVERSITY

ARO is a scientific journal published by the Koya University. ARO is a journal of original scientific research, global news, and commentary. The Aro Scientific Journal is a peer-reviewed, open access journal that publishes original research articles as well as review articles in all areas of Natural Science and Technology. ARO has been accepted for indexing in the Emerging Sources Citation Index (ESCI), a new edition of Web of Science™ as of Feb 2016 .

ARO the Scientific Journal Office
Koya University University Park
Danielle Mitterrand Boulevard
Koya KOY45
Kurdistan Region - F.R. Iraq

ISSN: 2410-9355 (print version) ISSN: 2307-549X (electronic version) DOI: 10.14500/2307-549X